REOVIRUS ENHANCES EGRESS IN EXTRACELLULAR VESICLES THAT PROTECT VIRUS PARTICLES AND FACILITATE MULTIPARTICLE INFECTION

By

Sydni Caet Smith

Dissertation

Submitted to the Faculty of the

Graduate School of Vanderbilt University

in partial fulfillment of the requirements

for the degree of

DOCTOR OF PHILOSOPHY

in

Microbe-Host Interactions

May 10th, 2024

Nashville, Tennessee

Approved:

Heather Pua, M.D. Ph.D. (Chair)

Alissa Weaver, Ph.D.

Andrea Pruijssers, Ph.D.

John Karijolich, Ph.D.

Lars Plate, Ph.D.

Kristen Ogden, Ph.D. (Mentor)

DEDICATION

To my family—thank you for your endless support and love, for your unwavering encouragement, for working so hard to provide the best in life, and for shaping me into the person I am. To my friends—thank you for the many laughs, for standing by me, and for being a home away from home. Thank you is too small a sentiment, but no words can really capture the extent of my gratitude.

ACKNOWLEDGEMENTS

First and foremost, I would like to thank Dr. Kristen Ogden, my mentor. Kristen, you took a chance on me after only knowing me for a week. Thank you for trusting that I would do a good job taking up the mantle as your second graduate student, for welcoming me into your lab team, and for believing in me then and every day since. You have shaped my critical thinking skills, helped give me the confidence to ask questions, encouraged me to be curious and share my ideas, taught me to believe in my voice and the things I have to say, and you've shown me how to have fun whilst doing so. Under your tutelage, I have grown farther than I thought I could and achieved more than I thought I would. Thank you for everything. I am truly and sincerely grateful, and I am honored to have had the opportunity to work alongside you and learn from you these past several years.

Thank you to my committee, including Heather Pua, Alissa Weaver, Andrea Pruijssers, John Karijolich, and Lars Plate. Your guidance, feedback, enthusiasm for my project, and support have truly been invaluable every step of the way. Each and every one of you have helped me become a better scientist, and I am grateful to you all for always being so willing to make room in your busy schedules for all of our meetings and conversations. Thank you for believing in my abilities and pushing me farther than I knew I could go. I would like to thank personally thank Heather Pua, for being such a wonderful and supportive Chair, and Alissa Weaver for so generously providing presentation opportunities and for your wealth of expertise. I would especially like to thank Andrea Pruijssers for your genuine and sincere mentorship, for always having my best interests at heart, for encouraging my career growth, for helping me navigate the world of

interviews and industry, and for connecting me to your network. You are a role model to me in more ways than one.

I would also like to thank the entire BRET Office for the resources you provide and the way you impact student's lives, including mine. Special thanks go to Kate Stuart and Ashley Brady, for always lending a helping hand and a clear mindset, and for always having my best interests at heart, as you do for every student who walks through your doors. Thank you to the Department of Pathology, Microbiology, and Immunology at Vanderbilt University, especially our DGS Maria Hadjifrangiskou, for allowing me a space and ample resources to train, learn, and grow.

Over the past several years, I have had the incredible opportunity to bond with some of the best and brightest minds, and they can all be found in the Ogden lab and Denison lab. Each and every one of you have made a positive impact in my life, and I will never forget all of our conversations, jokes, and laughs. I will dearly miss sharing stories and bits of our lives with one another daily, as we have done for the past several years. You all made the time spent in lab zip by, especially Tia Hughes, Samantha Grimes, Laura Stevens, and Jordan Anderson-Daniels. Special thanks and heartfelt appreciation go out to Julia Diller and Tim Thoner. Thank you for never hesitating to take me under your wings, for always making sure I felt listened to, and for always being there to celebrate the big and little wins with me. Thank you to my previous PI and mentor, Dr. Shaw, who continues to mentor and inspire me to this day as a paragon of positivity and the ability to truly balance a love of hard work with a genuine love for life and living. You

helped my passion for science take root and allowed it to flourish under your tutelage, and I aspire to your level of leadership some day.

None of the work in this dissertation would be possible without my wonderful collaborators. Thank you to Evan Krystofiak and Jenny Schafer at the Vanderbilt University Cell Imaging Shared Resource Core for assistance with sample preparation, imaging, and analysis. Special thanks to Evan who, in every sense of the phrase, “took the EV and ran with it”. We have been collaborating almost since day one of my thesis project, and we have visualized things I never dreamed we would be able to see. Thank you for always thinking outside the box and for sharing your significant expertise and years of experience. Thank you to Terry Dermody and the entire Dermody lab, not only for your collective wealth of knowledge and support, but for cheering on myself and every member of the Ogden lab just as warmly and fervently as you might cheer on your own lab mates and friends. You all always strive for the upper echelon of scientific research, and I appreciate every conversation, laugh, and de-brief about the weather that we have ever shared. Thank you to the laboratory of Andries Zjilstra, and to his then-graduate student Ariana von Lersner, for sharing your specialized technique and time with us.

This work could not have been carried out without the following funding sources: National Institutes of Health (R01AI155646 to Kristen Ogden; 1F31AI167541 to Sydni Caet Smith), the National Center for Advancing Translational Sciences (CTSA Award no. UL1 TR002243), and by Dolly Parton Pediatric Infectious Diseases Research Funds.

Additionally, I would like to thank Eric Skaar and the Chemical Biology of Infectious Diseases Training Program (NIH T32AI112541), for giving me access to numerous opportunities and for initially forging the path of my next career steps at Pfizer. Services at the Vanderbilt Cell Imaging Shared Resource performed through Vanderbilt University Medical Center's Digestive Disease Research Center were supported by National Institutes of Health grant P30DK058404 Core Scholarship.

Table of Contents

LIST OF FIGURES

CHAPTER I: INTRODUCTION

Part I: Virus egress has historically been attributed to virus structure

The egress mechanisms of many viruses remain largely understudied. Viral infection of host cells has long been proposed to occur via standalone entities of “free” virus units that traffick from cell to cell [1]. The mechanism of viral egress has traditionally been attributed to virus structure (**Fig. 1**). Enveloped viruses can enter cells by binding to specific receptors on the cell membrane surface, after which the virus fuses directly with the plasma membrane to release the viral core, or the virus is further sorted into the endocytic pathway [2]. Enveloped viruses can then bud directly from the plasma membrane, as with human immunodeficiency virus and influenza virus, or virus particles bud into an exocytic pathway, as with hepatitis C virus [3-5]. Both mechanisms involve the virus particle acquiring an envelope directly from the host cell plasma membrane, which is usually additionally studded with viral proteins [6]. The hallmark of enveloped virus egress is its nonlytic nature, wherein the procedure of viral egress itself does not compromise the cell membrane, although cells may eventually lyse due to infection stress or immune cell cytotoxicity [2]. Contrastingly, non-enveloped viruses, including poliovirus, coxsackievirus, rhinovirus, norovirus, and hepatitis A virus (HAV), have been thought to exit cells lytically [5,7-10]. Non-enveloped viruses, like enveloped viruses, interact with cell surface receptors upon entry. However, because non-enveloped viruses are not wrapped in a host cell membrane, they cannot fuse directly to the plasma membrane, and are instead most often taken up via endocytosis [11]. This relatively straightforward, structure-based delineation in

virus egress phenotype changed in 2013, when a group of researchers reported the presence of both enveloped and non-enveloped released HAV [12]. Another traditionally non-enveloped virus, hepatitis E virus, was also reported to escape from cells in an enveloped state [13]. Both of these viruses appeared to rely on vesicle biogenesis molecules and pathways in order to attain their enveloped form. Additional studies revealed that coxsackievirus, rhinovirus, and poliovirus exit cells prior to cell lysis, and escape in association with vesicles [7,14,15]. Since these early studies, and in contrast to historical dogma, multiple additional viruses have been discovered to employ extracellular vesicles (EVs) as vehicles of nonlytic cellular egress, and the field of EV-associated virus egress is expanding rapidly in the wake of these discoveries [9].

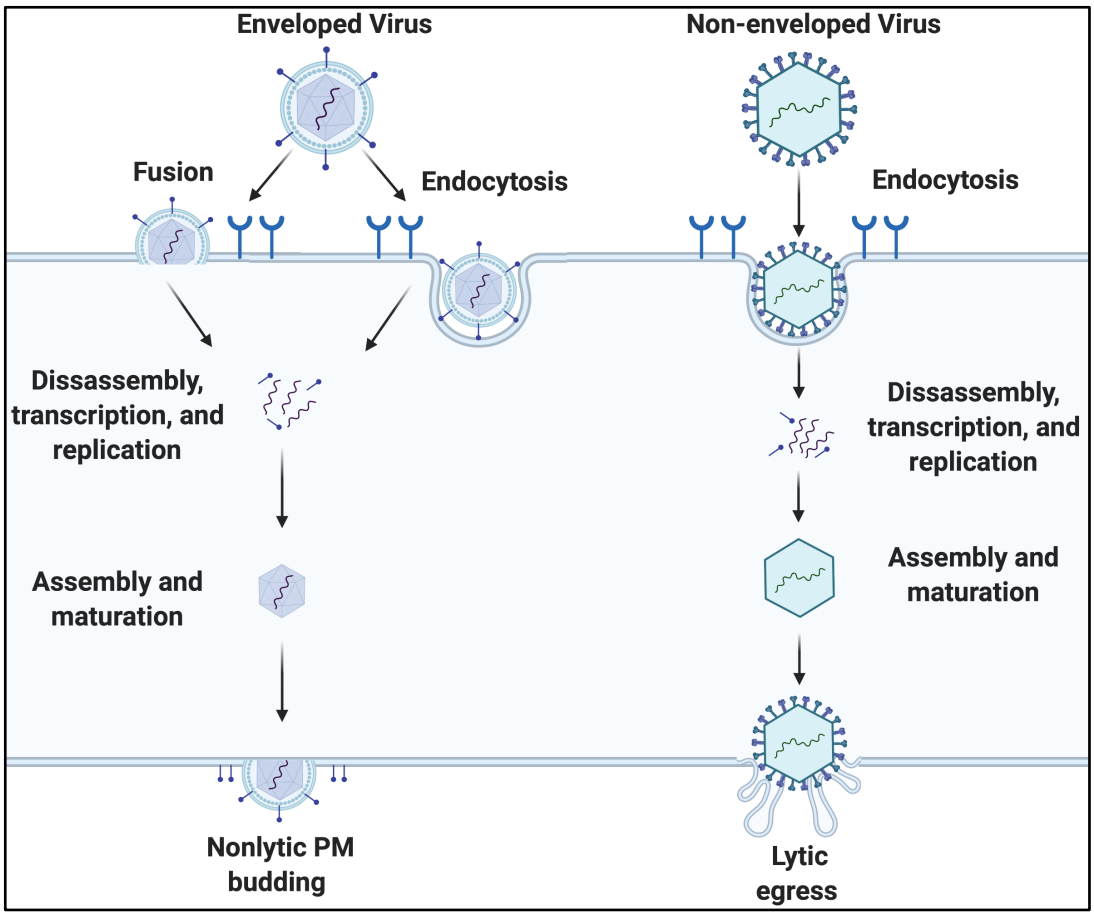

Figure 1. Enveloped virus egress differs from non-enveloped virus egress. Enveloped viruses may enter a cell via several mechanisms, including direct fusion with the plasma membrane and endocytosis. Non-enveloped viruses generally rely on interaction with specific cell receptors to enter cells via endocytosis. Following replication of both virus types, enveloped viruses acquire an envelope from the host cell, and egress nonlytically. Historically, it has been assumed that non-enveloped viruses rely on lytic egress.

Part II: Focus of dissertation and gaps in knowledge

When I began my dissertation project, very little was known regarding reovirus egress. Reovirus is a non-enveloped virus that does not cause disease in humans, and it is considered a potential oncolytic therapeutic due to its propensity to lyse cancer cells. Many steps of the reovirus infection cycle have been elucidated, including cell entry,

replication, packaging, tropism, interaction with and modulation of certain cellular pathways, and pathogenesis and spread in an animal model. Historical tenets the reovirus field have assumed that, because reovirus is non-enveloped, it must egress only via a lytic mechanism. However, this theory has only extremely rarely been investigated, and thus a considerable question has remained in the reovirus field for decades: does reovirus egress truly always rely on lysis, and is this the only route of egress? Recently, a nonlytic form of reovirus egress was defined, in which host cell-derived vesicles assist reovirus in exiting the cell without disturbing the plasma membrane. Additionally, the egress mechanism of two viruses in the same order as reovirus were linked to a different form of host cell-assisted nonlytic egress, this time involving direct association with host cell-derived extracellular vesicles (EVs). After reading about many instances of evolutionary distinct viruses employing EVs as vehicles of nonlytic egress, I was left to wonder whether reovirus might also take advantage of EVs during egress. Therefore, I sought to determine how reovirus escapes from infected cells, and I endeavored to address specific gaps in knowledge, including: i) does reovirus egress from infected cells in association with EVs, ii) does this egress strategy occur across multiple cell types, iii) what is the influence of reovirus egress strategy on infection of downstream cells, and iv) does reovirus infection alter EV release (**Fig. 2**)?

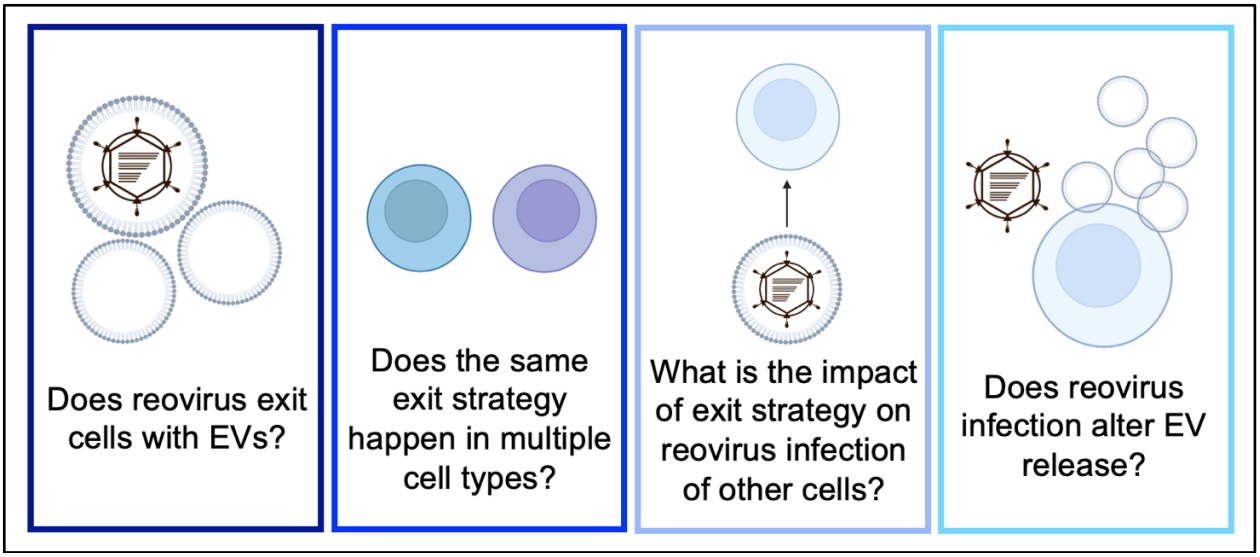

Figure 2. Gaps in knowledge. Several gaps in knowledge surrounding the mechanisms and influences of reovirus egress remain. These include: i) does reovirus egress in association with EVs, ii) does the same or similar egress mechanism occur in other cell types, iii) what is the effect of egress strategy on reovirus infection of other cells, and iv) does reovirus infection alter whole-cell EV release?

Part III: Viruses can employ extracellular vesicles as vehicles of nonlytic egress

Extracellular vesicles: Function, biogenesis, and subpopulations

Early in my dissertation research, I hypothesized that nonlytic reovirus egress might rely on association with EVs. EVs are generally defined as lipid bilayer-bound structures that are naturally released from cells. EVs were initially thought to play a role in removing cell waste and unneeded compounds, but have since been shown to function in cell-to-cell communication by transporting, storing, and protecting selective molecules such as proteins, lipids, metabolites, and nucleic acids as internal cargo during intracellular transit [16,17]. EVs additionally aid cells in regulating homeostasis and are fine-tuned based on the physiological status of the cell, allowing for short-range and long-range targeted delivery of specific cargo to recipient cells [18]. EVs have been isolated from

biological fluids including blood, saliva, milk, urine, and amniotic fluid [19-21]. To date, all cells have been found capable of releasing EVs, a process which has remained highly conserved throughout the evolution of bacteria, mammals, and plants [22-24].

If, during the course of my studies, I found that reovirus employs EVs as vehicles of nonlytic egress, then understanding what the type of EV with which reovirus associates could help elucidate a previously undefined set of cellular pathways with which reovirus interacts and potentially modulates. Many subpopulations of EVs have been characterized and are generally differentiated based on their cell of origin, size, composition, and cell biogenesis pathway [16]. EVs are widely acknowledged to be highly heterogenous and exist as complex and often overlapping populations, and the separation methodologies available often yield EV fractions that may be enriched in one subpopulation or another, but that overall remain dappled at best [25]. Though definitions in the EV field are constantly being revised, there are three broadly recognized EV categories: i) small exosomes (30-150 nm), ii) medium microvesicles (100-1000 nm), and iii) large apoptotic blebs (50-5000 nm) [26,27].

Exosomes are formed via inward budding of endosomal membranes during maturation of multivesicular bodies; multivesicular bodies either traffick to lysosomes for degradation an recycling, or they traffick to the plasma membrane where their exosome cargo is released via invagination of the inner leaflet of the multivesicular body, followed by exosome release from the cell via exocytosis [28]. Exosome cargo is shuttled from the

Golgi apparatus to endosomes, or are internalized at the plasma membrane before being sorted into endosomes [29]. Exosome cargo is enriched in molecules including DNA, mRNA, miRNA, heat-shock proteins, enzymes, cytoskeleton molecules, and signaling molecules[28].

Microvesicles are formed primarily directly at the plasma membrane, where the curvature of the plasma membrane increasingly protrudes or buds outward. Protein-degrading enzymes induce cytoskeleton destabilization of the plasma membrane, and calcium increase further weakens and increases flexibility of the plasma membrane until the microvesicle pinches off and is released from the cell [30]. Microvesicle cargo is localized to the plasma membrane and directed towards sites of budding through anchoring to the inner leaflet of the plasma membrane or through the cargo molecules' affinity for lipid rafts [31]. Microvesicle cargo is enriched in molecules including enzymes, heat-shock proteins, signaling molecules, histone fragments, and pieces of producer cell cytoplasm [28].

Although these two EV subpopulations are generated at different sites in the cell, exosomes and microvesicles retain common intracellular biogenesis mechanisms and sorting machineries that cloud our ability to definitively delineate subpopulations. Multiple previous studies have implicated the presence of proteins including CD9, CD63, CD81, ALIX, and TSG101 as being enriched in exosome populations [32-35]. Although microvesicles are generally less well-studied compared to exosomes, it appears that

annexin A1, matrix metalloproteinases including MMP2, and certain glycoproteins and integrins are enriched in microvesicles [34,36-40]. However, the markers enriched in one EV or another depend significantly on the producer cell line, and even the biogenesis pathway used to traditionally define EV subpopulations can differ markedly depending on the cell type in question [26,41]. Furthermore, the cargo that EVs carry can be markedly modulated based on the physiological state of the producer cell, and the stimulus that triggers EV biogenesis [35]. For microvesicles especially, given their origin at the plasma membrane surface, markers are heavily cell type-dependent.

Apoptotic blebs are highly heterogenous, but are known to be released from cells undergoing programmed cell death [42]. Apoptotic bleb formation follows a specific array of steps as the cell breaks down, including enucleation, expansion, and retraction. During the retraction phase, cell debris is packed into the blebs as they pinch off from the rest of the cell to form blebs [28]. Apoptotic blebs carry a wide and seemingly random array of cellular products, though recent studies have provided evidence that heat-shock proteins, lipoproteins, cytosolic proteins, and oncogenes were enriched [43,44]. Apoptotic blebs play an important role in removing aged and damaged tissue, promoting embryo development, and recycling biomolecules [45].

Medium-sized secretory autophagosomes (300-500 nm) are a more recently described subcategory of EV. Autophagy is a degradative pathway that plays a critical role in degrading large quantities of the cytoplasm to break down lipid, protein, and

carbohydrate molecules to maintain cellular homeostasis, and autophagosomes are produced in all eukaryotic cells [46]. Autophagosomes are double-membraned when trafficking within the cell, and can be formed from several intercellular membranes including the endoplasmic reticulum, the mitochondria, and the plasma membrane [47]. Secretory autophagosomes form when double-membraned autophagosomes fail to fuse with lysosomes during the normal recycling pathway, and instead shuttle to the cell surface and fuse to the plasma membrane to release single-membraned vesicles [48]. Secretory autophagosome release has been observed in several eukaryotic cells, and enriched cargoes include entire organelles, synuclein, amyloid β protein, and IL1β [49-51]. Thus, although three broadly recognized EV categories are currently defined, many more EV subpopulations exist outside of and overlapping with these categories.

Viruses egress in exosomes, secretory autophagosomes, and microvesicles

In recent years, viruses from distinct families have been found to take advantage of a variety of EV subpopulations to aid their escape from infected host cells (**Fig. 3**) [9]. Based on the rapidly-expanding index of viruses that employ EV-mediated strategies of egress, I hypothesized that reovirus might use a similar mechanism of nonlytic egress. Poliovirus, coxsackievirus, rhinovirus, zika virus, bluetongue virus, and varicella zoster virus egress within secretory autophagosomes [15,52-55]. Viruses including BK polyomavirus, norovirus, HAV, hepatitis E virus, hepatitis C virus, enterovirus 71, torque tene virus, dengue virus, west nile virus, langat virus, severe fever with thrombocytopenia syndrome virus, porcine reproductive and respiratory syndrome virus, and pegivirus egress in

association with exosomes [12,13,56-67]. Marseillevirus escapes in giant, multiparticle ER-derived EVs, JC polyomavirus egresses in EVs carrying both exosome and microvesicle markers, and encephalomyocarditis virus-associating EVs carry secretory autophagosome and microvesicle markers [68-70]. The above list is not exhaustive, as the EV-virus field is constantly and rapidly expanding, but it highlights the breadth of different viruses and EV subpopulations capable of permitting such an escape strategy. Despite the field's recent progression in knowledge, there remain many viruses whose egress mechanisms are a mystery, including reovirus, and the influence of egress mechanisms on infection are only just beginning to be revealed.

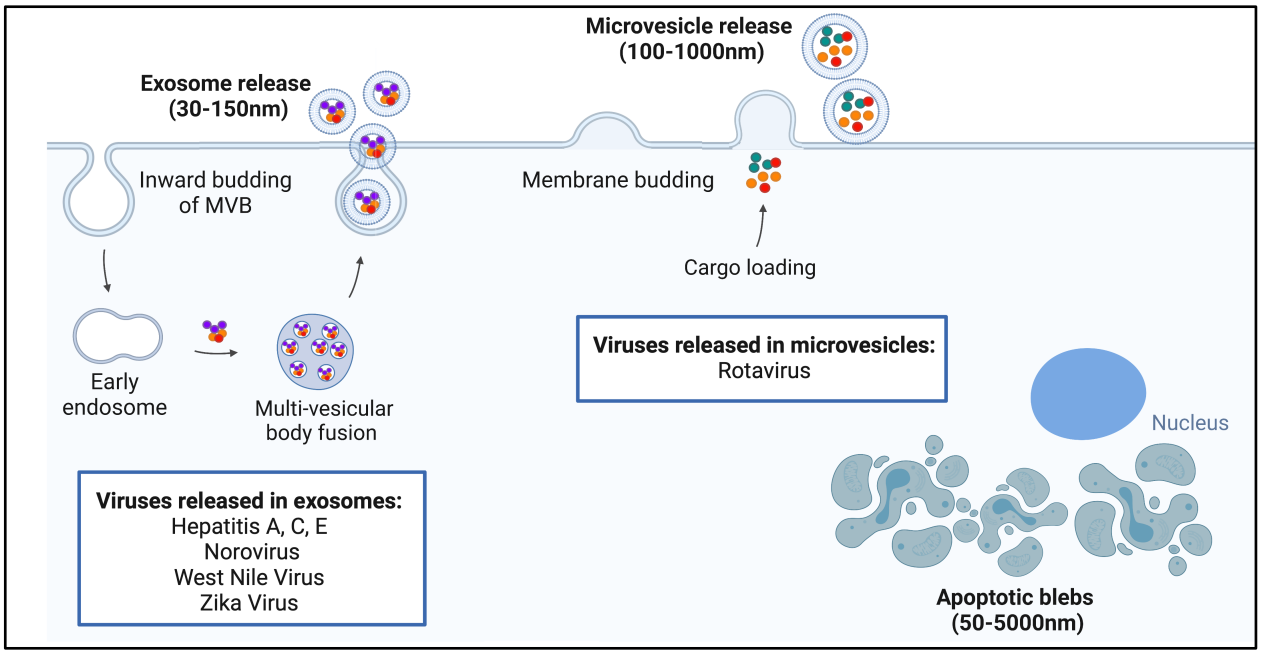

Figure 3. Evolutionarily distinct viruses associate with different EV subpopulations. The biogenesis pathways of exosomes involve budding of the inner leaflet of the multivesicular body, followed by release via exocytosis. Viruses associated with exosomes during egress include Hepatitis A, Hepatitis C, Hepatitis E, Norovirus, West Nile virus, and Zika virus (list not exhaustive). Microvesicles form via progressive curvature and final pinching of the plasma membrane. Rotavirus egresses in association with microvesicles. Apoptotic blebs form when a cell undergoes regulated cell death.

Rotavirus egress in microvesicles occurs *in vitro* and *in vivo*

After finding multiple prior studies in which viruses belonging to many different families utilize EVs as a mode of exit, I wanted to further investigate whether viruses more closely related to reovirus use EVs during egress. Rotavirus is in the same order as reovirus, the order Reovirales. Rotavirus causes acute gastroenteritis and in the pediatric population is responsible for 30 – 50% of severe diarrheal illnesses [71]. At the time of writing this dissertation, one of the only viruses found to be released in plasma membrane-derived microvesicles *in vitro* and *in vivo* is rotavirus.

Multiple rotavirus particles have been documented being released *in vivo* and *in vitro* in medium-sized EVs [57]. Following bead-based capture of medium and small EVs released from rotavirus-infected H69 lung carcinoma cells, MA104 monkey kidney cells, and Caco-2 intestinal epithelial cells, authors investigated several EV hallmarks. By employing super-resolution microscopy, the authors found that rotavirus particles associate with plasma membrane-bound structures whose size and propensity to protrude outward directly from the plasma membrane closely resembles the biogenesis pattern of microvesicles. Additionally, using lipidomic and proteomic studies and markers of medium EVs, autophagosomes, and small EVs, the authors revealed further evidence that EVs from rotavirus-infected cells bear canonical microvesicle hallmarks. Using negative-stain EM imaging, the authors provided evidence that multiparticle medium EV-associated rotavirus clusters are shed in the stool of infected mice. Interestingly, medium EV association provoked a biologically relevant increase in rotavirus virulence; when mice

were inoculated with EVs or free rotavirus and compared to free rotavirus, an inoculum containing five times the number of genome copies of free rotavirus as EV-contained rotavirus was required to recapitulate the number of infected cells and the severity and duration of diarrhea symptoms. Thus, evidence exists that EV-mediated virus egress in the order Reovirales occurs in an animal model (**Fig. 4**).

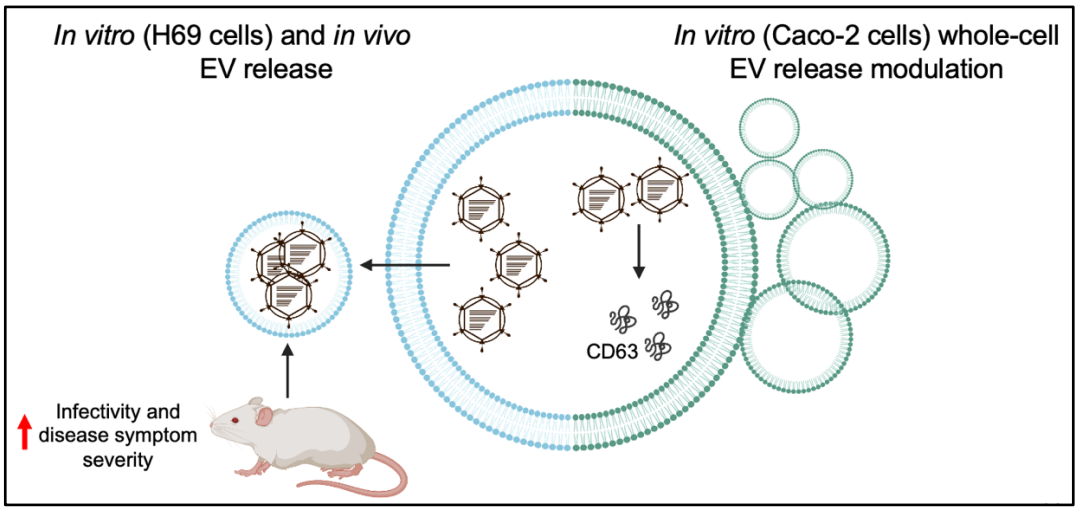

Figure 4. Rotavirus egress in microvesicles occurs *in vivo*, and rotavirus may interact with EV biogenesis molecules. Compared to free virus particles, rotavirus associated with medium EVs increased disease symptom severity in a mouse model. Additionally, rotavirus interacts with the EV biogenesis molecule CD63 to upregulate EV abundance compared to uninfected cells.

Part IV: Extracellular vesicle-mediated egress can influence virus infection

Extracellular vesicles affect virus neutralization

After finding published evidence that the mechanism of egress can directly influence rotavirus infection in a mouse model, I wanted to investigate whether the mechanism of egress might also influence reovirus infection. If reovirus egress is linked to EV association, then what are some ways in which EVs might impact virus infection?

Our current understanding of the influence of egress mode on infection, particularly relating to egress in EVs, is in its nascent stage. Current literature provides evidence that EV-facilitated egress potentially influences: i) antibody-mediated neutralization, ii) cell entry and receptor interactions, and iii) multiparticle infection (**Fig. 5**). EV-mediated egress and transport may alter immune system detection of ongoing viral infection. For viruses such as JC polyomavirus, enterovirus 71, HAV, rotavirus, and hepatitis E virus, EV association can, to varying degrees, protect viral particles from antibody-mediated neutralization [12,69,72-74]. Not only can EVs provide virus particles with a shield to escape from immune detection, EVs can carry immune-modulatory molecules. Phosphatidylserine, a phospholipid that is generally universally displayed on the surface of EVs, serves as a potent down-regulator of anti-inflammatory immune responses and can function as a phagocytic uptake signal, allowing viruses to persist undetected and thereby possibly increasing the likelihood that EV-associated viruses enter target cells [75-77].

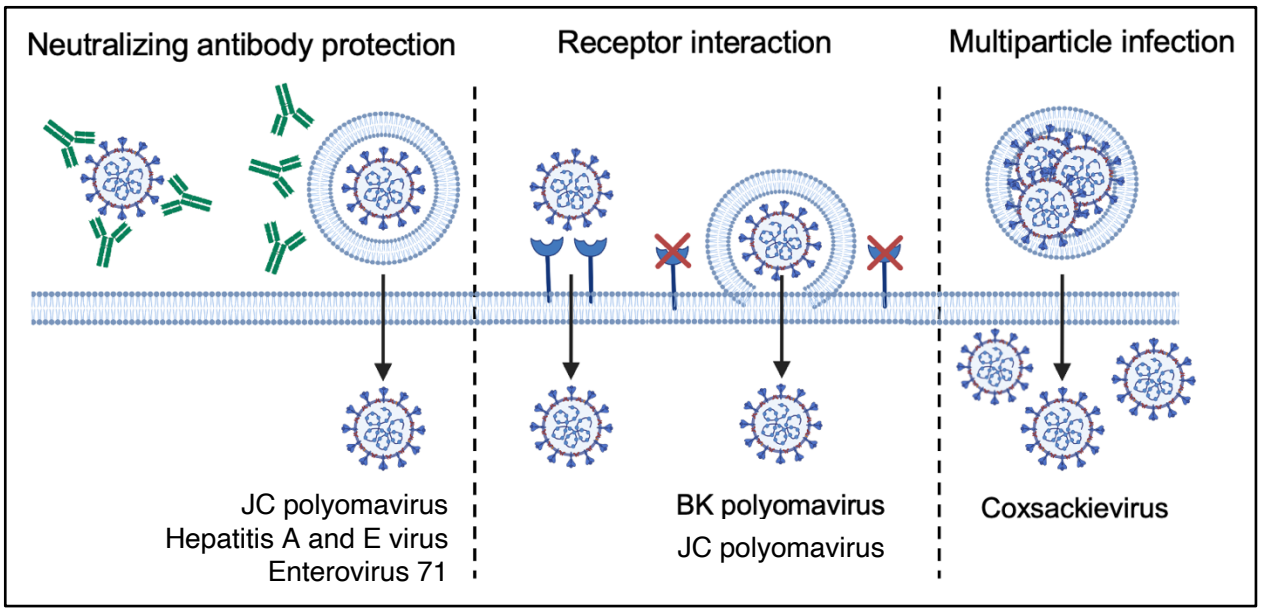

Figure 5. EV-mediated egress can influence virus infection. EV association potentially protects virus particles from antibody-mediated neutralization, alters virus interaction with and reliance on cell receptors during entry, and groups virus particles together to form multiparticle units that can collectively infect a recipient cell.

Extracellular vesicles influence virus entry

One universal requirement applies to most viruses; regardless of evolutionary origin, viruses must adhere to and enter into permissive host cells and take advantage of intracellular machinery in order to replicate. Different viruses rely on different and oftentimes highly specific host factors to achieve cell adhesion and entry, but some common themes exist. For many viruses, initial contact with the cell is achieved by binding to oligosaccharides on the cell surface [78]. Following adhesion, viruses usually interact with specific proteinaceous receptors in order to coordinate entry into the cell, which commonly involves endocytic pathways [10,79]. Thus, viruses generally enter cells via specific receptor interactions. In contrast, EV uptake into cells can be mediated via a variety of phagocytic and fusion pathways, including cell surface binding to integrins and

proteoglycans, micropinocytosis, micropinocytosis, phagocytosis, caveolae-mediated endocytosis, clathrin-mediated endocytosis, lipid raft interaction, and via direct fusion with the plasma membrane; entry via endocytic pathways, however, seems to be a common trait across EV subpopulations [26]. EVs additionally can deliver viruses and viral genomes to non-susceptible cells, thereby permitting viruses to gain access to cells they may otherwise naturally not be able to breach. EV-transported BK polyomavirus, which interacts with sialylated glycans similarly to reovirus, did not utilize cell receptors when transmitted in EVs, suggesting a mechanism of receptor-independent EV fusion with the plasma membrane to release viral cargo [56]. JC polyomavirus additionally did not require canonical receptors, suggesting an alternative entry pathway [80]. Contrastingly, productive infections established by poliovirus, norovirus, and HAV still required each virus's respective host cell receptor, suggesting a mechanism by which EVs must become disrupted in order to allow the virus to interact with its host cell receptor.

Extracellular vesicles influence multiparticle virus infection

EVs have the capacity to enclose multiple virus particles. EV association may permit a group of virus particles to simultaneously, collectively infect the same cell—this represents a previously undescribed mechanism of infection termed *en bloc* transport, which occurs both *in vitro* and *in vivo* [15]. Not only can EVs transmit virus bundles *in vitro* and *in vivo*, but they can also transmit viruses *en bloc* virus between animals [15,57,81]. Due to host cell permissivity and viral sensitivity to cellular immune defenses, a "threshold" of multiplicity of infection must be reached to successfully infect a cell [82-85]. EV-mediated

multiparticle transport can enhance viral multiplicity of infection in a recipient cell compared to independent units of free virus, thereby increasing the chances of a virus establishing productive infection. Additionally, EV-mediated multiparticle containment may increase the productivity of infection by enabling complementation and rescue of noninfectious virus particles containing dysfunctional genome segments. Specifically, multiparticle aggregation has been shown to increase poliovirus complementation during infection, and EV-mediated multiparticle aggregation has been reported for rotavirus [15,57,86]. Additionally, the adhesion of multiple reovirus particles to gut bacteria increased genetic complementation [86,87]. In coxsackievirus coinfected cells, 7-38% of EV-contained particles contained mixed parental genomes. Despite these advances in knowledge, however, the influence of EV-associated egress on downstream virus infection and replication kinetics, multiparticle transport, and immune evasion remains incompletely understood for many viruses.

Viruses can modulate extracellular vesicle release and composition

EV-mediated virus egress may be orchestrated by the virus itself, as large-scale viral modulation of EVs has been demonstrated for multiple viruses. Direct viral interaction with EV biogenesis pathways and molecules has been shown to alter whole-cell EV release patterns and EV-mediated viral release. In Caco-2 cells, rotavirus significantly increased the quantities of EVs released from infected cells; compared to EVs released from uninfected cells, these EVs inhibited T cell function and proliferation [88]. Rotavirus protein VP6 was reported to co-precipitate with the EV biogenesis protein CD63, which

plays a role in endosomal sorting, suggesting a potential direct link between EV biogenesis and rotavirus infection. When caspase inhibitors were applied to rotavirus-infected Caco-2 cells, EV markers decreased in prevalence, suggesting a potential point of EV modulation [89]. Furthermore, Zika virus was recently reported to modulate the activity and gene expression of exosome biogenesis molecule SMPD3 to facilitate small EV-mediated Zika virus release [90]. Epstein-Barr virus induces the upregulation whole-cell EV protein secretion and interacts with biogenesis protein CD63 to regulate its own exosome packaging [91]. Poliovirus remodels intracellular membranes and lipid pools, enterovirus 71 infection induces the formation of autophagosomes, and coxsackievirus proteins increase the formation of autophagosomes [7,92,93]. Additionally, viruses modulate EV composition and prevalence. Influenza A infection induces upregulation of 900 proteins in the EV proteome [94]. HIV and human cytomegalovirus-infected cells release EVs displaying viral capsid proteins that induce physiological changes in recipient cells [95]. Thus, by regulating EV abundance, composition, and biogenesis pathways, virus infection regulates whole-cell EV release patterns to potentially promote EV-mediated viral egress. Given the interaction of multiple viruses with EV biogenesis pathways, and the documented influence of rotavirus infection on egress pathway modulation, I wondered whether reovirus might similarly interact with the host cell to promote its escape in a specific route of egress.

Part V: Reovirus egress mechanisms remain unclear

Reovirus: background, replication, and strain-specific variations

For decades, the mechanisms of reovirus egress have remained poorly understood. Reovirus is an ideal model in which to study egress due to a wealth of foundational literature defining many aspects of the replication cycle and well-established *in vitro* and *in vivo* models. Additionally, its genetic tractability has permitted engineering of mutant, reassortant, and genetically barcoded viruses [96,97]. Thus, reovirus is a relatively straightforward virus to work with, and its genetic malleability makes it an ideal candidate to ask and answer questions relating to virus interaction with and modulation of host cell egress pathways. Additionally, different strains of reovirus have been classified and researched; some of these strains interact with host cells in markedly different ways. Thus, by using multiple different strains, it is possible to glean additional insight into how reovirus interaction with the host cell might modulate different strategies of egress.

Reovirus is a member of the order Reovirales, which contains pathogens that cause disease in a wide range of human and animal hosts. Viruses in the order Reovirales contain 9-12 double-stranded RNA segments capable of reassorting to generate genetic diversity. Specifically, reovirus is non-enveloped and contains ten double-stranded RNA segments. Reovirus encodes a group of 4 small (S1-S4), 3 medium (M1-M3), and 3 large (L1-L3) segments. These segments are contained within a double-layered, icosahedral, proteinaceous core. While reovirus is capable of infecting humans, it is rarely associated with disease, though reovirus infection has been linked to onset of celiac disease [98-100]. Based on its capacity to lyse tumor cells, reovirus is currently in clinical trials as an

oncolytic therapeutic [101]. Two strains of reovirus, type 1 Lang (T1L) and type 3 Dearing (T3D), will be discussed throughout the course of this dissertation.

Though we currently lack a clear idea how reovirus egress is governed, there is a great deal that we do understand regarding reovirus infection. Reovirus replication is entirely cytoplasmic (**Fig. 6**) [102]. Reovirus interacts with specific cell receptors and enters the cell through the endocytic pathway. Reovirus entry into permissive cells is mediated via binding to host cell receptors. Reovirus attachment protein σ1 binds to junctional adhesion molecule-A (JAM-A) and sialic acid. Reovirus binding to cells requires JAM-A interaction, but does not require sialic acid binding, though this is thought to increase viral adhesion to the cell surface. Reovirus strains interact with different sialylated glycans; T3D can engage α-2,3-, α-2,6-, and α-2,8-sialylated glycans, while T1L only engages α-2,3-sialylated glycans. Additionally, the NOGO-66 Ngr1 receptor on neuronal cells may affect reovirus binding in the brain [103]. Binding and subsequent infection can be neutralized by strain-specific antibodies, some of which target and bind the reovirus attachment protein σ1 [104,105]. Following uptake via the clathrin-mediated endocytic pathway, reovirus particles are sorted into early, late, and recycling endosomes. Only those particles which traverse the early and late endosomes can yield productive progeny virus, and host cell microtubule association is thought to play an important role in correct reovirus sorting to the correct endosomal pathway. Then, the virus is proteolytically uncoated and converted to an infectious subvirion particle (ISVP) via removal and cleavage of outer-capsid proteins, including σ3 and μ1, and penetrates into the cytoplasm

where the core synthesizes viral transcripts, which are then translated by host cell machinery [102]. ISVPs can additionally be formed by proteases in the intestinal lumen of an animal and penetrate early endosomes. Viral proteins accumulate in the cytoplasm and form replication factories that function as sites of particle assembly and maturation [102,106,107]. Viral replication factories are assembled by interactions of the reovirus nonstructural proteins μNS and σNS, which interact with and remodel tubules and vesicles derived from the endoplasmic reticulum[106,108]. Specifically, previous work has suggested that σNS plays a particular role in recruiting reovirus RNA segments to sites of viral replication factories [109]. Replication factories are thought to protect viral RNA from host cell immune recognition. Throughout the infection cycle, reovirus replication factories are dynamic, and factories that begin as small and punctate fuse together and become larger over time as infection progresses [110,111]. Strain-specific factory morphology is determined by the reovirus polymerase cofactor μ2; T1L factories traffick along microtubules and have a morphologically filamentous shape, whereas T3D factories do not associate with microtubules and thus retain a globular phenotype [112]. Following replication, genomic segments are packaged, and virus particles are re-coated. The host cell cytoskeleton plays a role in genome packaging; the capacity to successfully bind microtubules results in higher rates of correct packaging of “full” or “genome-containing” virions compared to “empty” or “genomeless” particles [113]. In the final step of the replication cycle, mature reovirus particles are released from cells; from this point on, the reovirus field as a whole lacks information on what happens next in the replication cycle, as investigations into the mechanism of reovirus egress have remained largely undone

for decades. Despite the wealth of literature defining steps of the reovirus replication cycle and infection, the mechanism of reovirus egress, whether lytic or nonlytic, remains unclear [10].

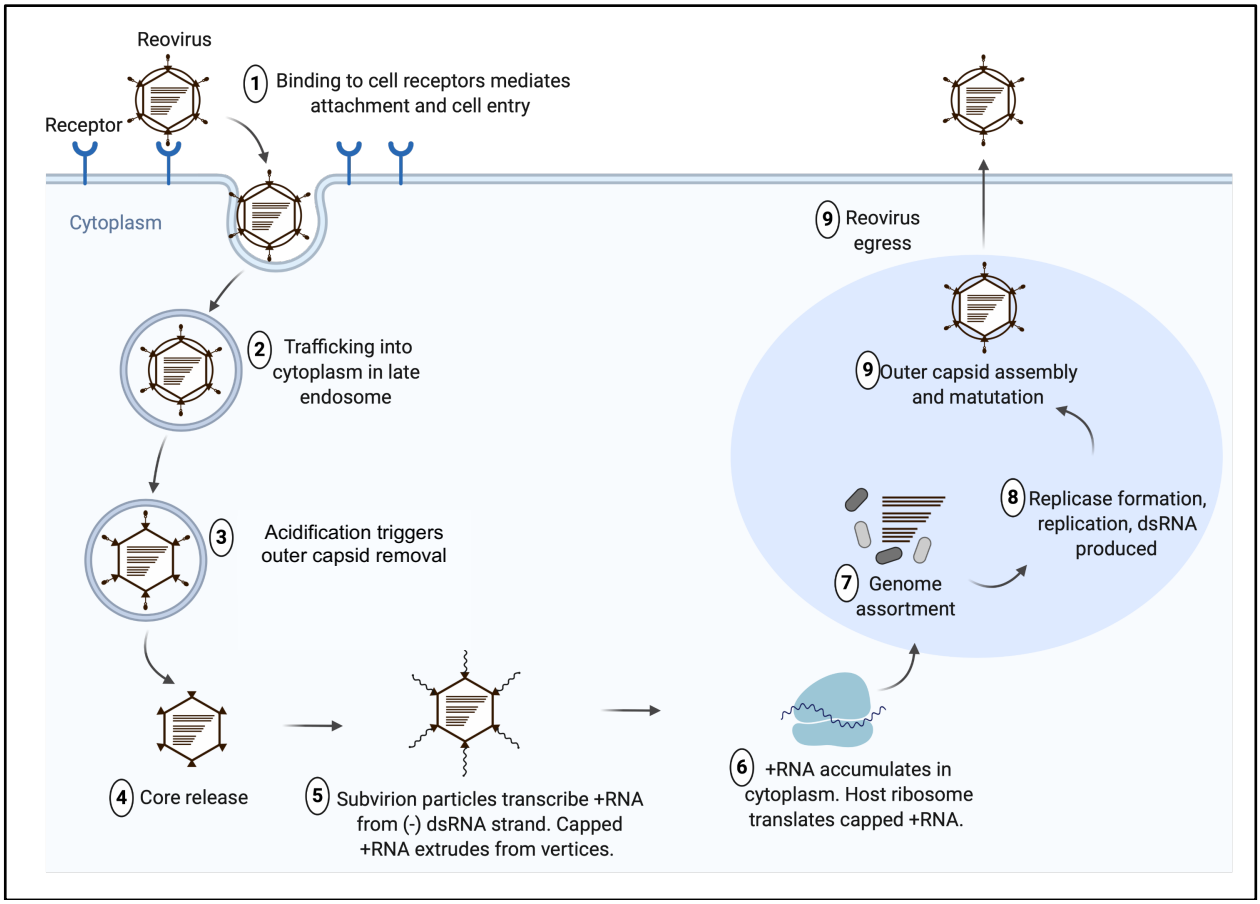

Figure 6. Reovirus replication occurs in the cytoplasm. Reovirus entry relies on interaction with specific cell surface receptors. Reovirus enters the cell via the endocytic pathway, where acidification triggers virus uncoating. The uncoated virus core is released into the cytoplasm, where transcription and translation occur. Virus replication, assembly, and maturation take place in viral replication factories. Mature virus particles egress from cells using mechanisms that are not entirely understood.

T1L and T3D reoviruses are well-documented to differ in their pathogenesis, tropism, and capacity to induce apoptosis, with T3D inducing apoptosis more efficiently than T1L [114-118]. Interestingly, there appears to be little connection between apoptosis

induction and progeny virus yield, and prior observations indicate that large quantities of infectious virus remain associated with cell debris following cell death induction[115,119,120]. Attachment, disassembly, and membrane penetration are important steps in cell death induction [102]. For T3D to induce maximum levels of apoptosis, binding of both JAM-A and sialic acid are required by the reovirus attachment protein σ1; strong cell adhesion is thought to route virus to correct endocytic compartments, where apoptosis signaling is initiated. Once T3D is uncoated, membrane penetration must occur efficiently for apoptosis induction to continue. Additionally, T3D activates NF-kB, initiator caspases, and effector caspases to a significantly higher degree than T1L [117]. Apoptosis can be elicited by mitochondrial damage via the intrinsic pathway or activation of death receptors via the extrinsic pathway, and additionally by activation of initiator and effector caspases. Reovirus interacts with the NF-kB apoptosis pathway; specifically, T3D induces NF-kB early in the infectious cycle and inhibits it later in infection. Likewise, T1L induces NF-kB early in the infectious cycle, but fails to inhibit it later in infection, leading to low amounts of apoptosis induction in T1L-infected cells. Interestingly, when NF-kB is inhibited late in infection, T1L can induce apoptosis efficiently. In a mouse model, reovirus infects M cells and then transits to Peyer's patches, where spread occurs hematogenously, in the case of T1L, or neurally, in the case of T3D. In mice, T3D infection is lethal when high viral loads in the brain are achieved, whilst T1L infection rarely is lethal. Thus, though T1L and T3D share many similar structural and genomic characteristics, key differences in their infection phenotype abound.

Four segments encode proteins that make up the reovirus outer capsid, and some of these segments strain-specifically effect reovirus replication: S1, S4, M2, and L2. The S1-encoded σ1 protein determines strain-specific tropism in a mouse model. T1L major outer-capsid proteins are readily cleaved to form the ISVP in the mouse intestine, leading to an increase in infectivity; for T3D, attachment protein σ1 is additionally cleaved during ISVP conversion, which results in substantial loss in receptor binding and infectivity in the intestine [121]. Since T3D σ1 is sensitive to proteolysis, T3D fails to spread systemically via the central nervous system in a mouse model; however, when inoculated intra-cranially, T3D replicates to high titers in the brain and induces neuronal necrosis and lethal encephalitis [122]. In contrast, T1L σ1 protein is insensitive to proteolysis, leading to high titers in the intestine, systemic spread through the central nervous system, and the induction of nonlethal hydrocephalus [102]. The S4-encoded σ3 protein regulates the efficiency of viral mRNA translation. The T1L σ3 protein is cleaved more rapidly, leading to efficient disassembly, while the T3D σ3 protein is cleaved more slowly, leading to less efficient disassembly [123]. The M2-encoded μ1 protein regulates viral virulence, and is documented to control endosomal membrane penetration efficiency. The L2-encoded λ2 protein forms the core spike, and associates with the nonstructural protein μNS. Given the evident differences in T1L and T3D interaction with host cells and their plasma membranes, and their differences in pathogenesis and spread, it is possible that their routes of egress also differ from one another. Thus, it is important to study both of these virus strains in order to gain a more complete picture of reovirus egress mechanisms and how they might differ based on reovirus's ability to interact with the host cell. When

reovirus egresses, it does so as a mature virus particle with a fully intact outer capsid coat; the four determinants described above that make up the outer capsid represent the most likely interacting partners with the host cell during reovirus egress, because it is the outer capsid that is structurally exposed to the host cell environment during the process of egress. Illuminating the reovirus determinants involved in egress mechanism(s) will offer further insight into reovirus modulation of and interaction with the host cell, and may provide uncover further strain-specific variations.

Reovirus modulation of the host cell, and further strain-specific variations

Reovirus extensively remodels cellular processes during its replication cycle (**Fig. 7**). Reovirus induces interferon expression and represses interferon signaling, a process that requires the presence of accessible viral RNA in the cytoplasm of the host cell [102]. Strain-specific differences determine the induction of interferon, with T3D inducing significantly more interferon than T1L. This phenotype has been linked to the M1, S2, and L2 gene segments, with M1 specifically driving interferon signaling repression in T1L, but not in T3D. Reovirus infection additionally facilitates autophagic machinery induction, induces alteration in the localization of and number of lysosomal compartments, de-acidified lysosomes, interacts with lysosome-derived structures, and induces major remodeling of the endoplasmic reticulum in and around virus replication factories to build these replication factories using endoplasmic reticulum-derived tubules and vesicles [106,124,125]. Furthermore, reovirus inhibits the synthesis of cell RNA and proteins, a marked change in the cellular proteome matrix which is usually noted by 8 h post reovirus infection

[126]. T3D specifically is capable of cell cycle arrest at the G2/M checkpoint to a greater extent than T1L, and this strain-specific difference segregates with the S1 gene segment [127]. Reovirus also induces the upregulation of many key cellular proteins, most notably those involved in cell growth, oxygen transport, and cell structure organization [106,124,128,129]. Like reovirus, rotavirus also modulates the host cell during its infection cycle. Specifically, rotavirus interacts with lipid rafts and remodels microfilaments, a process that has been linked to egress, and co-localizes with autophagic proteins at sites of viral replication [130,131]. Rotavirus protein interaction with specific EV biogenesis molecules prior to upregulation of EV release has been elucidated [88]. Thus, there exists precedent for another virus in the Reovirales order to interact directly with EV biogenesis molecules, and I question whether reovirus might do the same in order to promote its potential release in association with EVs. Although reovirus interaction with EV biogenesis molecules has yet to be elucidated, there are several ways in which reovirus interacts with the host cell that might intersect with its ability to interact with EV pathways.

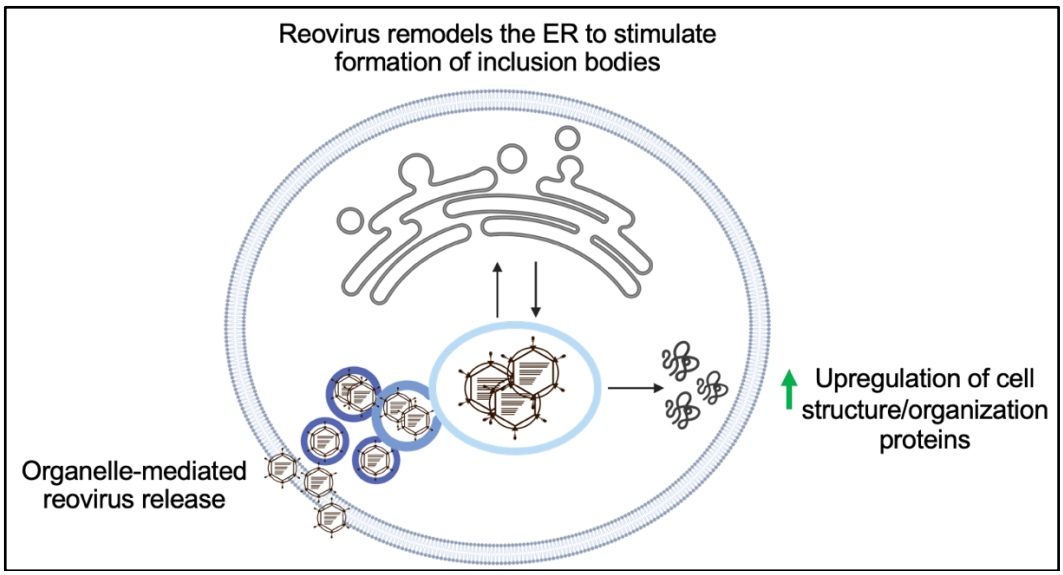

Figure 7. Reovirus extensively remodels the host cell during its infection cycle. Reovirus remodels the endoplasmic reticulum (ER), upregulates proteins involved in cell structure and protein organization, and remodels membrane-bound organelles to facilitate egress.

Precedent for a nonlytic form of reovirus egress

Historical tenets of the reovirus field have long assumed that due to its nonenveloped structure, reovirus must egress lytically, but for years reovirus egress mechanisms have remained poorly defined. Reovirus infection initiates lysis in some types of cells, including HeLa cells and Madin Darby canine kidney cells [120,132]. Reovirus lysis appears to be mediated via activation of NF-κB which in turn activates cellular apoptosis signaling [10]. However, in human brain microvascular endothelial cells (HBMECs) and in primary human airway epithelia, reovirus exits cells without inducing lysis [125,133,134]. HBMECs and primary human airway epithelia may more closely model the cells reovirus infects in animals than the immortal HeLa cell line. How, then, does reovirus exit these cells, and what is the influence of the mode of egress on downstream reovirus infection?

As noted above, precedent exists for rotavirus, a member of the order Reovirales, to undergo EV-mediated egress *in vivo* and *in vitro* [57]. Other members of the order Reovirales appear to employ nonlytic routes of egress as well. Bluetongue virus egresses via lysis and, during the early stages of infection, nonstructural protein NS3 interacts with the EV biogenesis molecule TSG101 to induce cell extrusion and subsequent budding in EVs that contain lysosome and exosome markers [54,135]. Phytoreovirus, a major agricultural pathogen, egresses in vesicular compartments [136]. Multivesicular bodies traffick to and engulf newly matured virus assemble at the periphery of the viral replication factory, and then traffick along cytoskeletal actin filaments using myosin motors. Once at the plasma membrane, the virus-containing multivesicular bodies release the virus particles via exocytosis, and the virus particles retain association with these exosome structures in the extracellular space.

A nonlytic mechanism of reovirus egress has also been described. In nonpolarized HBMEC cells, lysosome-derived membrane-bound structures termed “sorting organelles” appear to gather mature reovirus particles from cytoplasmic reovirus factories [125]. These sorting organelles carry markers of lysosomes, primarily LAMP-1, and morphologically resemble lysosomes as well. Mature reovirus particles are transported from the replication factory into the sorting organelle through specific membrane-fusion points. It appears that mature virus particles are specifically selected for loading into the sorting organelles, and the authors hypothesize that observed filaments, possibly actin-derived, may be responsible for this highly directed form of selection and tethering. Groups of

mature virus particles are then shuttled from the sorting organelle to the basal side of the plasma membrane in smaller “membranous carriers,” which fuse with the plasma membrane and then release free particles non-lytically. Thus, at least one mechanism of non-lytic reovirus egress has been elucidated in at least one cell type. I theorize that reovirus egress mechanisms may be cell-type specific, though previous studies of nonlytic egress in other cell types are highly limited. HBMECs and primary human airway epithelia may more closely model the cells reovirus infects in animals than the immortal HeLa cell line, so reovirus egress in a nonlytic fashion may be a closer model to how egress proceeds in an animal model. The question remains: is this the only non-lytic egress mechanism of which reovirus is capable?

Part VI: Summary of findings

When I began working on my dissertation, I wanted to determine how reovirus is released from infected cells, and I wanted to further understand how the mode of reovirus egress influences downstream infection of recipient cells. Using two strains of reovirus that differ in membrane disruption phenotypes and a virus I engineered to contain genetic barcodes, I provide evidence that reovirus infection enhances the release of EVs from infected cells and that infectious units of reovirus can egress from cells in association with large and medium EVs. In some cases, medium EVs can shield reovirus particles from antibody-mediated neutralization and protease degradation protection, and large and medium EVs can transmit multiple reovirus particles between cells (**Fig. 8**). Reovirus-infected medium EVs are resistant to mechanical and detergent disruption and can

withstand storage under a range of conditions. Though canonical EV markers proved heterogenous, the visual biogenesis pattern and size of reovirus-associating medium EVs may be consistent with microvesicles. In some cases, I supplement my reovirus work using a strain of rotavirus, rSA11. Overall, my work reveals mechanisms by which reovirus may escape immune system defenses and overcome cellular thresholds to infection, enhancing the likelihood of productive infection (**Fig. 8**). These findings, which enhance our field's current understanding of the effect of egress strategy on virus infection, may apply broadly to other viruses, including highly pathogenic viruses that are released in and travel in association with EVs (**Fig. 8**). Further insights into the mechanisms and effects of EV-mediated virus egress may help inform our viral vaccination strategies and delivery of viral vectors, including for oncolytic reovirus therapeutics (**Fig. 8**).

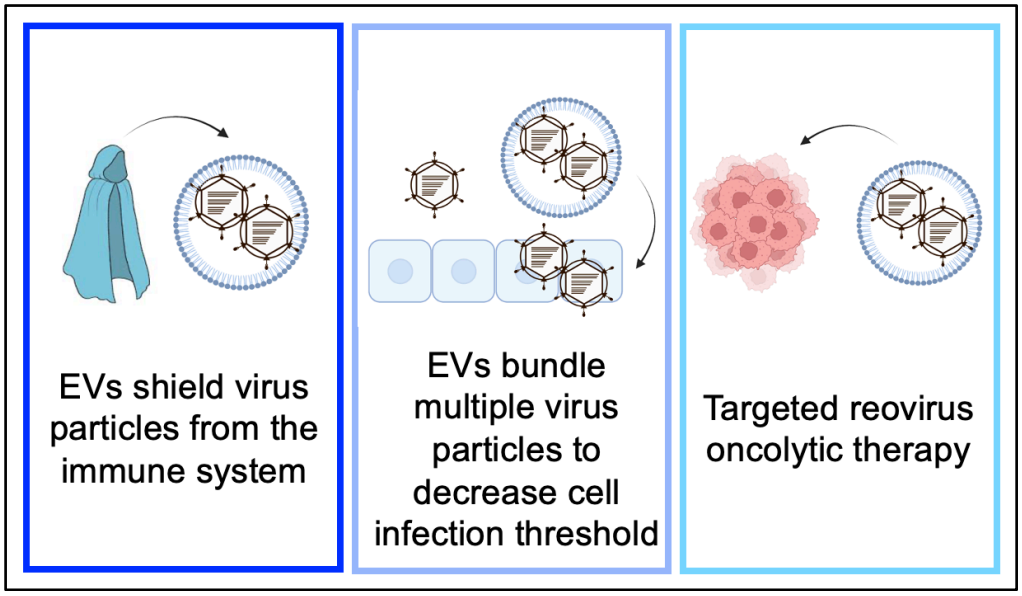

Figure 8. EV-mediated viral egress could impact public health measures. EV-mediated virus egress may affect our understanding of viral infection, including: i) EV-facilitated shielding of virus particles from the immune system, ii) EV-mediated increase in infectivity of viral particles, and iii) therapeutic targeting of EV-bundled virus particles to host sites.

CHAPTER II: REOVIRUS EGRESSES FROM INFECTED CELLS ENCLOSED IN EXTRACELLULAR VESICLES AND AS FREE VIRUS

Smith SC, Krystofiak E, Ogden KM (2024) Mammalian orthoreovirus can exit cells in extracellular vesicles. PLoS Pathog 20(1): e1011637.
https://doi.org/10.1371/journal.ppat.1011637

CO-AUTHOR CONTRIBUTIONS

Preparation and imaging of all samples for negative-stain electron microscopy and thin section transmission electron microscopy was conducted by Dr. Evan Krystofiak at Vanderbilt University. Dr. Krystofiak also assisted in large part with troubleshooting and optimizing electron microscopy-based experiments and conditions. I conducted all other work, in close intellectual collaboration with Dr. Kristen Ogden.

INTRODUCTION

The egress mechanisms of many viruses, including reovirus, remain largely understudied. In recent years, multiple viruses belonging to several families have been found capable of employing EVs as vehicles of non-lytic cellular egress from cells [9,137]. EVs are generally defined as membrane-bound structures released from cells, which remove cellular waste and function in intercellular communication by transporting

molecules such as proteins, lipids, and nucleic acids [26,138,139]. Many subpopulations of EVs have been characterized and are generally differentiated based on their cell of origin, size, composition, and cellular biogenesis pathway [16]. Although EVs are highly heterogenous, there are three broadly recognized EV categories i) small exosomes (30-150nm) which form via inward budding of inner leaflet of multivesicular bodies followed by exocytosis at the plasma membrane, ii) medium-sized microvesicles (100-1000nm) which form via outward extrusion of and budding from the plasma membrane, and iii) large apoptotic blebs (50-5000nm) which form via plasma membrane blebbing when a cell undergoes apoptosis [16,27,42,140,141]. Several markers have been defined in previous literature as being enriched in one EV subtype or another; however, because of overlap in EV markers between subtypes and because the lipid bilayer of microvesicles is derived from the plasma membrane, the exact molecular composition and thus, defining markers, are highly dependent on the parental cell. Because EVs are composed of lipid bilayers, they are generally thought to be sensitive to disruption via detergent treatment, including detergents such as sodium dodecyl sulphate (SDS), Triton X-100, Tween 20, and sodium deoxycholate (DOC) [16,142]. Depending on the category and size of EV, differences in detergent sensitivity exist; apoptotic blebs and microvesicles are overall more highly sensitive to detergent disruption than exosomes [142].

When I began working on my project, which had the primary aim of uncovering the mechanism(s) of reovirus egress, I discovered a wealth of viruses, some belonging to the same order as reovirus, which egressed in association with EVs; therefore, I wondered

whether EVs may likewise play a role in reovirus egress. Several viruses, such as BK polyomavirus, HAV, and enterovirus 71 egress in association with small exosome EVs during their egress [12,56,61,72]. Enteric viruses including bluetongue virus, poliovirus, and coxsackievirus egress in association with secretory autophagosomes, which are specialized medium EVs (300-900 nm) that form when double-membraned autophagosomes fuse with the plasma membrane to release single-membraned vesicles [14,15,48,54,143-145]. To date, the only virus known to be released in microvesicles *in vitro* and *in vivo* is rotavirus, a member of the order Reovirales that causes acute gastrointestinal infection and is a leading cause of diarrheal mortality in infants and young children in the developing world[57]. *In vivo*, EV-contained rotavirus displayed markedly increased virulence compared to free rotavirus particles, including augmented disease symptom severity and increased numbers of infected cells[57]. Furthermore, some viruses which include rotavirus, Zika virus, and Epstein-Barr virus appear to upregulate EV release, which may promote EV-mediated virus egress [88,90,146]. However, despite the multitude of discoveries made in recent years as more of an interest has been taken in the EV-virus egress field, there remain many viruses whose egress mechanisms are poorly understood, reovirus among them.

Reovirus, which serves as a focus of this dissertation, is a nonenveloped virus. Due to its nonenveloped structure, historical tenets of the field have assumed that reovirus egresses after lysing cells, but for many years, this assumption has remained unconfirmed. Two strains, T1L and T3D, differ in their ability to induce apoptosis; prior

observations provide evidence that large quantities of infectious reovirus remain associated with cell debris following cell death induction [147]. Mechanisms of reovirus egress are traditionally poorly understood. Like rotavirus and bluetongue virus, reovirus is a member of the order Reovirales which includes pathogens that cause disease in a wide range of human and animal hosts. Based on its capacity to lyse tumor cells, reovirus is currently in clinical trials as an oncolytic therapeutic [101]. Reovirus replication occurs in the cytoplasm [102]. Reovirus binds to specific cell receptors and enters cells through the endocytic pathway. Following endocytic uptake and uncoating, viral proteins accumulate in the cytoplasm and form replication factories that function as sites of particle assembly and maturation [102,106,107]. Viral replication factories are assembled by interactions of the reovirus nonstructural proteins μNS and σNS, which interact with and remodel vesicles derived from the endoplasmic reticulum[106,108]. Following replication and re-coating in the replication factory, mature reovirus particles are then released from cells either lytically or non-lytically, depending on the cell type.

Reovirus infection initiates lysis in some types of cells, including HeLa cells and Madin-Darby canine kidney cells [120,132]; however, in human brain microvascular endothelial cells (HBMECs) and in primary human airway epithelia, reovirus exits cells in the absence of lysis [125,133,134]. In HBMECs, lysosomally-derived membranous structures termed “sorting organelles” appear to gather mature reovirus particles from site of reovirus replication factories [125]. Groups of reovirus particles are then shuttled to the plasma membrane in smaller “membranous carriers,” which fuse with the plasma

membrane and release free reovirus particles non-lytically. Reovirus infection appears to upregulate the formation of sorting organelles in the host cell, and additionally appears to re-structure and re-organize their spatial location within the cell. While a non-lytic egress mechanism in one cell type has been characterized, non-lytic egress pathways in other cell types currently remain a mystery, and alternative mechanisms of nonlytic reovirus egress, including potential EV-facilitated routes of escape, have yet to be identified.

Despite the field's wealth of knowledge surrounding reovirus entry and the general reovirus replication cycle, there remains a large puzzle piece missing that must be elucidated in order for us to gain a complete picture of reovirus infection—it is currently unclear what mechanism(s) controls reovirus egress [10]. Given the multitude of other viruses that egress using EVs as nonlytic escape vehicles, including two viruses in the same order as reovirus (rotavirus and bluetongue virus), I was interested in investigating whether reovirus employs similar EV-associated egress tactics. I wondered whether membrane disruption capacity may play a role in how reovirus egresses from cells, so I employed two strains of reovirus which differ in their ability to induce cellular lysis. Studies of EV-mediated virus egress usually endeavor to identify the EV subtype with which the virus associates, typically by investigating EV size, EV biogenesis pattern, and EV markers. I wanted to discover with which specific EV subtype, if any, reovirus associates using these field-tested methods. If reovirus does associate with EVs, does that population represent infectious units of virus, does EV-mediated egress occur in more than one cell type, how stable is the interaction, and is the association a specific

encapsidation of virus or a result of non-specific virus binding to EV membranes? Furthermore, I was interested in investigating whether reovirus infection, like rotavirus and other viruses, alters EV release. Overall, with these studies, I endeavored to take a closer look at EV-reovirus egress.

RESULTS

Reovirus protein co-fractionates with EV-enriched fractions released from cells irrespective of plasma membrane integrity phenotype

Given reovirus's capacity to egress lytically in some cell types and non-lytically in others, I first questioned whether membrane disruption plays a role in how reovirus egresses from cells, so I employed two strains of reovirus, T1L and T3D. I began by evaluating the effects of T1L and T3D replication on plasma membrane integrity in murine L929 fibroblasts (L cells), which are susceptible to reovirus infection and well-documented to produce high viral yields [148]. To assess the efficiency of reovirus replication in this cell type, I adsorbed L cells with either T1L or T3D reovirus and harvested infected cell culture supernatant every 24 h for a total of 96 h. I quantified total virus titer, including both virus replicating inside of cells and virus released from cells, at each time point using a fluorescent focus assay (FFA). Although the inoculum contained identical infectious units, cell binding observed at the 0 h post infection (p.i.) timepoint appeared to vary between the two strains, as T1L titer immediately after adsorption was significantly lower than that of T3D (**Fig. 9A**). However, replication for both viruses was efficient and reached similar peak titers by 48 h p.i. and continued to replicate efficiently throughout the remainder of the timecourse. I next assessed the capacity of both reovirus strains to alter cell membrane integrity. After adsorbing L cells with T1L or T3D reovirus or medium alone

(mock), I evaluated plasma membrane disruption using trypan blue staining of cell monolayer and supernatant every 24 h for 96 h. Compared to T1L-infected and mock-infected cells, significantly higher amounts of T3D-infected cells are trypan blue positive, and nearly all cells are disrupted by 96 h p.i. (**Fig. 9B**). In contrast, at most timepoints, T1L infection yielded significantly lower levels of trypan blue-positive cells that are comparable to mock-infected cells, indicating minimal plasma membrane disruption. To complement our trypan blue staining approach, I evaluated cell cytotoxicity as a proxy for plasma membrane damage using a lactase dehydrogenase assay. Our results echoed our initial trypan blue-based approach, wherein fluorescence-based quantitation of LDH release into the supernatant of infected or mock-infected cells indicated that T3D induces significantly more cell cytotoxicity than T1L, which failed to induce more damage than mock-infected cells (**Fig. 9C**). Thus, although T1L and T3D both replicate efficiently in L cells, these strains exhibit significant differences in their capacity to disrupt cell membranes. Therefore, I suspected that these viruses may employ different egress strategies.

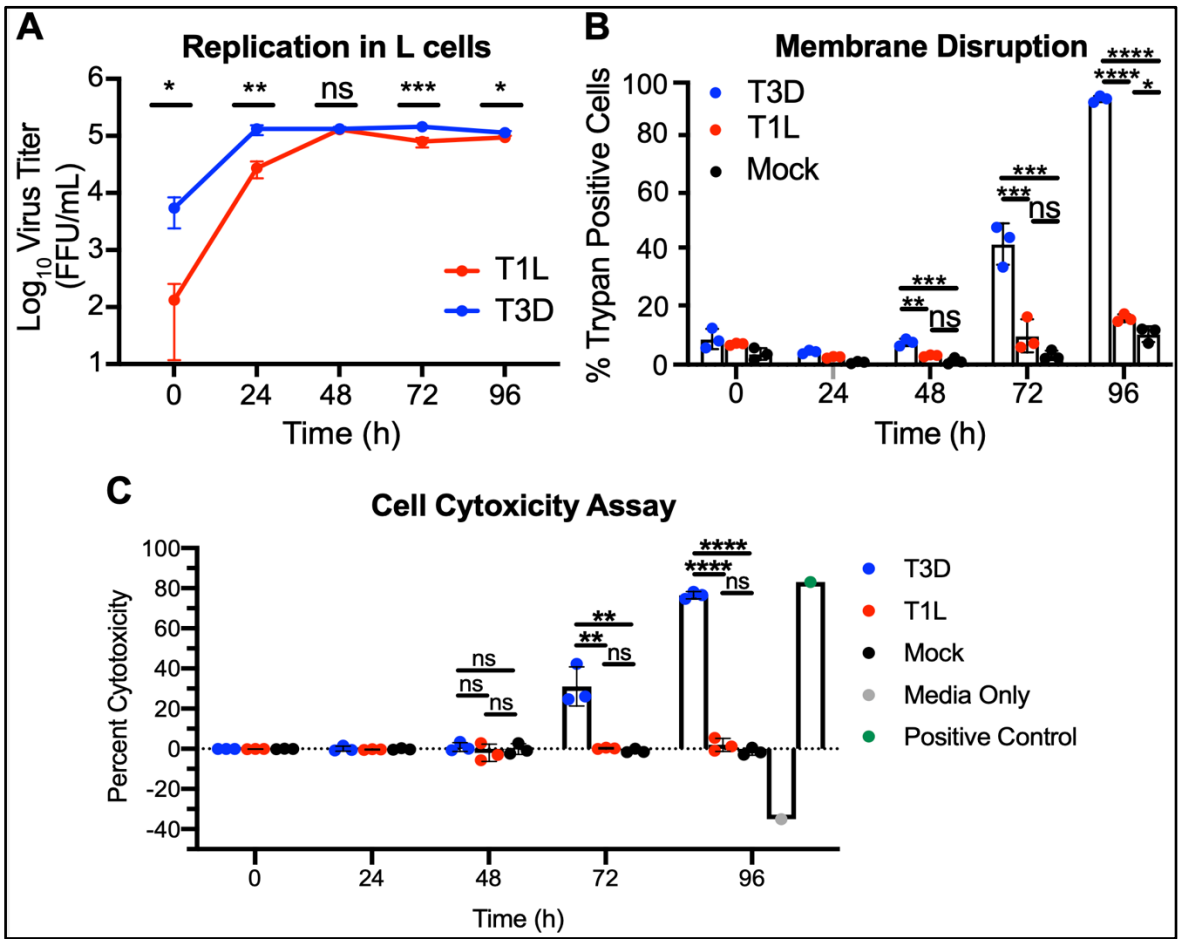

Figure 9. Despite similar replication efficiency, reovirus plasma membrane disruption is strain specific. L cells were adsorbed with three individual clones of T1L or T3D reovirus at an MOI of 1 PFU/cell. (A) Every 24 h, cell lysates were collected, and virus in the supernatant was quantified by FFA. Error bars indicate SD. $n = 3$. *, $P < 0.05$; **, $P < 0.01$; ***, $P < 0.001$ by two-sample unpaired T test. (B) Cell membrane disruption was quantified for T1L-, T3D-, and mock-infected cells every 24 h for 96 h using trypan blue staining. Error bars indicate SD. $n = 3$. *, $P < 0.05$; **, $P < 0.01$; ***, $P < 0.001$; ****, $P < 0.0001$ by one-way ANOVA with Tukey's multiple comparisons. (C) Cell membrane disruption was quantified for T1L-, T3D-, and mock-infected cells every 24 h for 96 h using an LDH assay. A media-only negative control and a kit-specific positive control quantified in triplicate at 96 h are shown. Error bars indicate SD. n = 3. **, $P < 0.01$; ****, $P < 0.0001$ by one-way ANOVA with Tukey's multiple comparisons.

Next, to evaluate how reovirus might associate with fractions that are enriched for EVs, I adsorbed L cells with T1L or T3D and used sequential differential centrifugation to fractionate EV populations. The centrifugation conditions are chosen based on EV field

specifications which are known to enrich for certain sizes of EVs; 2,000 × *g* enriches for large EVs, and 10,000 × *g* enriches for medium EVs (**Fig. 10A**) [16]. Centrifugation at 100,000 × *g* is anticipated to pellet a mixed population of small EVs and free reovirus particles [16,148]. These fractions are not "pure" populations of any one type of EV; rather, they represent an enrichment based on size and density. However, I anticipate that apoptotic blebs would primarily be enriched in the large EV fraction, microvesicles in the medium EV fraction, and exosomes in the small EV fraction [16]. Due to their size and density, free reovirus particles are not anticipated to pellet at 2,000 × *g* or 10,000 × *g* unless they are directly associated with larger structures [148]. This point will be tested directly in **Figure 14**. To determine whether reovirus protein associates with each EV-enriched fraction, I harvested infected L cell supernatant every 24 h for 96 h and used sequential centrifugation to enrich for large EV, medium EV, and small EV/free virus fractions. I resolved equal loading volumes of each sample via immunoblotting and quantified the reovirus λ3 structural protein signal associated with each fraction. I found that reovirus structural protein associated with fractions enriched for each EV size, and reovirus-EV protein association increased with infection time (**Fig. 10B-E**). By 96 h p.i., I detected T1L protein associated in approximately equivalent proportion with large EV, medium EV, and small EV/free virus fractions (**Fig. 10B-C**). Likewise, at 96 h p.i., I detected T3D protein associating approximately equivalently with medium EVs and with the small EV/free virus fraction, though T3D protein association with the large EV fraction was comparatively lower (**Fig. 10D-E**). Thus, although some strain-specific EV-reovirus protein association differences exist between both reovirus strains, overall I detect clear

association of reovirus structural protein with fractions released from infected cells that are enriched for large EVs, medium EVs, and small EVs/free virus.

Next, to determine whether the reovirus protein associated with EV fractions represented infectious reovirus, I used a plaque assay to determine the titers of T1L and T3D associated with large EV, medium EV, and small EV/free virus fractions. The 72 h p.i timepoint was chosen for this analysis because there are high amounts of detectable reovirus-EV association (**Fig. 10C, 2E**) without the near complete plasma membrane disruption induced by T3D at 96 h p.i. (**Fig. 9B-C**). Infectious reovirus was detected in all EV fractions (**Fig. 10F**). For T3D, I detected high infectious virus titers associated with fractions enriched for large EVs, medium EVs, and small EVs/free virus, with the most consistently high titers associated with large EVs (**Fig. 10F**). For T1L, infectious virus associated with fractions enriched for large EVs and medium EVs were variable and sometimes lower than those present in the small EV/free-virus fraction; in general, however, titers were high, and these noted differences were not statistically significant (**Fig. 10F**).

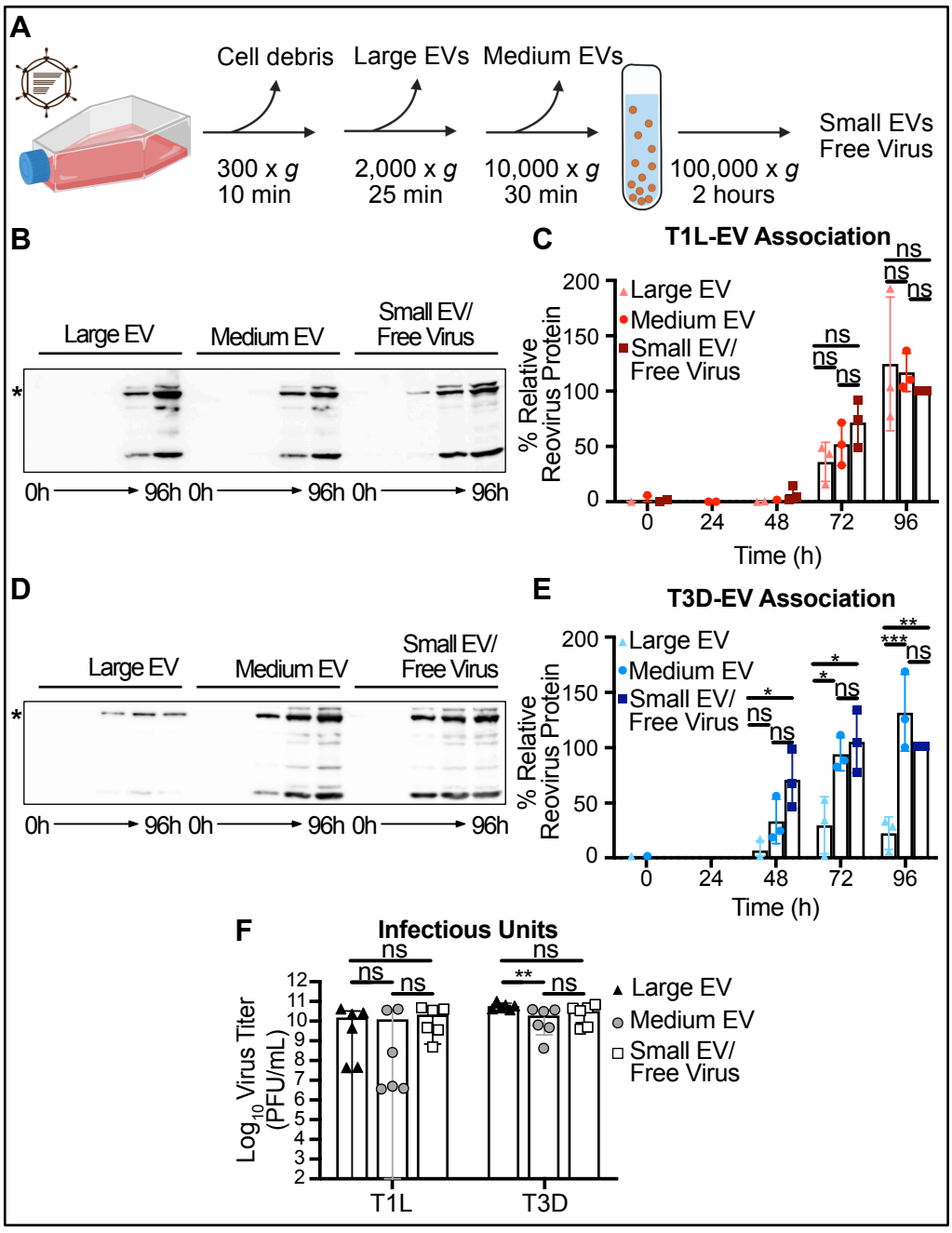
A
Cell debris
Large EVs
Medium EVs
300 x g
10 min
2,000 x g
25 min
10,000 x g
30 min
100,000 x g
2 hours
Small EVs
Free Virus
B
Large EV
Medium EV
Small EV/
Free Virus
*
0h
96h
0h
96h
0h
96h
C
T1L-EV Association
Large EV
Medium EV
Small EV/
Free Virus
% Relative
Reovirus Protein
Time (h)
ns
D
Large EV
Medium EV
Small EV/
Free Virus
*
0h
96h
0h
96h
0h
96h
E
T3D-EV Association
Large EV
Medium EV
Small EV/
Free Virus
% Relative
Reovirus Protein
Time (h)
F
Infectious Units
Log10 Virus Titer
(PFU/mL)
Large EV
Medium EV
Small EV/
Free Virus
T1L
T3D

Figure 10. Reovirus protein co-fractionates with EV-enriched fractions released from cells. L cells were adsorbed with three individual clones of T1L or T3D reovirus at an MOI of 1 PFU/cell. (A) Schematic showing the EV fraction enrichment protocol described in the text. (B-E) Infected cell supernatants were collected every 24 h for 96 h. Mock-infected supernatant was collected at 96 h, but reovirus protein was not detected. Reovirus protein association with large EV, medium EV, and small EV/free virus fractions was quantified following SDS-PAGE and immunoblotting. Representative immunoblots probed using reovirus antiserum for T1L (B) and T3D (D) and graphs showing results quantified from three independent immunoblots for T1L (C) and T3D (E) are shown. Asterisk denotes the reovirus λ3 protein band used for quantitation. Error bars indicate SD. $n = 3$. *, $P < 0.05$; ***, $P < 0.001$ by one-way ANOVA with Tukey's multiple comparisons prior to normalization. Protein signal was normalized as a percentage of maximum by dividing each adjusted volume value by the highest measured value within the blot. (F) Infected-cell supernatants were harvested at 72 h, and viral infectious units associated with each EV fraction were quantified by plaque assay. Error bars indicate SD. $n = 3$. **, $P < 0.01$ by two-way ANOVA with Tukey's multiple comparisons.

Finally, I was curious whether EVs may package entire pieces of reovirus replication factories, which exist as large cytoplasmic sites of viral replication and maturation that represent the last "step" of the replication cycle directly prior to egress. To determine whether reovirus nonstructural protein associates with each EV-enriched fraction, I harvested supernatant from infected L cells at 72 h p.i. and enriched for large EV, medium EV, and small EV/free virus fractions. I resolved equal loading volumes of each sample via immunoblotting and quantified the reovirus σNS nonstructural protein signal associated with each EV fraction (**Fig. 11A**). I observed that T1L σNS protein (**Fig. 11B**) associates only with the small EV/free virus fraction, whereas T3D σNS protein (**Fig. 11C**) associates with both the medium and large EV fractions. Thus, strain-specific differences in how reovirus protein associates with different EV fractions persist. Altogether, however, these data suggest that regardless of the capacity for reovirus to induce cell membrane disruption during infection, infectious T1L and T3D reovirus are

released from cells in association with cell-derived structures that are harvested under conditions that enrich for EVs.

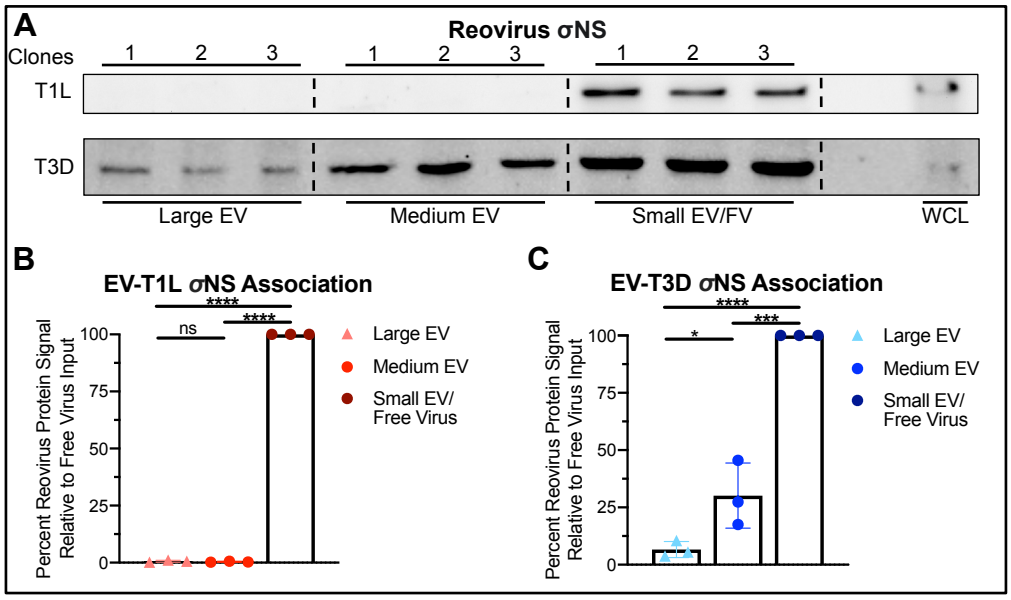

Figure 11. Reovirus nonstructural proteins associate with EV fractions in a strain-specific manner. (A-C) L cells were adsorbed with three individual clones (C1-C3) of T1L or T3D reovirus at an MOI of 1 PFU/cell for 72 h. Reovirus nonstructural protein association with large EV, medium EV, and small EV/free virus fractions was quantified following SDS-PAGE and immunoblotting (A) for T1L σNS (B) or T3D σNS (C). Error bars indicate SD. n = 3. *, $P < 0.05$; ***, $P < 0.001$; ****, $P < 0.0001$ by one-way ANOVA with Tukey's multiple comparisons prior to normalization. Protein signal was normalized as a percentage of maximum by dividing each adjusted volume value by the highest measured value for each clone within the blot.

Extracellular reovirus visually associates with large and medium EVs

To visualize the cell-derived structures with which reovirus associates, I adsorbed L cells with T1L or T3D reovirus. I harvested cell supernatants at 72 h p.i., enriched for large EVs or medium EVs by sequential centrifugation, and imaged each fraction using negative-stain transmission electron microscopy (EM). Large EV and medium EV fractions were generally enriched for the target EV size of interest but were not homogenous (**Fig. 12**). Large EVs purified from reovirus-infected cell supernatants

contained enveloped structures hundreds to more than a thousand nanometers in diameter with membranes that often appeared thin and non-uniform, potentially due to a loss of the contents within the large EVs (**Fig. 12B-C**). In some cases, the EV structures in this fraction were smaller, appeared to have thicker membranes, and formed aggregates. I observed reovirus particles measuring about 80 nm in diameter adhered to, or in some cases possibly enclosed within, these structures. In contrast, mock-infected supernatant fractions enriched for large EVs contained primarily smaller EVs (**Fig. 12A**). When I visualized medium EVs purified from supernatants of reovirus-infected cells (**Fig. 12E-F**), I observed vesicles measuring ~ 600 nm in diameter. These EVs and tended to have rounder, more uniform shapes with well-defined membranes. I observed reovirus particles associating with these medium EVs, though it was often unclear whether particles were on the interior or exterior of the EVs. I observed single viral particles, pairs of particles, and multiparticle clusters (**Fig. 12B-C, E-F**). Similar to mock-infected fractions enriched for large EVs, our mock-infected fractions enriched for medium EVs contained EVs that are smaller than those enriched from reovirus-infected cells (**Fig. 12D**). Overall, these findings suggest that centrifugation enriches for large and medium EVs, although these fractions do appear to contain at least partially heterogenous EV populations. Furthermore, T1L and T3D reovirus both associate with large and medium EVs; however, it is unclear whether the reovirus particles are bound on the exterior of the EVs or packaged internally.

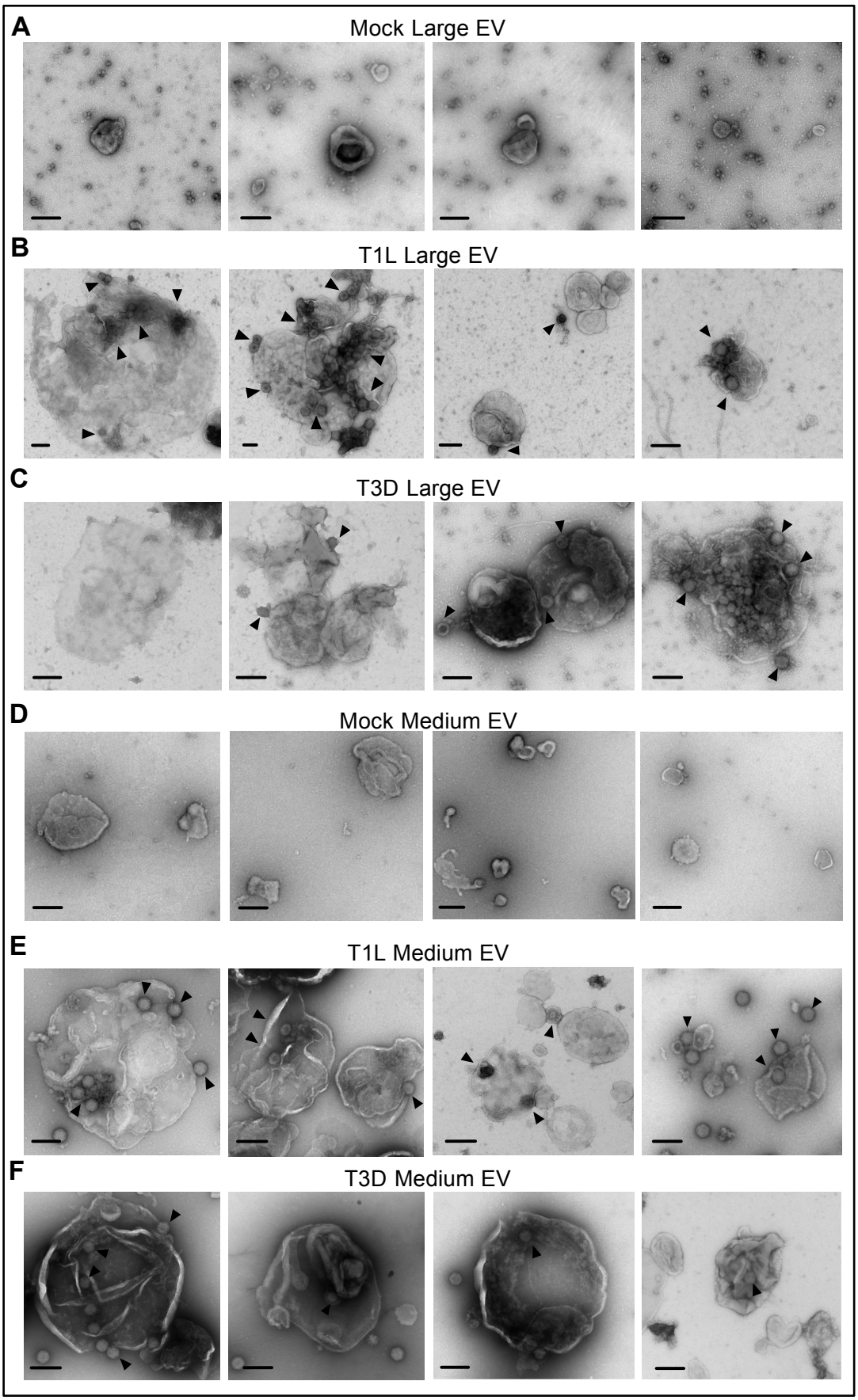
A
Mock Large EV
B
T1L Large EV
C
T3D Large EV
D
Mock Medium EV
E
T1L Medium EV
F
T3D Medium EV

Figure 12. Extracellular reovirus visually associate with large and medium EVs. L cells were adsorbed with medium alone (mock) or with reovirus strain T1L or T3D at an MOI of 1 PFU/cell for 72 h. Cell supernatants were collected and enriched by sequential centrifugation to enrich for large EVs (A-C) or medium EVs (D-F), which were visualized using negative-stain EM. Scale bars = 200 nm.

I next wanted to determine whether reovirus particles are packaged inside of EVs enriched in the medium EV fraction. To begin to address this question, I infected L cells with T1L for 72 h and harvested the medium EV fraction via centrifugation. EVs were resuspended in a fixative solution and sliced thinly to visualize a cross-section of the EVs, then imaged using transmission electron microscopy (TEM). Importantly, I observed multiple instances wherein T1L reovirus particles appeared to be contained on the interior of these medium EVs (**Fig. 13**). In some cases, I observed virus particles associating with smaller membrane-bound structures that are further contained inside the larger medium EV structures. Thus, T1L particles inside of medium EVs are potentially contained by two sets of membranes. However, some of the virus particles contained within these smaller membrane-bound structures appeared disrupted, and did not have the usual whole, round shape that I have previously observed (**Fig. 12 and 13).** Thus, based on the visual nature of the virus particles, it is difficult to determine whether the virus particles inside or outside of the smaller membrane-bound structures are those comprising the infectious EV-associated reovirus fraction that I have previously quantified (**Fig. 10F and 13**). Overall, it appears that T1L particles may be enclosed within medium EVs. Despite this interesting trend, these experiments represent only a single experiment. Further experimental optimization steps and more extensive imaging will need to be undertaken to support

these initial observations, and the question of whether or not reovirus is packaged internally will be explored and discussed in further detail in Chapter III.

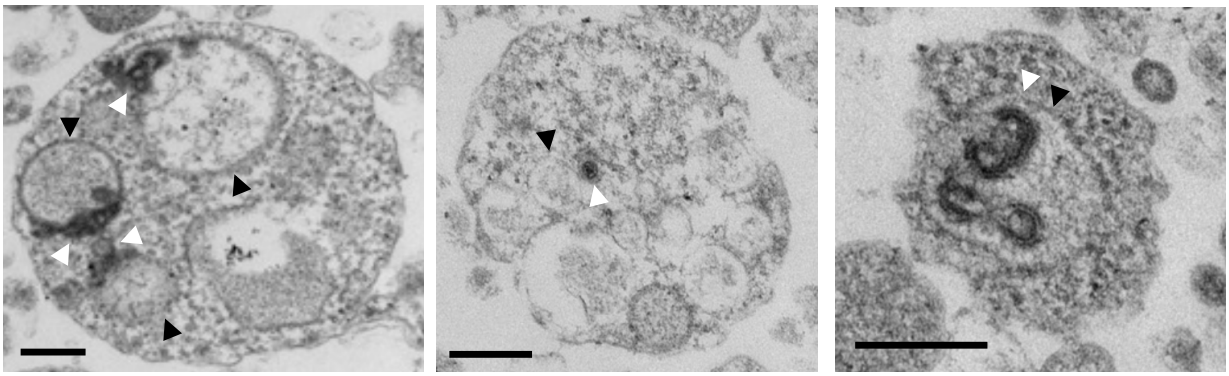

Figure 13. Cross-sectioning electron microscopy reveals interior packaging of reovirus particles. At 30hpi with T1L reovirus at an MOI of 1PFU/cell, L cells were fixed in 1% glutaraldehyde, washed thrice in PBS -/-, embedded in epoxy resin, and sectioned using a microtome set to 70nm thickness. Thin sections were then visualized using transmission electron microscopy. Black arrowheads indicate membrane-bound structures packaged inside of the EVs. White arrowheads indicate virus particles. Scale = 200nm.

Extracellular reovirus fails to associate with small EVs

I anticipated that the final step in the sequential centrifugation protocol enriched for a mixed population of small EVs and free reovirus particles. To determine whether small EVs could be separated from free reovirus particles, I infected L cells with T1L or T3D for 72 h, harvested the supernatant, and concentrated large EV-depleted and medium EV-depleted supernatant on an iodixanol cushion (**Fig. 14A**). I applied the resulting small EV/free virus pellet to an iodixanol gradient and centrifuged overnight. I collected 12 × 1 ml fractions, with fraction 1 representing the top of the gradient and fraction 12 representing the bottom of the gradient. I resolved collected fractions and immunoblotted for reovirus proteins and a protein marker of small EVs, CD81 (**Fig. 14B-**

E) [16,149]. Gradient-separated T1L-infected cell supernatants yielded a strong CD81-positive small EV signal in fractions 7-9, which was distinct from the reovirus protein signal detected in fractions 10-12 (**Fig. 14B-C**). Gradient-separated T3D-infected cell supernatants exhibited a similar phenotype; I detected CD81 in fractions 7-10 and reovirus proteins in fractions 9-12, with peak signals of each in distinct fractions (**Fig. 14D-E**). For T1L and T3D, fraction 7 contained small EVs, which resembled exosomes based on their small size and cup-shaped morphology [150,151]; I did not detect reovirus particles in this fraction (**Fig. 14F-G**). Fraction 10 contained mainly protein aggregates, with some small EVs scattered sparsely throughout (**Fig. 14H-I**). I did not detect any T1L particles in this fraction, and although I did detect T3D particles, I did not observe physical association of the reovirus particles with the small EVs. Fraction 11 contained free T1L and T3D virus particles, with no small EVs (**Fig. 14J-K**). These findings suggest that reovirus particles do not associate with small EVs, and a subset of reovirus egresses from L cells as free virus particles that fail to associate with any EV population.

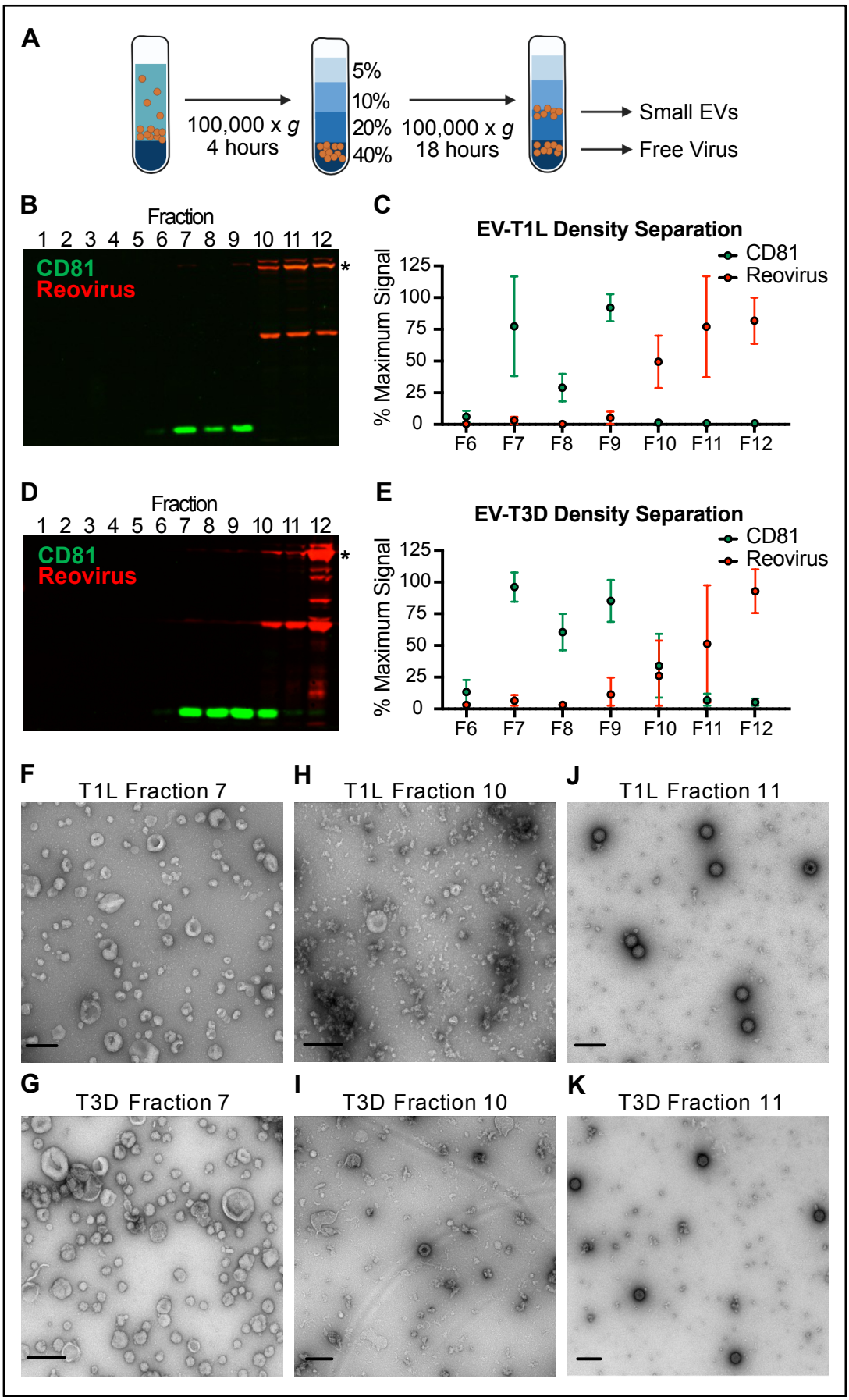
A
100,000 x g
4 hours
5%
10%
20%
40%
100,000 x g
18 hours
Small EVs
Free Virus
B
Fraction
1 2 3 4 5 6 7 8 9 10 11 12
CD81
Reovirus
*
C
EV-T1L Density Separation
CD81
Reovirus
% Maximum Signal
125
100
75
50
25
0
F6 F7 F8 F9 F10 F11 F12
D
Fraction
1 2 3 4 5 6 7 8 9 10 11 12
CD81
Reovirus
*
E
EV-T3D Density Separation
CD81
Reovirus
% Maximum Signal
125
100
75
50
25
0
F6 F7 F8 F9 F10 F11 F12
F
T1L Fraction 7
H
T1L Fraction 10
J
T1L Fraction 11
G
T3D Fraction 7
I
T3D Fraction 10
K
T3D Fraction 11

Figure 14. Extracellular reovirus particles fail to associate with small EVs. L cells were adsorbed with three individual clones of reovirus strains T1L or T3D at an MOI of 1 PFU/cell for 72 h. Cell debris, large EVs, and medium EVs were cleared from infected-cell supernatants. (A) The resulting supernatant was centrifuged on a 60% iodixanol cushion to concentrate small EVs and free virus particles. The pellet was loaded onto a 5-40% iodixanol gradient. Twelve 1-ml fractions were collected and analyzed. (B-E) T1L-infected (B-C) or T3D-infected (D-E) iodixanol gradient fractions were resolved using SDS-PAGE and immunoblotting to detect CD81 (green) and reovirus proteins (red). (B, D). Relative CD81 and reovirus protein signals in fractions 6-12 were quantified in three independent experiments. Asterisk denotes the reovirus λ3 protein band used for quantitation. (C, E). Error bars indicate SD. (F-K) Contents of fractions 7 (F, G), 10 (H, I), and 11 (J, K) were imaged using negative-stain EM. The reovirus strain used to infect the cells from which gradient-separated supernatant fractions were collected is indicated. Scale bars = 200 nm.

Extracellular reovirus association with EVs is not an artefact of spontaneous binding

I next sought to determine whether reovirus association with EVs is primarily mediated through nonspecific external adhesion. Given my prior results providing evidence against reovirus association with small EVs (**Fig. 14**), I evaluated the capacity for reovirus to associate with large EV and medium EV fractions harvested from mock-infected cells. I collected large EV and medium EV fractions from T1L-infected, T3D-infected, and mock-infected L cells at 72 h p.i. I incubated free T1L and T3D virus particles with equivalent volumes of large EVs and medium EVs harvested from mock-infected cells, or with vehicle buffer, and re-pelleted each fraction at respective centrifugation speeds. Using Coommassie blue staining, I determined that thrice the number of uninfected cells was required to yield approximately equivalent protein amounts in each uninfected EV-enriched fraction compared to reovirus-infected EV-enriched fractions (**Fig. 15A-B**). By immunoblotting for reovirus protein, I found that the amount of protein from free T1L virus and free T3D virus that spontaneously associates with uninfected large and medium EVs was markedly lower than the amount of reovirus that associates with

EVs during infection (**Fig. 15C, 14E**). Additionally, free reovirus particles did not voluntarily pellet at 2,000 × g or 10,000 × g unless associated with the EV structures that I enriched in the large and medium EV fractions (**Fig. 15C-F**). Furthermore, the spontaneous association of T1L virus with large and medium EVs from mock-infected cells was significantly lower than the free T1L virus input (**Fig. 15D**). Interestingly, although the spontaneous association of T3D virus with uninfected large and medium EVs is also significantly lower than the free T3D virus input, I do observe slightly elevated spontaneous T3D association with large and medium uninfected EVs compared to T1L (**Fig. 15F**). Thus, though strain-specific differences in the efficiency of spontaneous reovirus-EV binding do appear to exist, nonspecific virus adhesion to large and medium EVs is unlikely to fully explain the association of these particles with the EVs during egress, and I conclude that spontaneous EV association does not make up the majority of the population of egressing reovirus. Moreover, I conclude that the reovirus-EV association I detected in prior experiments appears to be a specific interaction, as the amount of reovirus that I observe that spontaneously binds to EVs is minimal compared to the reovirus that associates with EVs during the course of infection.

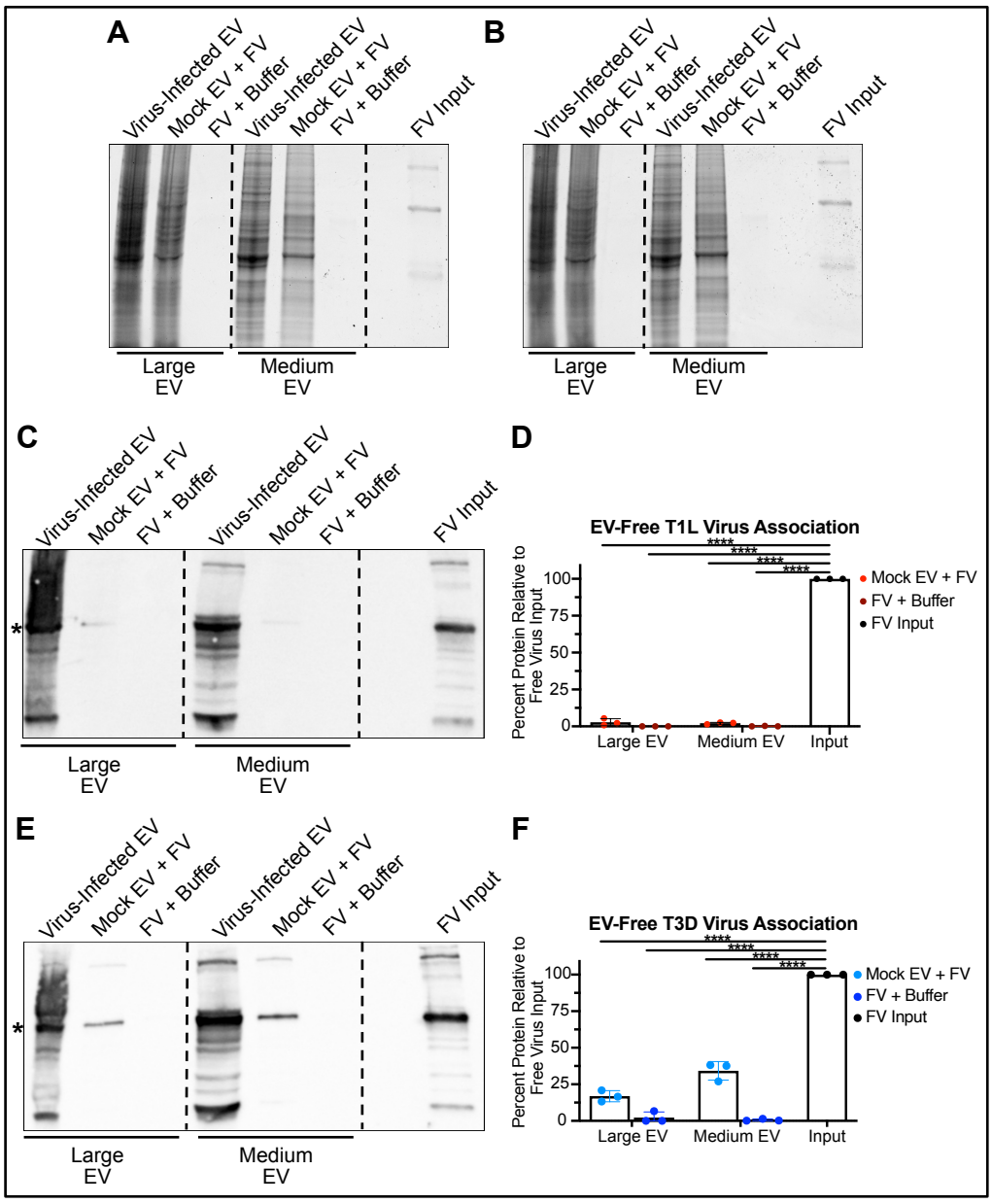
A
Virus-Infected EV
Mock EV + FV
FV + Buffer
Virus-Infected EV
Mock EV + FV
FV + Buffer
FV Input
Large EV
Medium EV
B
Virus-Infected EV
Mock EV + FV
FV + Buffer
Virus-Infected EV
Mock EV + FV
FV + Buffer
FV Input
Large EV
Medium EV
C
Virus-Infected EV
Mock EV + FV
FV + Buffer
Virus-Infected EV
Mock EV + FV
FV + Buffer
FV Input
*
Large EV
Medium EV
D
EV-Free T1L Virus Association
Percent Protein Relative to Free Virus Input
100
75
50
25
0
****
****
****
****
Mock EV + FV
FV + Buffer
FV Input
Large EV
Medium EV
Input
E
Virus-Infected EV
Mock EV + FV
FV + Buffer
Virus-Infected EV
Mock EV + FV
FV + Buffer
FV Input
*
Large EV
Medium EV
F
EV-Free T3D Virus Association
Percent Protein Relative to Free Virus Input
100
75
50
25
0
****
****
****
****
Mock EV + FV
FV + Buffer
FV Input
Large EV
Medium EV
Input

Figure 15. Reovirus fails to spontaneously associate with EVs to a significant degree. (A-F) L cells were adsorbed with three individual clones of T1L or T3D reovirus at an MOI of 1 PFU/cell. In parallel, triple the amount of L cells were adsorbed with media (mock). After 72 h, large and medium EVs were harvested via centrifugation from reovirus-infected cells to constitute the "virus-infected EV" samples and from mock-infected cells. 1×10^9 total PFU of free reovirus particles were mixed and incubated with large or medium EVs from mock-infected cells (mock EVs) or with virion storage buffer (buffer), then re-pelleted at respective centrifugation speeds. Equal volumes of all T1L (A, C, D) and T3D (B, E, F) samples were resolved by SDS-PAGE and Coomassie staining (A-B) or by SDS-PAGE with immunoblotting using anti-reovirus serum (C-F). The spontaneous association of free reovirus with mock large and medium EVs was quantified and compared to free T1L virus input (D) or free T3D virus input (F). Error bars indicate SD. n = 3. ****, $P < 0.0001$ by two-sample unpaired T test.

Medium EV populations containing reovirus are inseparable using density-dependent gradients

Due to their small size, reovirus particles will not pellet at speeds less than 100,000 × g, and should not be present in an EV fraction centrifuged at 10,000 × g unless directly associated with large EV structures (**Fig. 15**). After visualizing medium EVs associating with and potentially containing many reovirus particles (**Fig. 12 and 13),** I hypothesized that a subpopulation of reovirus-containing medium EVs may be separable from the non-virus-containing medium EV population based on a difference in density. I had prior success employing iodixanol gradients to separate populations of small EVs and free reovirus particles based on density (**Fig. 14**). Thus, I employed an iodixanol gradient-based method, wherein the concentrated medium EV fraction was layered atop a discontinuous gradient of iodixanol concentrations ranging from 20%-40% to separate different medium EV populations based on density (**Fig. 16A**) [152]. I then collected a total of 24 × 0.5 ml fractions, with fraction 1 representing the top of the gradient and fraction 24 representing the bottom of the gradient. I quantified the reovirus protein association

with each harvested iodixanol fraction by immunoblotting for reovirus signal (red) and for medium EV signal (green) (**Fig. 16B**). I observed that the medium EV signal was spread throughout all fractions, with the highest signal contained in Fraction 21. This observation indicates that within the medium EV-enriched fraction, there is a wide range of EV densities. Thus, the medium EV-enriched fraction likely contains a heterogenous population. However, this density-dependent separation method was not successful in separating a reovirus-containing EV fraction from the rest of the medium EV population, as I detected reovirus protein in all fractions. Thus, further experimentation is needed to identify methods to separate out a reovirus-associating medium EV fraction.

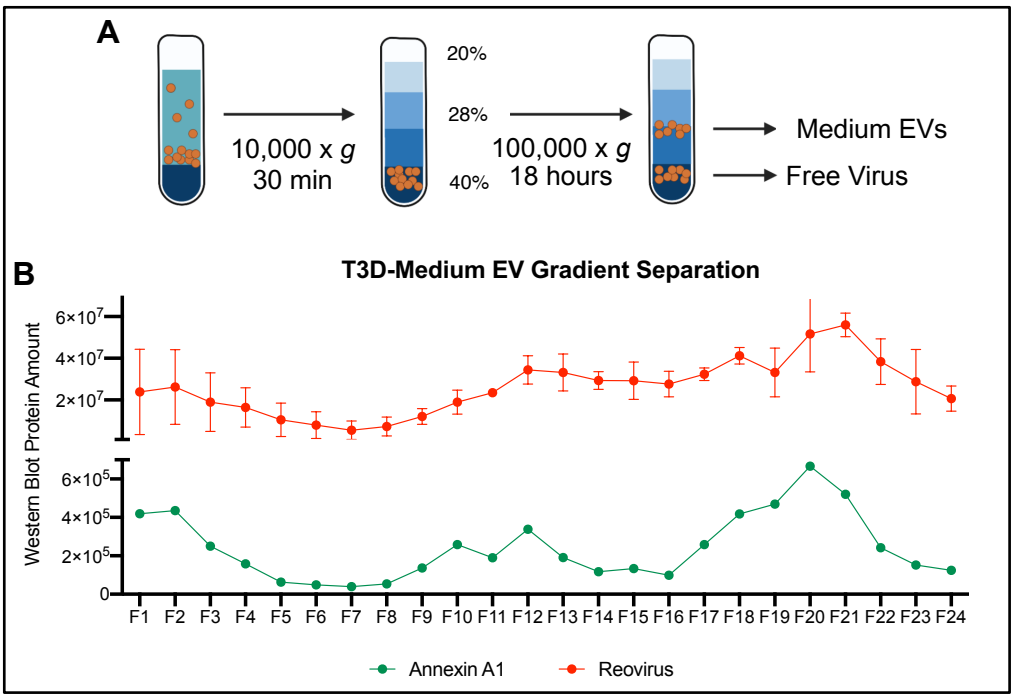

Figure 16. Subpopulations of reovirus-filled EVs are not divisible using density-dependent gradient centrifugation. (A) L cells were adsorbed with T3D at an MOI of 1 PFU/cell. After 72 h, the indicated centrifugation steps were used to pellet medium EVs on an iodixanol cushion. The resulting medium EV pellet was moved to a new ultracentrifuge tube, and then a 20-40% discontinuous iodixanol gradient was layered on top. A total of 24 × 0.5ml fractions were harvested to separate medium EV subpopulations. (B) Iodixanol gradient fractions were resolved via SDS-PAGE and immunoblotting using polyclonal anti-reovirus serum (red) and monoclonal annexinA1 antibody (green).

Medium EVs are resistant to mechanical and detergent stressors

I next sought to assess the stability of virus association with medium EVs. I chose to investigate medium EVs because I had previously observed reovirus particles present inside of this EV fraction, and additionally, rotavirus has been documented as being packaged inside of this EV fraction (**Fig. 13**) [57]. I began by focusing on whether various detergents disrupt infected medium EVs. I used both ionic and nonionic detergents which have been previously published to disrupt EVs; detergent-treated virus-infected EVs are often used in the virus-EV field as a "free virus" control, and I wanted to determine whether

detergent treatment would yield another, more easily-obtained free virus fraction to use as a control in my experiments. Given that microvesicles are more susceptible to detergent-based disruption, and that SDS and Triton X-100 were shown to be more effective at lysing EVs at lower concentrations compared to DOC or Tween 20, I hypothesized that either SDS or Triton X-100 would disrupt the medium EV fraction, as evidenced by a loss in reovirus association with medium EVs after detergent treatment, because reovirus will not pellet in significant quantities unless associated with a larger EV structure (**Fig. 15**) [142]. I treated medium EVs harvested from T1L- and T3D-infected L cells with increasing concentrations of SDS, DOC, Triton X-100, and Tween 20 detergent for 30 min at room temperature, and then re-harvested remaining medium EVs via centrifugation. I observed that under the conditions tested, T1L and T3D association was lost following SDS treatment, but not DOC, Triton X-100, and Tween 20 disruption (**Fig. 17A-B**). It is surprising that these EVs remain stable against three out of four tested detergents [81]. Previous literature did provide evidence that, depending on the cell type, EV disruption resilience against certain concentrations of detergents varied based on cell type; perhaps EVs released from L cells are unexpectedly stable, and can withstand unusually high amounts of certain detergents, but are susceptible to SDS [142].

I next focused on the stability of virus association with medium EVs following mechanical disruption and various storage conditions. I was interested in investigating mechanical disruptors and storage-based stressors that closely mirror experimental conditions routinely used field-wide in the study of reovirus, and therefore I included

conditions such as freeze-thawing, sonication, and storage at 4◦C and -80◦C [148]. As a comparator for T3D-infected medium EVs, I used rotavirus-infected EVs, which have been previously found to be environmentally stable [81]. Given the resilience of rotavirus-associated medium EVs against environmental stressors, I hypothesized that reovirus-associated medium EVs would likewise be fairly resistant against mechanical disruption and storage conditions. I found that, compared to EVs left untreated, rSA11 association with medium EVs was resistant to freezing and thawing and short periods of sonication, but was sensitive to treatments involving long sonication periods, though these differences were not statistically significant (**Fig. 17C**). In contrast, T3D association with medium EVs was resistant to all mechanical treatment conditions (**Fig. 17C**). Additionally, association of both rSA11 and T3Dwith medium EVs withstood a range of short- and long-term storage conditions without exhibiting notable loss (**Fig. 17D**). Thus, it appears that reovirus and rotavirus association with medium EVs is quite stable against mechanical and temperature/storage stressors. Therefore, my earlier hypothesis, based on prior literature, that virus association with medium EVs would not be markedly disrupted by mechanical disruption and storage was supported [81].

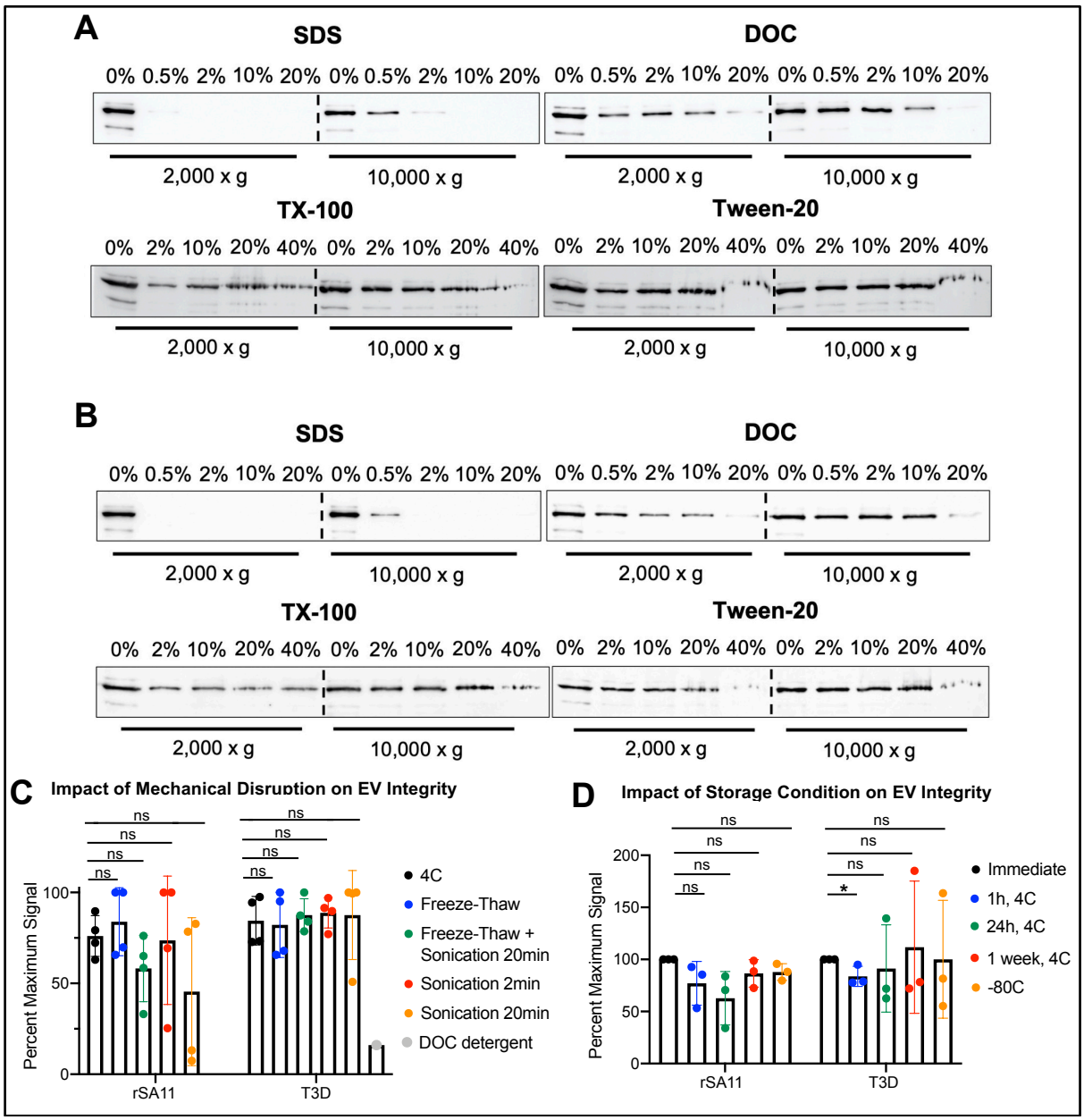
A
SDS
DOC
0% 0.5% 2% 10% 20% 0% 0.5% 2% 10% 20%
0% 0.5% 2% 10% 20% 0% 0.5% 2% 10% 20%
2,000 x g
10,000 x g
2,000 x g
10,000 x g
TX-100
Tween-20
0% 2% 10% 20% 40% 0% 2% 10% 20% 40%
0% 2% 10% 20% 40% 0% 2% 10% 20% 40%
2,000 x g
10,000 x g
2,000 x g
10,000 x g
B
SDS
DOC
0% 0.5% 2% 10% 20% 0% 0.5% 2% 10% 20%
0% 0.5% 2% 10% 20% 0% 0.5% 2% 10% 20%
2,000 x g
10,000 x g
2,000 x g
10,000 x g
TX-100
Tween-20
0% 2% 10% 20% 40% 0% 2% 10% 20% 40%
0% 2% 10% 20% 40% 0% 2% 10% 20% 40%
2,000 x g
10,000 x g
2,000 x g
10,000 x g
C
Impact of Mechanical Disruption on EV Integrity
Percent Maximum Signal
100
50
0
ns
rSA11
T3D
4C
Freeze-Thaw
Freeze-Thaw + Sonication 20min
Sonication 2min
Sonication 20min
DOC detergent
D
Impact of Storage Condition on EV Integrity
Percent Maximum Signal
200
150
100
50
0
ns
*
rSA11
T3D
Immediate
1h, 4C
24h, 4C
1 week, 4C
-80C

Figure 17. Medium EVs are resistant to mechanical and detergent treatment. (A-B) L cells were adsorbed with three individual clones of T1L or T3D reovirus at an MOI of 1 PFU/cell. Medium EVs harvested via centrifugation from T1L-infected (A) and T3D-infected (B) cell supernatants were mock-treated with media or treated with increasing concentrations of SDS, DOC, Triton X-100, or Tween-20 detergent for 30 min at room temperature. EVs were re-harvested via centrifugation, and reovirus association with each fraction was quantified via SDS-PAGE and immunoblotting using anti-reovirus serum. (C-D) L cells were adsorbed with three individual clones of T3D reovirus at an MOI of 1 PFU/cell. Caco-2 cells were adsorbed with three individual clones of rSA11 rotavirus at an MOI of 0.01 PFU/cell. Medium EVs harvested via centrifugation from T3D-infected or rSA11-infected cell supernatants were split into equivalent volumes and each sample was subjected to a range of mechanical and detergent treatments. (C) Medium EVs were stored at 4°C while treatments took place, including i) two (T3D) or three (rSA11) freeze-thaw cycles, ii) freeze-thaw plus sonication for 20 min, or iii) sonication for either 2 min or 20 min. As a control, T3D medium EVs were additionally treated with 20% DOC detergent for 30 min at room temperature. After treatment, medium EVs were re-harvested via centrifugation, and reovirus-EV association was measured using SDS-PAGE and immunoblotting with anti-reovirus serum. ns, not significant by two-sample paired T test. Error bars indicate SD, n = 4. (D) One aliquot of medium EVs was centrifuged immediately upon collection. The remaining aliquots of medium EVs were subjected to different temperature and time-dependent storage conditions, including i) 4°C for 1h, ii) 4°C for 24h, iii) 4°C for 1 week, or iv) -80°C storage for 1 week. After storage, medium EVs were re-harvested via centrifugation, and reovirus-EV association was measured using SDS-PAGE and immunoblotting with anti-reovirus serum. *, $P < 0.05$ by two-sample paired T test. Error bars indicate SD, n = 3.

EV-associated reovirus subpopulations are of unknown marker origin, but visually egress like microvesicles

To begin understanding the cellular origin of the EVs that reovirus associates with, I assessed the markers that define the large EV, medium EV, and small EV populations harvested from T1L-infected and T3D-infected L cells. I selected markers that are widely used in the EV literature to define microvesicles (medium EVs), exosomes (small EVs), and autophagosomes (large-to-medium EVs). I enriched large EVs, medium EVs, and small EVs/free virus using centrifugation and resolved the resulting samples using SDS-PAGE and immunoblotting to detect reovirus protein or EV protein markers. I volume-

matched samples (left panel) or protein-matched samples (middle panel) and compared to mock-infected whole cell lysate (right panel). Interestingly, no one marker or group of markers successfully defined any EV population, and there were no clear differences between T1L-infected EVs and T3D-infected EVs (**Fig. 18**). Markers that, according to literature, are enriched for one EV population or another were instead heterogenous in the L cell-derived EVs **(Fig. 18)**. For example, the large EV fraction, which I would expect to be enriched for apoptotic blebs, contained strong microvesicle (ANXA1), exosome (CD81), and autophagosome (LC3A/B) markers. Based on the prevalence of the autophagosome marker LC3A/B in the large EV fraction, I hypothesize that most secretory autophagosomes are enriched in the large EV fraction [15]. The medium EV fraction, which I would expect to contain microvesicles, contained mostly faint markers; of these, the strongest signal populating this fraction was microvesicle (ANXA1), and exosome (TSG101 and ALIX). The small EV fraction, which I would expect to contain exosomes, was mostly populated by exosome markers (CD81, TSG101, ALIX). The small EV fraction was, however, additionally populated with autophagosome marker LC3A/B. I hypothesize that this heterogeneity is due to cell origin, as EV markers are highly dependent on their parental cell and widely acknowledged in EV literature to be heterogenous between EV subpopulations, and to date there has been no prior literature that has defined EV markers originating from L929 murine fibroblast cells. Thus, these selected common EV markers may not be appropriate for defining these L cell-derived EV fractions.

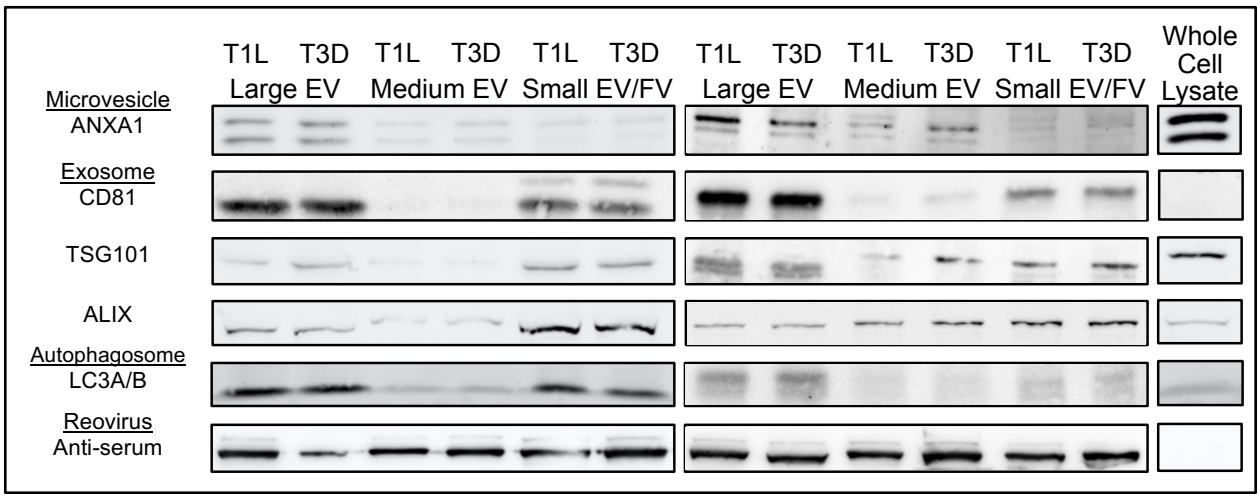

Figure 18. Reovirus-associated EV types are unclear based on marker differentiation. L cells were adsorbed with medium alone (whole cell lysate) or with T1L or T3D reovirus at an MOI of 1 PFU/cell. At 96 h p.i., cell monolayers were lysed to make whole cell lysate, or cell supernatants were enriched for large EV, medium EV, and small EV/free virus fractions. Equal loading volumes (left) or equal sample protein amounts (right) were resolved by SDS-PAGE and immunoblotted using antibodies targeting protein markers of microvesicles (ANXA1), exosomes (CD81, TSG101, ALIX), and autophagosomes (LC3A/B), or reovirus proteins.

Based on the heterogeneity of the EV marker data above, I next wanted to employ an alternative method to gain a better understanding the cellular origin of the EV subpopulation with which reovirus egresses. I decided to visualize the point of reovirus egress; if reovirus egresses in association with microvesicles, I would expect to see distinct protrusion or “budding” of the plasma membrane. If reovirus egresses in association with apoptotic blebs, I would expect to see evidence of larger-scale cell blebbing as the cell underwent apoptosis. To visualize T1L and T3D egress from cells, I adsorbed L cells with T1L or T3D reovirus, and visualized a thin cross-section of the whole cell monolayer using TEM imaging. In rare occurrences, I detected single T1L or T3D particles associating with plasma membrane structures that appeared to be budding outwards (**Fig 19A-B**). I observed T1L or T3D virus particles present as single particles,

pairs of particles, or clusters of multiple particles present in association with, and potentially packaged inside of, EV-like structures that are distinct but proximal to the plasma membrane (**Fig 19A-B**). These EV-like structures ranged in diameter from ~ 400 nm to ~ 600 nm, which is similar to the size of microvesicles. I additionally used confocal microscopy to visualize how T1L and T3D egress from cells. I stained infected and mock-infected L cells to visualize cell nuclei, reovirus protein, and cell membrane. Mock-infected cells reveal that our anti-reovirus antibody is not cross-reactive with cell structures and is specific for reovirus protein only (**Fig 19E**). Similar to the phenotype observed for T1L using thin-section TEM, confocal microscopy reveals that T1L and T3D visually appear to bud from the plasma membrane surface in association with plasma membrane-stained EVs (**Fig 19C-D**). Thus, the phenotype of at least one mechanism of reovirus egress appears consistent with the biogenesis of microvesicles, which bud outward from the plasma membrane prior to pinching-off and release [26,27,141]. Further confocal microscopy and thin-section TEM imaging must be conducted to confirm these initial observations.

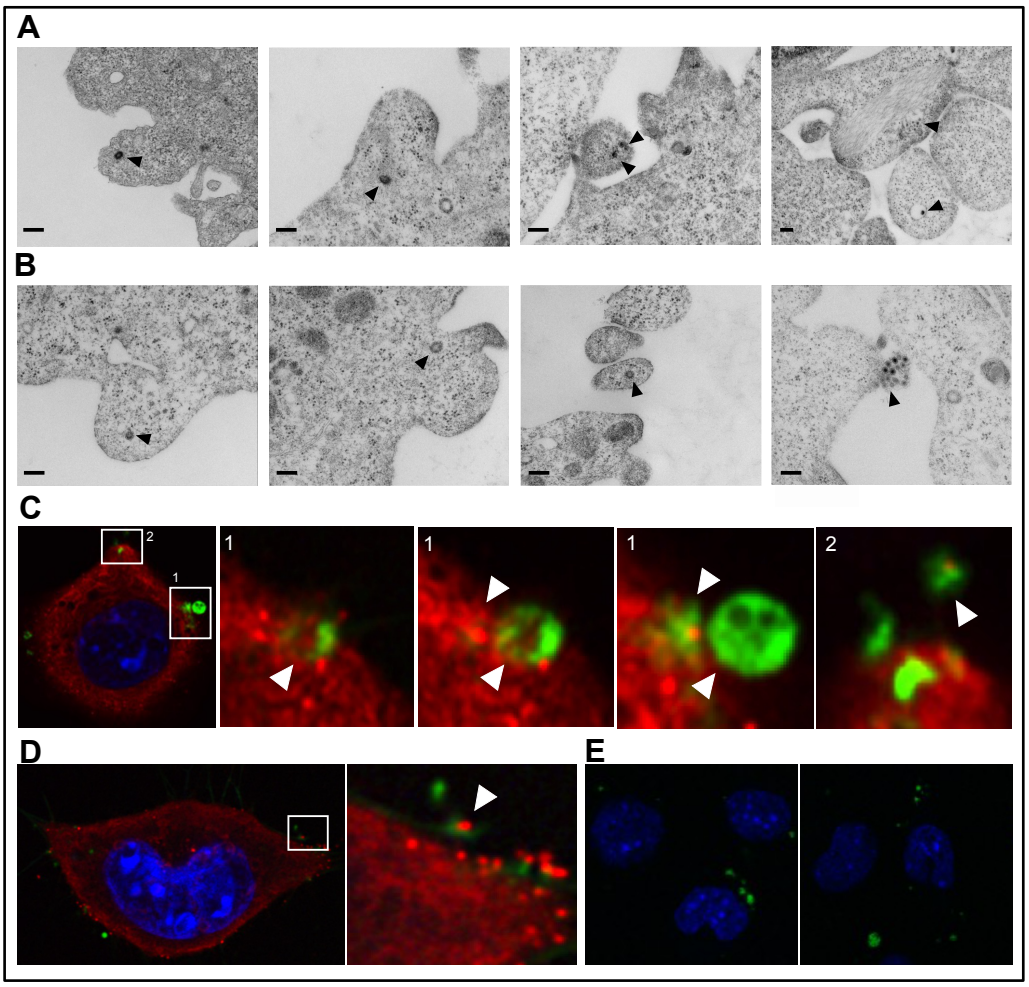

Figure 19. EV-mediated reovirus egress is potentially consistent with microvesicle biogenesis. (A-B) TEM of T1L-infected (A) or T3D-infected (B) L cells at 24 h p.i. Arrows point to viral particles observed near membrane-bound structures budding from the plasma membrane in or around cells. Scale bar = 200 nm. (C-E) L cells were grown to confluency on 1 mm glass coverslips. At 72 h p.i., T1L-infected (C), T3D-infected (D), and mock-infected (E) L cells were stained for plasma membrane (green, CellBrite 488), reovirus protein (red, polyclonal anti-reovirus serum), and cell nucleus (blue, DAPI). Stained samples were subjected to airyscan Z-stack imaging using the Zeiss LSM 880 confocal microscope. Inset 1 of panel (C) indicates several Z-stack layers of the same area of the cell, taken from bottom to top. White triangles indicate areas of reovirus (red) and plasma membrane-derived vesicle (green) colocalization.

EV-mediated reovirus egress occurs in more than one cell type

To investigate whether EV-mediated reovirus egress occurs in cell types other than murine L929 fibroblasts, I used non-polarized human colon epithelial Caco-2 cells, which

more closely resemble the intestinal epithelial cells reovirus infects in mammals [102]. I compared titers of T1L and T3D following infection of Caco-2 cells to those following infection of L cells during a time course of infection (**Fig. 20A-B**). Although T1L replicated significantly less efficiently in Caco-2 cells at an MOI of 5 PFU/cell than in L cells at an MOI of 1 PFU/cell, T1L titer increased throughout the time course by more than 500-fold (**Fig. 20A**); T3D replication in Caco-2 cells and L cells was comparable (**Fig. 20B**). Following infection of Caco-2 cells, plasma membrane disruption and cell cytotoxicity phenotypes for both viruses were similar to what I observed in L cells, with T3D inducing significantly higher levels of membrane disruption compared to T1L (**Fig. 20C-D**). Thus, both strains of reovirus appear to replicate efficiently and display the same plasma membrane disruption phenotypes in both L cells and Caco-2 cells.

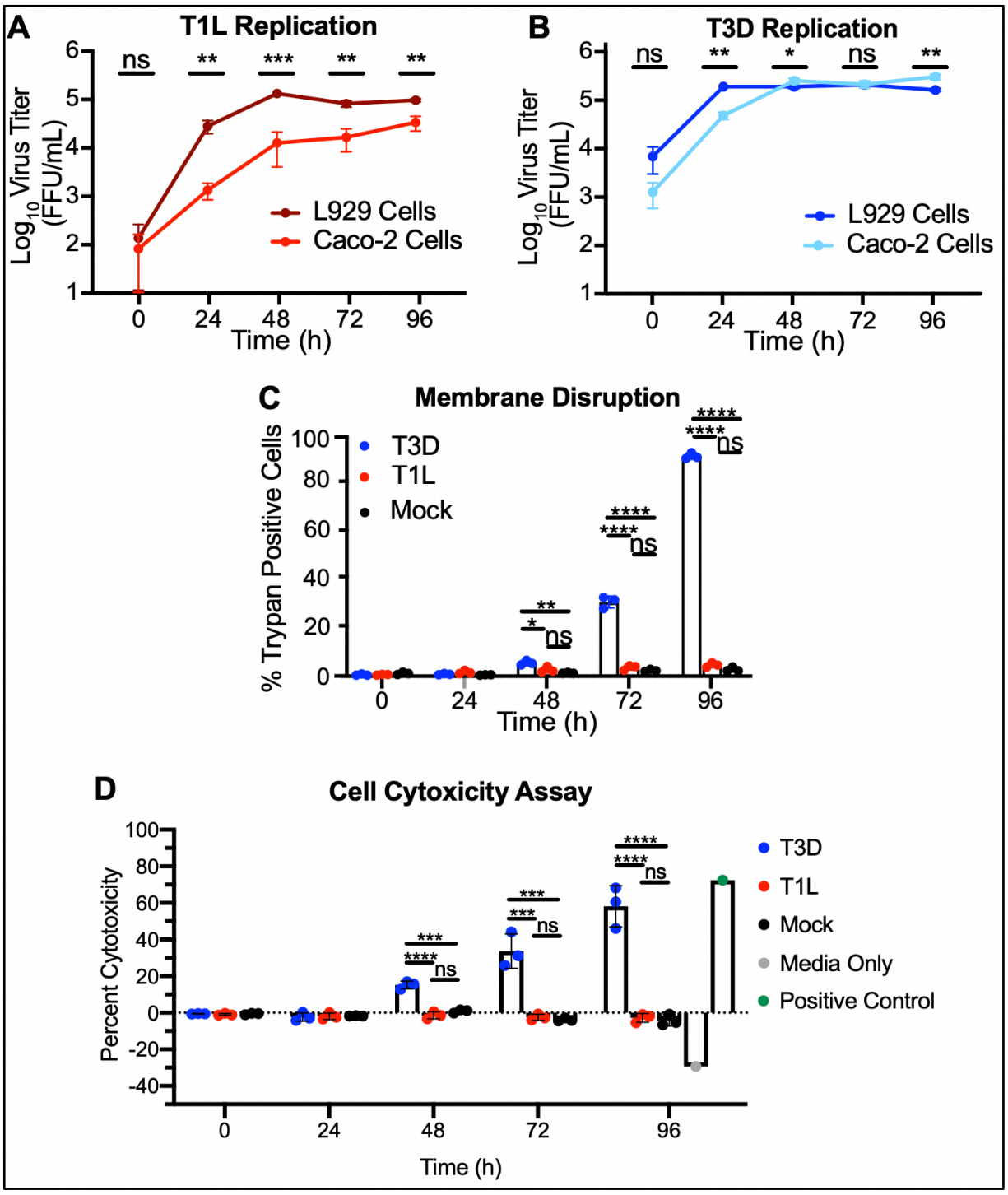
A
T1L Replication
Log10 Virus Titer (FFU/mL)
ns
**
***
**
**
L929 Cells
Caco-2 Cells
Time (h)
B
T3D Replication
Log10 Virus Titer (FFU/mL)
ns
**
*
ns
**
L929 Cells
Caco-2 Cells
Time (h)
C
Membrane Disruption
% Trypan Positive Cells
T3D
T1L
Mock
Time (h)
D
Cell Cytoxicity Assay
Percent Cytotoxicity
T3D
T1L
Mock
Media Only
Positive Control
Time (h)

Figure 20. Reovirus replication efficiency and plasma membrane disruption capacity is similar in a different cell type. (A-B) Caco-2 cells were infected with three individual clones of T1L (A) or T3D (B) at an MOI of 5 PFU/cell (Caco-2), as quantified in L cells. At the indicated timepoints, cell lysate was collected, and virus titers were determined by FFA. Results for T1L or T3D infection of L cells at an MOI of 1 PFU/cell are duplicated from **Fig. 1A** for ease of comparison. Error bars indicate SD. $n = 3$. *, $P < 0.05$; **, $P < 0.01$; ***, $P < 0.001$ by two-sample unpaired T test. (C) Caco-2 cells were adsorbed with three individual clones each of reovirus strains T1L or T3D at an MOI of 5 PFU/cell. Cell membrane disruption was quantified for T1L-, T3D-, and mock-infected cells every 24 h for 96 h using trypan blue staining. Error bars indicate SD. $n = 3$. *, $P < 0.05$; **, $P < 0.01$; ****, $P < 0.0001$ by one-way ANOVA with Tukey's multiple comparisons. (D) Caco-2 cells were adsorbed with media (mock) or with three individual clones of T1L or T3D reovirus at an MOI of 5 PFU/cell. Cell membrane disruption was quantified for T1L-, T3D-, and mock-infected cells every 24 h for 96 h using an LDH assay. A media-only negative control and a kit-specific positive control quantified in triplicate at 96 h are shown. Error bars indicate SD. n = 3. ***, $P < 0.001$; ****, $P < 0.0001$ by one-way ANOVA with Tukey's multiple comparisons.

Next, I investigated the association of reovirus structural and nonstructural protein with each EV fraction. I observed that while T1L protein association was equivalent among all fractions in L cells, T1L protein association with Caco-2-derived medium EV fractions was significantly less relative to small EV/free virus fractions (**Figs. 10C and 21A**). While T3D structural protein association with large EV fractions from L cells was significantly lower relative to the medium EV and small EV/free virus fractions, T3D protein association with all Caco-2-derived EV-enriched fractions was generally equivalent **(Figs. 10E and 21B**). Similar to observations with L cells, infectious reovirus was associated with all EV fractions released from Caco-2 cells (**Fig. 21C**). In most cases, the distribution of infectious virus titer associated with each fraction was roughly equivalent for a given virus, though significantly lower for T1L with the medium EV fraction. In contrast with the strain-specific phenotype I previously observed in L cells, neither T1L or T3D nonstructural protein σNS appeared to associate with any EV fraction derived from

Caco-2 cells (**Fig. 11 and 21D**)**.** Overall, I observed infectious reovirus association with EVs released from murine L cells and human Caco-2 cells, suggesting that this mechanism of EV-mediated reovirus egress is not unique to L cells and can occur in multiple cell types.

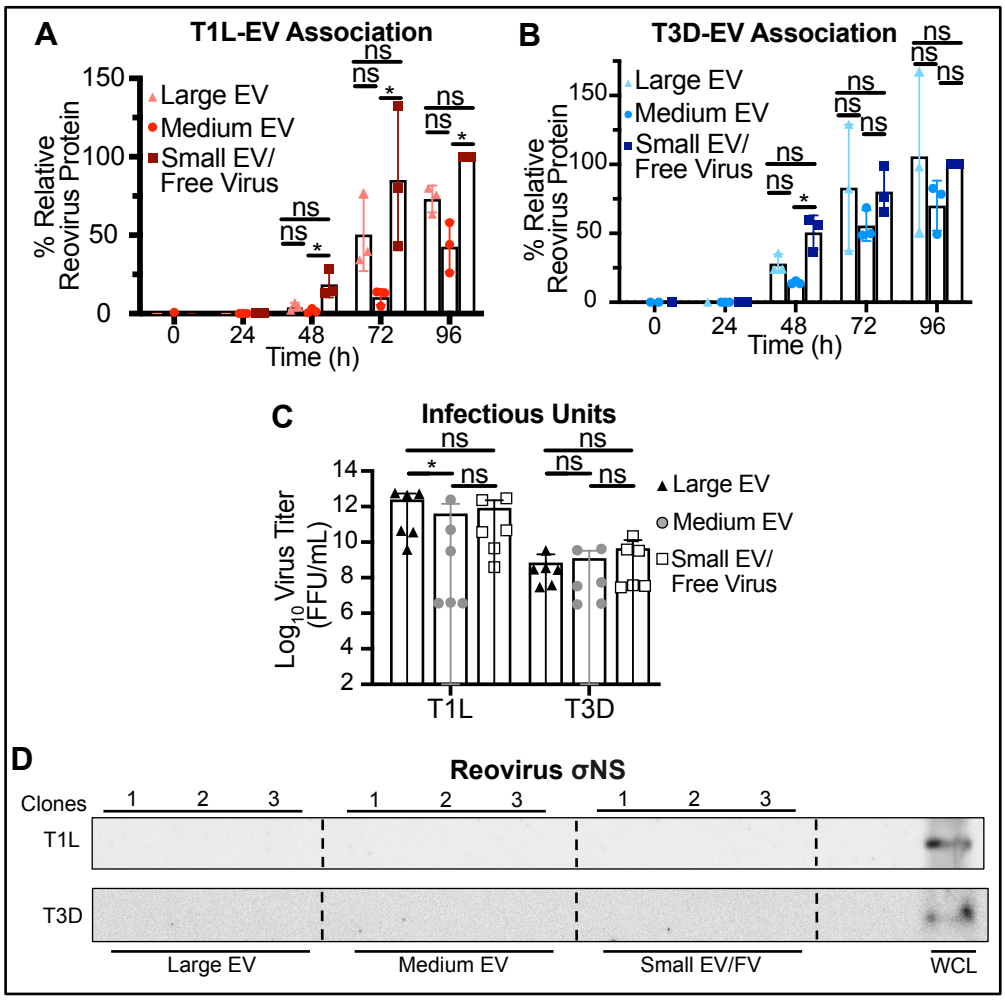

Figure 21. EV-mediated reovirus egress occurs in multiple cell types, but reovirus nonstructural protein association with EV fractions is cell type dependent. (A-B) Infected Caco-2 cell supernatants were collected every 24 h for 96 h. Mock-infected supernatant was collected at 96 h, but reovirus protein was not detected. Reovirus protein association with large EV, medium EV, and small EV/free virus fractions was quantified following SDS-PAGE and immunoblotting for T1L (A) or T3D (B). Error bars indicate SD. *n* = 3. *, P < 0.05 by one-way ANOVA with Tukey's multiple comparisons prior to normalization. Protein signal was normalized as a percentage of maximum by dividing each adjusted volume value by the highest measured value within the blot. (C) Infected-cell supernatants were harvested at 72 h, and viral infectious units associated with each EV fraction were quantified by plaque assay. Error bars indicate SD. *n* = 3. *, P < 0.05 by two-way ANOVA with Tukey's multiple comparisons. (D) Caco-2 cells were adsorbed with three individual clones (C1-C3) of T1L or T3D reovirus at an MOI of 5 PFU/cell for 72 h. Reovirus nonstructural protein association with large EV, medium EV, and small EV/free virus fractions was quantified following SDS-PAGE and immunoblotting for T1L σNS or T3D σNS.

SUMMARY AND RELEVANCE

Given its nonenveloped structure, reovirus egress has traditionally been attributed to plasma membrane lysis. In this data chapter, my primary aim was to further elucidate mechanisms of reovirus egress. Using two strains of reovirus that differ in membrane disruption capacity, I show that fully infectious units of reovirus can egress from two different cell types in association with EVs. Specifically, reovirus appears to associate with large and medium EVs, and does not appear to associate with small EVs. Nonspecific reovirus adhesion to large and medium EVs is unlikely to fully explain the association of these virus particles with EVs during egress, as I found that the amount of reovirus that spontaneously binds to EVs is minimal compared to the reovirus that associates with EVs during the course of infection. Thus, reovirus-EV association is not simply explained by artefactual binding of reovirus to plasma membrane molecules, including glycans and sialic acid, which are likely found on the surface of EVs and on cell debris. Furthermore, the EV population that reovirus employs for egress appears to resemble microvesicles, given the visual pattern of egress and promising pilot data revealing that at least one reovirus strain may be encapsulated inside of these medium EVs. Interestingly, the medium EVs with which reovirus associates appear highly environmentally stable. The findings presented in this chapter, which enhance our understanding of reovirus egress strategies in multiple cell types, may apply broadly to other viruses that are released in EVs and travel in association with EVs. Further insights into the mechanisms of EV-mediated viral egress may help inform improved viral

vaccination strategies and delivery of viral vectors, including delivery of oncolytic therapeutic reovirus to directed tumor treatment sites.

DISCUSSION

I envision a model in which reovirus uses at least three distinct pathways to exit infected cells: (i) by membrane lysis, (ii) associated with and possibly packaged within medium EVs, or (iii) using a mechanism involving “sorting organelles” and “membranous carriers” [10,125]. More than one reovirus egress pathway may function in each cell type we have tested thus far, and the pathways reovirus uses may vary by cell type. For example, bluetongue virus exits cells using both lytic and non-lytic strategies; in addition to inducing cell lysis, bluetongue virus also buds non-lytically from the plasma membrane in EVs that carry markers of lysosomes and exosomes [54,143]. In L cells and Caco-2 cells, T3D reovirus may employ a similar strategy in which free virus particles are released through lysis, while additional virus exits cells enclosed within medium EVs. In contrast, T1L reovirus egress occurs in the near-complete absence of membrane disruption, which is consistent with medium EV-associated egress but fails to explain free virus release (**Fig. 9B-C**). I propose that an additional host cell-assisted mechanism, perhaps akin to the non-lytic reovirus egress strategy previously described for reovirus in HBMECs, facilitates non-lytic T1L free virus egress[125]. It is additionally possible that free T3D virus egresses using a non-lytic mechanism. T3D does not induce significant membrane disruption at 48 h p.i. and yet I detect T3D protein association with the small EV/free virus fraction at this same timepoint (**Fig. 10E**)**.** Although T1L and T3D protein and infectious reovirus do appear to additionally associate with large EVs derived from both L cells and Caco-2 cells (**Fig.**

10B-F, Fig. 21A-C), I hypothesize that this association is due to free reovirus particles adhered to released cell debris and large EVs after their release from cells. This hypothesis is consistent with prior observations that large quantities of infectious virus remain associated with cell debris following cell death induction [147]. The more efficient association of T3D with large and medium EVs derived from mock-infected cells suggests that this adhesion may be more pronounced for T3D than T1L; I suspect that T3D's ability to induce cell membrane disruption to a far greater degree than T1L may be responsible for this phenotypic difference (**Fig. 15**)**.** Though this model seems plausible based on the data I have collected thus far, many additional questions remain; a combination of molecular and imaging approaches will reveal additional insights into the detailed mechanisms of EV-associated reovirus egress in the future. Ideas to address remaining gaps in knowledge will be discussed in further detail in Chapter V.

Based on the data currently presented in this chapter, it is difficult to pinpoint the specific EV subtype(s) with which reovirus associates. Techniques I have employed involving a range of differing densities of iodixanol gradient preparations have all been unsuccessful in separating a reovirus-containing medium EV fraction from the rest of the medium EV population; thus, I am currently unable to segregate the specific EV subpopulations with which reovirus associates (**Fig 16** and data not shown) [35]. If reovirus is packaged externally on the surface of EVs, it may be possible to employ an immunoprecipitation-based technique to pull down reovirus particles and thus to capture the EVs associated with said particles [153]. Data that will be presented in Chapter III suggest that reovirus particles are packaged on the interior of medium EVs, and on the

exterior of large EVs. Thus, the above strategy may be effective in allowing us to further define the large EVs with which reovirus appears to associate, but does not assist us in advancing our understanding of the subpopulation origins of reovirus-associated medium EVs. I attempted to demystify this query using EV-specific markers that are widely accepted in the field, but given the heterogenous spread of these markers throughout large, medium, and small EV fractions, these particular markers did not aid in defining any one particular EV subtype (**Fig. 18**) [20,34]. Large EV fractions contained markers enriched in microvesicles, secretory autophagosomes, and exosomes. Based on my EM imaging, I hypothesize that the large EV fraction mostly contains apoptotic blebs and cell debris, which, since these are generally defined as membrane-bound "chunks" of cell, would explain the presence of the plasma membrane-associated microvesicle and exosome markers [34]. Furthermore, based on their size, which ranges from 300-500 nm, and on prior literature which revealed success in capturing secretory autophagosomes at relatively low-speed centrifugation, I would expect secretory autophagosomes to pellet either in the medium or large EV fraction [15,48]. Due to the prevalence of the autophagosome marker LC3A/B in the large EV fraction, I hypothesize that most secretory autophagosomes are additionally enriched in the large EV fraction [15]. I additionally found that medium EV fractions contained markers of microvesicles and exosomes. Using negative stain EM, I have visualized EVs matching the size of microvesicles present in the medium EV fraction, which may explain the presence of microvesicle markers in this fraction; I have additionally visualized much smaller EVs present in this same fraction, which may explain the presence of exosome markers (**Fig.**

12E-F). Initial imaging observations provide more insight into the potential origin of the medium EV fraction. Using thin-section TEM and confocal microscopy, I captured instances in which egressing reovirus particles appear to be encapsulated inside of a protruding plasma membrane-encapsulated structure (**Fig. 19**). These protrusions ranged 400-800 nm in diameter, with 600 nm being the average diameter. The size of these structures is consistent with microvesicles or with secretory autophagosomes, but the budding-specific pattern is consistent only with the biogenesis of microvesicles. When I visualized cross-sections of reovirus-infected medium EVs, I observed some instances in which clusters or single T1L particles were encapsulated inside membrane-bound EV structures that measured around 600-800 nm in average diameter, which is consistent with the size range generally noted for microvesicles (**Fig. 13**). Additionally, I observed that small EV fractions contained markers of exosomes and weakly of secretory autophagosomes. I theorize that, because exosome biogenesis has been known to intersect with the autophagy pathway, and LC3 has been found on multivesicular body membranes and evidently plays a role in exosome formation, perhaps our small EVs additionally contain autophagic markers [154]. However, reovirus does not associate directly with this EV fraction, so these EVs are less of an interest. Taken altogether, I have observed distinct reovirus particle association with, and in some cases packaging within, membrane-bound structures that match the size of either secretory autophagosomes or microvesicles, and follow a biogenesis pattern consistent with microvesicle biogenesis. Future studies utilizing EV pathway-specific inhibitors may help to begin elucidating the

EV subpopulation that reovirus associates with and will be discussed further in Chapter V.

I observed that the association of reovirus with medium EVs is retained throughout a range of storage lengths, temperatures, and mechanical stressors (**Fig. 17**). Given the stability of rotavirus association with EVs in nature, these results are not wholly surprising [81]. Each of the conditions that I tested represents a common protocol practice used in the reovirus field and extends to general virology protocols as well. Given that reovirus association with medium EVs was retained throughout these disruptive conditions, with the exception of SDS treatment, it will be important for the reovirus field as a whole going forward to consider the potential effect of EVs in foundational assays such as stock preparation and storage, plaque assays, viral purification, and the like.

The strain-specific and cell type-dependent differences in detection of reovirus nonstructural protein σNS in association with EVs may reflect reovirus biology or have potential implications for release and protection. In L cells, I observed T1L and T3D nonstructural σNS protein association with the small EV/free virus fraction, and additional T3D nonstructural σNS protein association with the large and medium EV fractions (**Fig. 11**). Contrastingly, in Caco-2 cells, I observed a complete lack of σNS association with any EV fraction (**Fig. 21D**). I have shown that, corresponding with current literature, T3D induces apoptosis and membrane damage more efficiently than T1L (**Fig. 9B-C, Fig. 20C-D**). Although they are generally acknowledged to mostly be enriched in the large EV fraction, apoptotic blebs vary broadly in size and may be detected in any EV-enriched

fraction. Signal from σNS detected in large and medium EV fractions from L cells may primarily be derived from pieces of virus factories incorporated in apoptotic blebs, which would explain their absence in corresponding T1L fractions. Furthermore, replication factory morphology and host protein interactions also may alter σNS uptake into released EVs, particularly large and medium EVs released from the plasma membrane. Given the larger general size of the EVs enriched in the large and medium EV fractions, I speculate that pieces of T3D replication factories, which have a distinct globular morphology compared to the filamentous morphology of T1L replication factories, are potentially packaged into large and medium EVs. Bearing in mind the cytotoxic nature of T3D infection, these EVs may in turn package larger pieces of the cell during their biogenesis[51,69]. In either case, if T3D particles are packaged into the same EVs as σNS, they could potentially be protected from the environment by nonstructural proteins. This hypothesis will be further explored in the Discussion portion of Chapter III. Additionally, in L cells, T1L and T3D σNS protein may potentially bind to single-stranded host RNA that is strain-specifically packaged as cargo to varying degrees within EVs of each size category [155,156]. RNA binding, protein misfolding, or ubiquitinylation and sorting by EV biogenesis ESCRT complex proteins could serve as a mechanism to load T1L or T3D σNS into small EVs, which are known to package RNA and protein cargo [157-159]. Although exosome cargo can differ by cell type, it is currently unclear why σNS is present in reovirus-infected L cell-derived small EV fractions but not in any T1L- or T3D-infected Caco-2 cell-derived EV fractions.

Although it is presently a mystery whether the EV-mediated reovirus egress strategy occurs in humans or in an animal model, I do observe that this mechanism of egress occurs in more than one cell type, including a cell type that is a closer and more translational surrogate to the intestinal cells that reovirus naturally infects in an animal model. It is probable that EV-associated egress is biologically meaningful, as studies conducted in the last few years have accumulated evidence that EV-mediated egress is employed by evolutionary diverse viruses. Future studies will need to be undertaken in order to address the biological relevance of this mechanism of host cell-assisted reovirus egress, some possibilities for which will be discussed in Chapter V.

CHAPTER III: EXTRACELLULAR VESICLE-MEDIATED EGRESS CAN INFLUENCE REOVIRUS INFECTION

Smith SC, Krystofiak E, Ogden KM (2024) Mammalian orthoreovirus can exit cells in extracellular vesicles. PLoS Pathog 20(1): e1011637. https://doi.org/10.1371/journal.ppat.1011637

CO-AUTHOR CONTRIBUTIONS

Preparation and imaging of all samples for negative-stain electron microscopy and thin section transmission electron microscopy was conducted by Dr. Evan Krystofiak at Vanderbilt University. Dr. Krystofiak also assisted in large part with troubleshooting and optimizing electron microscopy-based experiments and conditions. The laboratory of Dr. Terence Dermody carried out all *in vivo* work. The laboratory of Dr. Andries Zjilstra, including Ariana von Lersner, carried out all EV microflow cytometry, EV staining, and EV fingerprinting analysis. I conducted all other work, in close intellectual collaboration with Dr. Kristen Ogden.

INTRODUCTION

In my previous chapter, I provided evidence that one of the possible routes of reovirus egress is via interaction with large and medium EVs. Since this mode of host cell-assisted reovirus egress is newly discovered, its effect on reovirus infection is

unknown. Egress mechanisms for rotavirus, a non-enveloped virus of the Reovirales order, have only recently been clarified. A foundational study discovered that rotavirus egresses in medium sized EVs *in vitro* and *in vivo* that are consistent with microvesicle EV subpopulations [57]. Using imaging techniques, the authors present evidence that rotavirus is contained within these EVs. In Chapter II, I provided evidence that infectious units of reovirus, like rotavirus, egress from cells in association with EVs. I observed select instances in which reovirus appeared to be packaged inside of highly environmentally stable medium-sized EVs that bud from the cellular plasma membrane in a manner that is reminiscent of microvesicle biogenesis. Despite the current wealth of knowledge giving us insight into how reovirus interacts with cell pathways and how the replication cycle proceeds in a cell, it is currently a mystery i) how the mechanism of egress effects downstream reovirus transport and infection, and ii) how reovirus interacts with EV biogenesis pathways.

The effect of EV-facilitated egress on enclosure and protection of reovirus particles against the extracellular milieu is unknown. EV-mediated transport potentially confers a higher probability of establishing productive viral infection, and EV-facilitated virus shielding may protect particles from immune detection and subsequent neutralization. For viruses including JC polyomavirus, rotavirus, enterovirus 71, hepatitis E virus, and HAV, association with EVs can confer varying levels of protection of viral particles from antibody-mediated neutralization [12,69,72,73]. However, when EV-contained virus interacted with a recipient host cell, EV-mediated neutralization protection was markedly diminished

for HAV. Overall, this suggests that EVs may not fully protect virus particles throughout the entire duration of transport, and virus uptake and entry may play a role in determining whether EVs remain whole or become disrupted. Moreover, a previous study established that large and medium EVs derived from Caco-2 cells protected a minority of rotavirus particles; rSA11 infectivity was retained by only 1.2-3.6% [73]. Not only do EVs provide a virus with a shield to escape immune detection, but EVs can additionally carry immune-modulatory molecules. Phosphatidylserine, a phospholipid that is generally universally displayed on the surface of EVs, serves as a potent down-regulator of anti-inflammatory immune responses, allowing viruses to persist undetected and thereby possibly increasing the likelihood that EV-associated viruses enter target cells [75-77]. By shielding virus particles, EVs enable viruses to enter cells with potentially greater ease, avoid triggering immune system alarms, promote virus protection from immune defenses that potentially arise, and protect virus particles from the extracellular environment, including protease degradation, chemical treatment, and disinfection protocols [81].

To date, whether large or medium EV association promote multiparticle reovirus transport is unclear, though the imaging I displayed in Chapter II suggests that multiple reovirus particles can associate with both of these EV subpopulations (**Fig. 12**). Given the size difference between most virus particles and EVs, an EV may additionally enclose multiple virus particles into a single, collective multiparticle unit. This may in turn enable collective virus infection of the same recipient cell [15,160]. Due to host cell permissibility and viral susceptibility to cellular immune defenses, a high multiplicity of infection “threshold”

must be reached to establish an infection in a cell [82-85]. The presence of bacteria has been found to enhance reovirus virulence, and multiparticle infection has been presented as a potential mechanism [87,161]. In coxsackievirus-coinfected cells, a marked percentage of EV-associated virus contained mixed parental genomes, suggesting the presence of a population of multiparticle infectious units [144]. I previously observed multiple reovirus particles in association with large EVs and with medium EVs; however, it is unclear at the present time whether these EV fractions promote multiparticle reovirus transport, and whether differences between these two EV populations influence the degree at which grouped transit occurs (**Fig. 12**).

Large-scale viral modulation of EVs has been demonstrated for multiple viruses, but whether reovirus induces EV modulation is unknown. In Caco-2 cells, rotavirus significantly increased the quantities of EVs released from infected cells; compared to EVs released from uninfected cells, these EVs inhibited T cell function [88]. Zika virus modulates exosome biogenesis proteins to facilitate EV-mediated Zika virus release, and dengue virus and Epstein-Barr virus induces the upregulation whole-cell EV protein secretion, especially small EVs [90,146,162]. Thus, viruses are capable of interacting with and modulating the host cell to upregulate EV release patterns in order to potentially promote their release in EVs. Though its interaction with specific EV pathways is currently understudied, reovirus does extensively modulate cellular processes [106,124,128-131]. Thus, it is possible that reovirus modulates EV pathways, though the effects of infection on EV modulation are currently unknown.

Currently, it is unknown whether reovirus actively orchestrates its release in EVs, and the biological relevance of this mechanism of escape *in vivo* has yet to be illuminated. Reovirus strains T1L and T3D, which were a focus of Chapter II and will remain a focus in this chapter, differ in their *in vivo* pathogenesis and ability to induce apoptosis, with T3D inducing significantly more apoptosis than T1L. Though the distinct mechanism of reovirus apoptosis induction is incompletely defined, this phenotype at least partially segregates with the attachment protein σ1 and the endosomal penetration protein μ1, both of which are major constituents of the reovirus outer capsid [115,163]. In a mouse model, strain-specific differences impact how reovirus spreads, and these differences are thought to segregate with the μ1 protein [116]. Therefore, there is documented history of two of the major reovirus outer capsid proteins, both of which are implicated in apoptosis induction, interacting with host cells in order to affect viral spread. One mechanism of reovirus spread, as I have shown in Chapter II, is via EV-mediated egress. I hypothesize that the reovirus outer capsid, which stands the greatest chance of physically interacting with EV biogenesis pathways during egress, is responsible for ensuring EV-mediated egress of mature reovirus particles. I question whether, as evidenced in a mouse model, differences in strain-specific apoptosis induction capacity influence the route of EV-mediated viral egress.

In Chapter II, I provided evidence that reovirus egresses in association with large EVs and medium EVs. The influence of EV-mediated egress on reovirus infection of recipient cells is a mystery, and I questioned whether large EV-mediated reovirus egress

influences infection differently than medium EV-mediated reovirus egress, because these EV fractions likely represent separate EV subpopulations. Therefore, in this chapter, I was interested in investigating several specific lines of questioning to fill these gaps in knowledge, including: i) do EVs truly enclose reovirus particles and if so, do EVs protect reovirus from antibody neutralization and protease degradation, ii) does reovirus orchestrate its release in EVs and if so, what reovirus determinants are responsible for playing this role, iii) does EV-facilitated egress promote multiparticle reovirus transport, and iv) does viral infection alter the abundance of EVs compared to uninfected cells?

RESULTS

Medium-sized EVs protect reovirus from neutralization and protease conversion

I first sought to increase my understanding of how EVs might shield reovirus particles from the extracellular environment during transit from one infected cell to the next recipient cell. To determine whether association with EVs can protect reovirus from antibody-mediated neutralization, I employed a plaque reduction neutralization assay. I enriched large EV, medium EV, and small EV/free virus fractions, as well as iodixanol gradient-separated free virus, from the supernatants of L cells infected with T1L or T3D for 72 h (**Fig. 22A**). I treated each fraction with reovirus strain-specific neutralizing antiserum or with medium alone and determined titers by plaque assay. I hypothesized that if reovirus is present as free particles or as particles adhered to the EV exterior, then the virus would be sensitive to neutralization, and the treated sample titer would be reduced relative to the untreated sample titer; however, if reovirus particles are enclosed within EVs as internal cargo, then the virus would be protected from neutralization, and

the treated sample titer would be comparable to the untreated sample titer. I found that when reovirus associated with large EV or small EV/free virus fractions, both T1L and T3D were neutralized to similar levels as free reovirus, with titers reduced on average by 100-fold (**Fig. 22B-E**). In contrast, when associated with the medium EV fraction, T1L and T3D titers were unaffected, demonstrating robust protection from neutralization. These findings suggest that T1L and T3D particles released from L cells are specifically packaged inside medium EVs, but not inside large EVs.

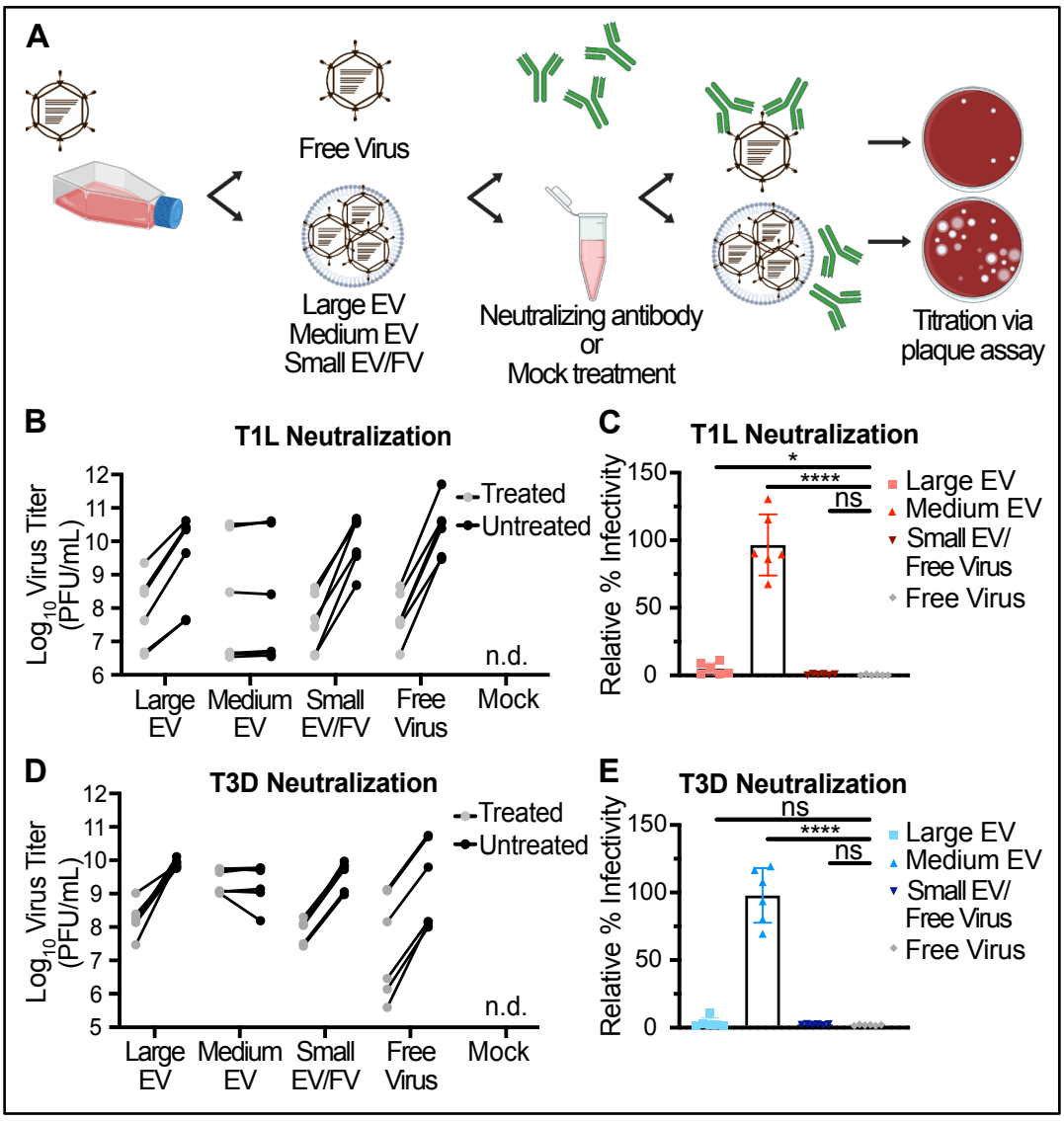

Figure 22. Reovirus particles can be protected from antibody-mediated neutralization via association with medium-sized EVs. (A) L cells were adsorbed with three individual clones of reovirus strains T1L or T3D at an MOI of 1 PFU/cell. After 72 h, EV-associated and free reovirus particles were enriched using sequential centrifugation and iodixanol gradient separation, as previously described, then incubated with σ1-specific reovirus antiserum (treated) or with diluent (untreated). Infectious units were quantified by plaque assay. (B-E) Plaque titer (B, D) and percent relative infectivity, quantified by dividing the treated infectious units by mock-treated infectious units and multiplying by 100 (C, E), for each sample are shown. Error bars indicate SD. "n.d." = not detected. *n* = two titers per sample in each of three independent experiments. *, $P < 0.05$; ****, $P < 0.0001$ by two-sample unpaired T test.

To validate my findings, I employed a complimentary approach in which I used the protease chymotrypsin to assess the protective capacity of EVs for virus particles.

Chymotrypsin treatment cleaves reovirus virions to infectious subvirion particles (ISVPs) *in vitro*, and this conversion can be visualized on an immunoblot. I reasoned that if EVs provide protection to reovirus particles, then reovirus virion particles would not be transformed from virion form to ISVP form, as evidenced first by the loss of σ3 protein and then by the conversion of the μ1C protein to δ protein [102]. Using a concentration of chymotrypsin at which I observed full conversion of virions to ISVPs in the small EV/free virus fraction, I treated large, medium, and small EVs enriched from infected L cells with 20 μg/mL of chymotrypsin. Then, I resolved viral structural proteins by SDS-PAGE and immunoblotting and quantified the loss or retention of σ3 or μ1C protein signal in chymotrypsin-treated samples relative to mock-treated samples (**Fig**. **23A, C**). For both T1L (**Fig. 23B**) and T3D (**Fig. 23D**) particles, the amount of σ3 and μ1C proteins retained post protease treatment compared to the untreated fraction was decreased overall when reovirus associated with large and small EVs. Although the σ3 protein signal retained post chymotrypsin treatment was not statistically significant in the medium EV fraction compared with the other fractions, likely due to high variability, it was the only EV fraction in which σ3 signal was detected. Thus, it appears that medium EVs are capable of at least partially protecting released reovirus from two components of the extracellular environment, neutralizing antibodies, and proteases.

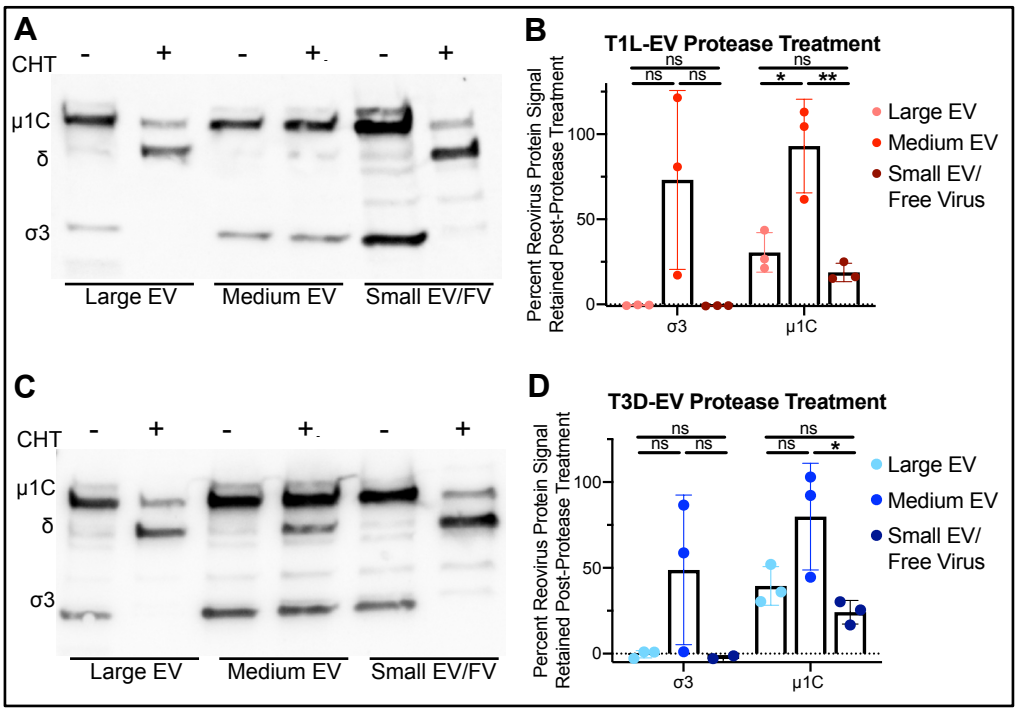

Figure 23. EVs partially protect reovirus from protease treatment. (A-D) L cells were adsorbed with three individual clones of T1L or T3D reovirus at an MOI of 1 PFU/cell for 72 h. Large, medium, and small EV/free virus fractions were harvested via centrifugation and each split into two aliquots containing equal volumes. One aliquot was left untreated (-), and the other aliquot was treated with 20 μg/mL of chymotrypsin (+). Reovirus T1L (A-B) and T3D (C-D) σ3 and μ1C proteins were visualized by and quantified by SDS-PAGE and immunoblotting using anti-reovirus serum. Shown are representative immunoblots for each virus strain alongside values quantified for the three clones. Error bars indicate SD. n = 3. *, $P < 0.05$; **, $P < 0.01$ by one-way ANOVA with Tukey's multiple comparisons.

EV-mediated virus neutralization protection is cell type- and virus strain-dependent

I was next interested in determining whether the observed protection that L cell-derived medium EVs provide reovirus particles held true in another cell type. Caco-2 cells, which are a human colonic epithelial cell line, are closer surrogates to the intestinal cells that reovirus would naturally infect *in vivo* compared to L cells, which are derived from murine fibroblasts. To determine whether reovirus particles are packaged inside Caco-2-derived EVs and protected from antibody neutralization, I again employed a plaque

reduction neutralization assay. I found that T1L was neutralized to similar levels as free reovirus when it was associated with Caco-2-derived large EVs and small EVs/free virus but was protected from neutralization when associated with medium EVs (**Fig. 24A-B**). Interestingly, T3D was efficiently neutralized to levels similar to free T3D reovirus when associated with any Caco-2-derived EV fraction, including the medium EV fraction which had previously protected T3D particles from neutralization in L cells (**Fig. 24C-D**). These findings suggest that T1L particles are packaged inside of medium EVs released from two cell types. However, EV-mediated protection appears to be virus-strain- and cell-type-dependent, as T3D is efficiently protected when associated with L cell-derived medium EVs, but T3D is inefficiently protected when it associates with Caco-2-derived medium EVs.

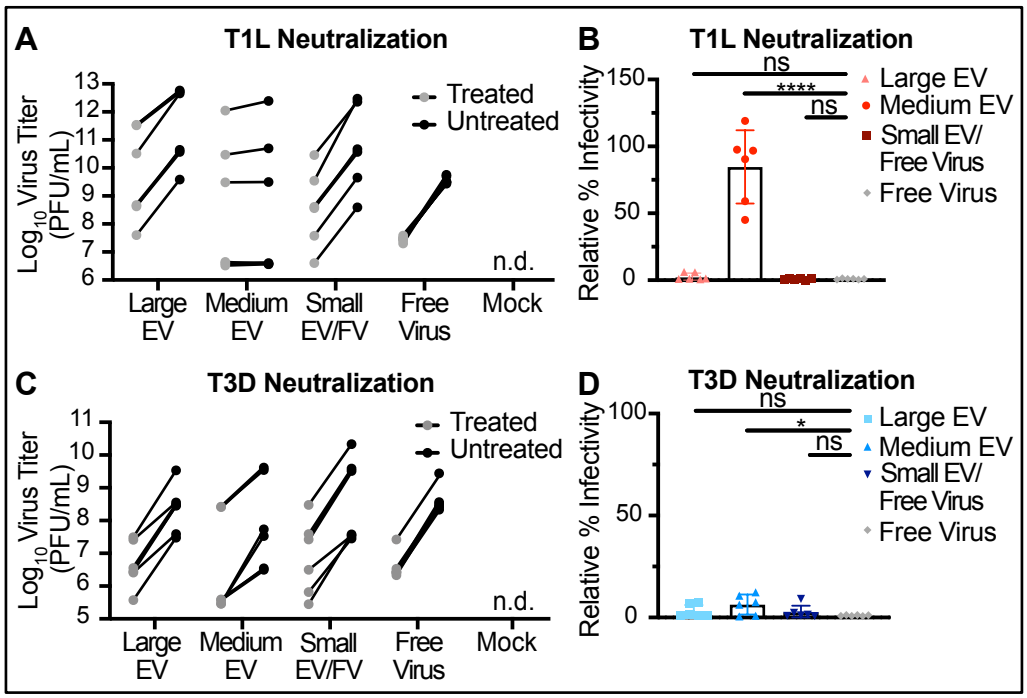

Figure 24. EV-mediated reovirus egress protection from neutralization may be reovirus strain- and cell type-dependent. (A-D) Caco-2 cells were adsorbed with three individual clones of reovirus strains T1L or T3D, as indicated, at an MOI of 5 PFU/cell, and supernatants were fractionated and treated with neutralizing antibody or left untreated as described previously. Infectious units were quantified by plaque assay. Plaque titer (A, C) and relative percent infectivity, quantified by dividing the treated infectious units by mock-treated infectious units and multiplying by 100 (B, D), for each sample are shown. Error bars indicate SD. "n.d." = not detected. *n* = two titers per sample in each of three independent experiments. *, $P < 0.05$; ****, $P < 0.0001$ by two-sample unpaired T test.

Next, I endeavored to further investigate the EV-mediated neutralization protection phenotype for another virus in the order Reovirales that has been reported to associate with medium EVs—rotavirus. To quantify rotavirus association with EVs, I infected Caco-2 cells with rotavirus strain rSA11 and used sequential centrifugation to enrich cell culture supernatants for populations of large/medium EVs and small EVs/free virus during a time course of 96 h. I resolved equal amounts of each sample by SDS-PAGE and immunoblotting and quantified rotavirus protein signal associated with each EV fraction. I observed roughly equivalent levels of rSA11 protein associated with the large/medium

EV and small EV/free virus fractions **(Fig 25A)**. Like T3D, rSA11 caused substantial plasma membrane disruption in Caco-2 cells **(Fig. 25B)**. To visualize how rSA11 associates with EVs, I employed negative-stain EM. Consistent with published data and with what I observe for reovirus, rSA11 particles visually clustered with medium EVs and failed to associate with small EVs **(Fig. 25C-D)**. As was true for negative stain EM images from reovirus-infected cells, it was difficult to discern whether rotavirus particles were adhered to the exterior or enclosed within the medium EVs. In some cases, the EVs appeared partially disrupted with particles directly adjacent to the vesicle. To ascertain whether rSA11 is packaged inside of protective Caco-2-derived medium EVs, I employed a plaque reduction neutralization assay. I found that rSA11 was neutralized efficiently under all conditions tested, including as free virus or when associated with any EV size class (**Fig. 25E-F**). Thus, although rSA11 evidently associates with EVs when released from Caco-2 cells, it is nevertheless accessible to neutralizing antibodies. Overall, it appears that Caco-2-derived medium EV protection of viruses is variable, as we observe robust neutralization protection for T1L reovirus, but not for T3D reovirus or rSA11 rotavirus.

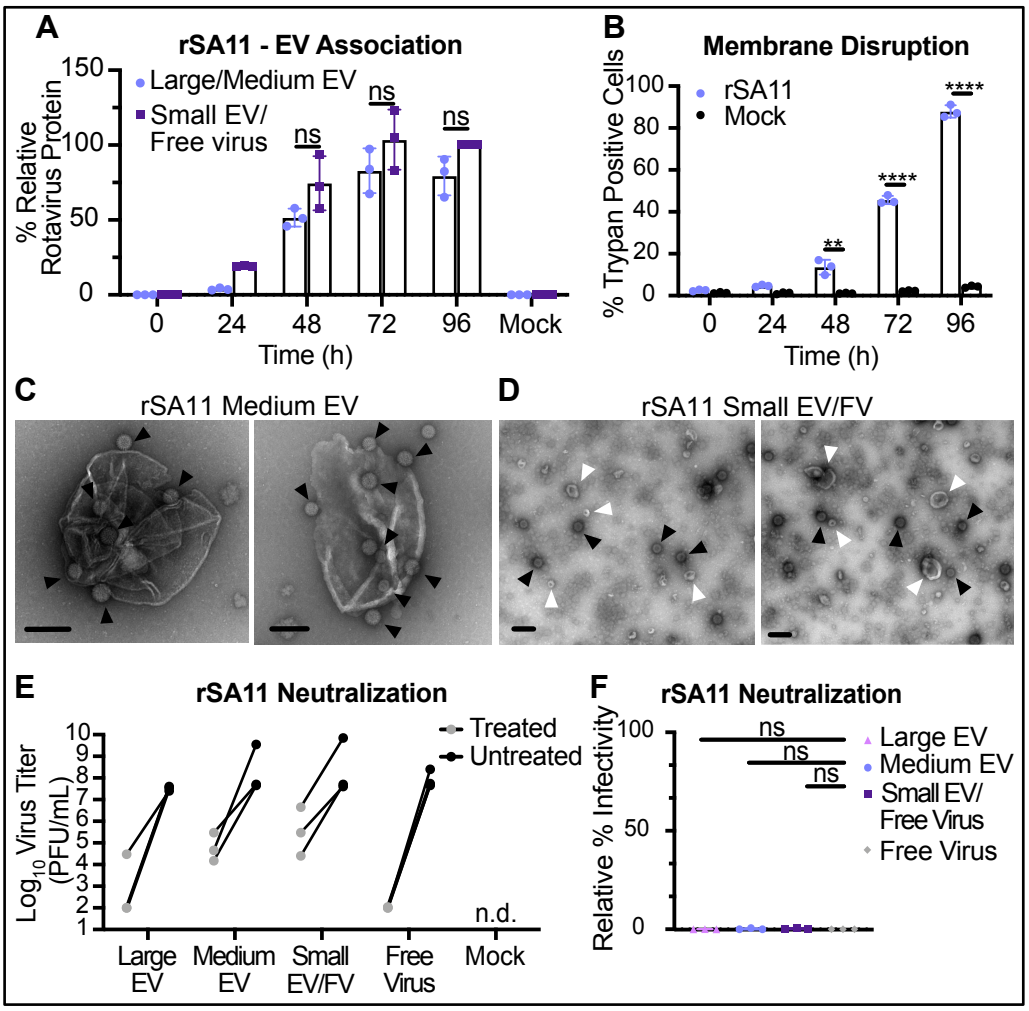

Figure 25. Rotavirus associates with Caco-2-derived EVs that fail to protect particles from neutralization. (A) Caco-2 cells were adsorbed with rSA11 rotavirus at an MOI of 0.01 PFU/cell. Every 24 h for 96 h, the large/medium EV fraction and the small EV/free virus fractions were harvested via centrifugation at 10,000 × *g* and 100,000 × *g* respectively. The amount of rotavirus protein associated with the large/medium EV and small EV/free virus particle fractions was resolved and quantified by immunoblotting using polyclonal rotavirus antiserum. Error bars indicate SD. *n* = 3. ns = not significant by Two sample unpaired T test. (B) Cell membrane disruption was quantified at the indicated time points by trypan blue staining. Error bars indicate SD. *n* = 3. **, P < 0.01; ****, P < 0.0001 by Two sample unpaired T test. (C-D) At 48h p.i., the large EV fraction, medium EV fraction, and the small EV/free virus particle fraction were harvested via centrifugation. Medium EV (C) and small EV (D) fractions were visualized using negative-stain EM (C-D). Scale bar = 200 nm. (E-F) Cell supernatants infected for 48 h with rSA11 were fractionated and treated with neutralizing antibody or left untreated, as described previously. Infectious units were quantified by plaque assay. Plaque titer (E) and relative infectivity level, quantified by dividing the treated infectious units by mock-treated infectious units and multiplying by 100 (F), for each sample are shown. Error bars indicate SD, n = 3. "n.d." = not detected. *n* = two titers per sample in each of three independent experiments. ns = not significant by two sample unpaired T test.

Next, I wanted to determine which reovirus determinants, if any, are linked to the cell type- and virus strain-dependent EV-facilitated neutralization protection phenotype I observed in Caco-2 cells. During reovirus replication, particles replicate and mature in cytoplasmic replication factories. The outer capsid proteins of mature virus particles are structurally most accessible for direct interaction with EV biogenesis molecules, and thus are the most likely candidates responsible for orchestrating host cell-mediated virus egress. Two of the four segments encoding proteins located on the outer capsid, S1 and M2, have additionally been linked to reovirus apoptosis induction capacity [115,122]. These two segments are of particular interest because I observed a lack of EV-mediated protection for rSA11 and T3D, both of which cause cell death and apoptosis in Caco-2 cells (**Fig. 9B-C and 20C-D**). I decided to engineer a pair of hybrid reoviruses with parental backbones but exchanged outer capsids, which additionally carry apoptosis induction determinants. I rescued the hybrid viruses using plasmid-based reverse genetics and made clonal stocks. To validate these hybrid particles, I employed electropherotyping and trypan blue assays. Electropherotyping of the hybrid virus featuring a T1L parental backbone with a T3D outer capsid (T1L-T3D O.C.) indicated correct incorporation of all segments (**Fig. 26A**). Trypan blue analysis revealed that in Caco-2 cells, plasma membrane disruption phenotypes of hybrid viruses took on an "intermediate" phenotype compared to wildtype (WT) viruses. At 96 h p.i., WT T3D induced roughly 75% cell membrane disruption, and T3D-T1L O.C. membrane disruption decreased to roughly 35%. WT T1L induced about 5% cell membrane disruption, and T1L-T3D O.C. membrane disruption increased to about 40% (**Fig. 26B**). Like T1L WT,

T1L-T3D O.C. was neutralized to similar levels as the free virus control when associated with large EVs and small EVs (**Fig. 24B and 26C-D**). Compared to T1L WT, which is robustly protected from neutralization, T1L-T3D O.C. protection fell to roughly 20% protection (**Fig. 24B and 26C-D**). Thus, by exchanging outer capsid segments between T1L and T3D, cell membrane disruption capacity and neutralization protection phenotypes appear to exchange between the two reovirus strains as well.

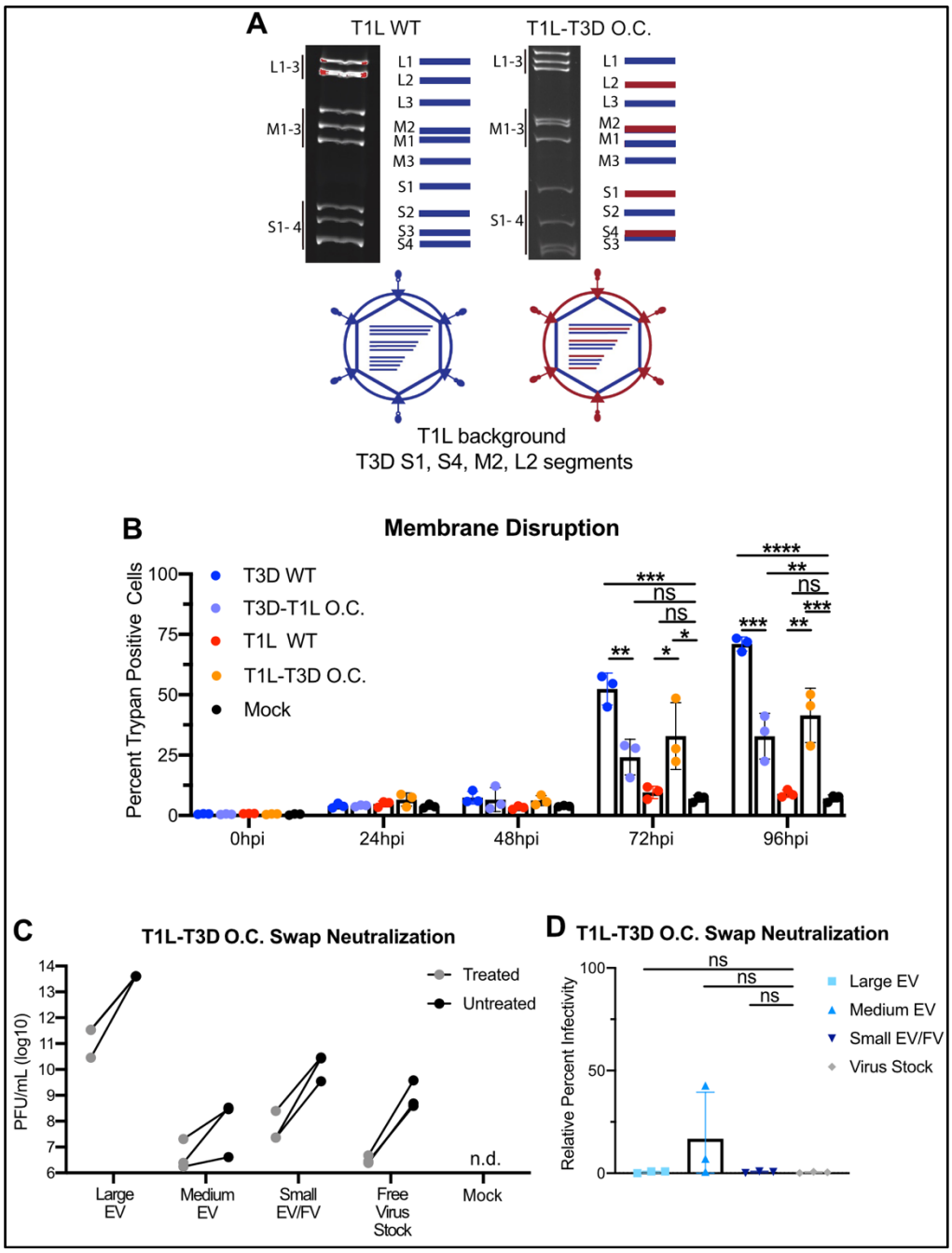
A
T1L WT
T1L-T3D O.C.
L1-3
M1-3
S1-4
L1
L2
L3
M2
M1
M3
S1
S2
S3
S4
T1L background
T3D S1, S4, M2, L2 segments
B
Membrane Disruption
Percent Trypan Positive Cells
T3D WT
T3D-T1L O.C.
T1L WT
T1L-T3D O.C.
Mock
0hpi
24hpi
48hpi
72hpi
96hpi
C
T1L-T3D O.C. Swap Neutralization
PFU/mL (log10)
Treated
Untreated
n.d.
Large EV
Medium EV
Small EV/FV
Free Virus Stock
Mock
D
T1L-T3D O.C. Swap Neutralization
Relative Percent Infectivity
Large EV
Medium EV
Small EV/FV
Virus Stock

Figure 26. Reovirus outer capsid determinants may play a role in virus strain-specific neutralization protection. (A) RNA was harvested from a T1L WT-infected L cell monolayer or a T1L-T3D O.C.-infected L cell monolayer, resolved in an SDS-10% polyacrylamide gel, ad stained using ethidium bromide. Migration of dsRNA segments of T1L WT were compared to those of T1L-T3D O.C. (B) Cell membrane disruption was quantified for T1L WT-, T1L-T3D O.C.-, T3D WT-, T3D-T1L O.C.-, and mock-infected cells every 24 h for 96 h using trypan blue staining. *, $P < 0.05$; **, $P < 0.01$; ***, $P < 0.001$; ****, $P < 0.0001$ by one-way ANOVA with Tukey's multiple comparisons. Error bars indicate SD. $n = 3$. (C-D) L cell supernatants infected for 72 h with 1 PFU/cell of T1L-T3D O.C. were fractionated and treated with neutralizing antibody or left untreated, as described previously. Infectious units were quantified by plaque assay. Plaque titer (C) and relative infectivity level, quantified by dividing the treated infectious units by mock-treated infectious units and multiplying by 100 (D), for each sample are shown. Error bars indicate S.D., $n = 3$. "n.d." = not detected. ns = not significant by two sample unpaired T test.

In vivo EVs may confer some level of reovirus neutralization protection

I was next interested in beginning to assess the biological relevance of EV-mediated reovirus egress. Our laboratory's collaborators, the laboratory of Dr. Terence Dermody, inoculated two litters of newborn mice with T1L and then harvested the colon contents of each mouse separately. I then used centrifugation to harvest large EV, medium EV, and small EV/FV fractions. To visualize the contents of these fractions, I employed negative stain EM. I observed that the large *in vivo* EV fraction contains primarily clusters of small EVs that aggregate together to form large clusters (**Fig. 27A**). Slightly larger small EVs were visualized as separate entities, but in most cases the EVs contained in this fraction were individually smaller than 100 nm in diameter. The medium *in vivo* fraction yielded a mixture of small, distinct EVs in addition to slightly larger medium EVs ranging in size from 300 nm to 400 nm (**Fig. 27B**). In some cases, these medium EVs were adhered to other medium EVs or with small EVs. As expected, the small EV fraction yielded a field of small EVs that were distinct and separated from one another (**Fig. 27C**). For all fractions visualized, I only rarely observed any virus particles, perhaps

due to the small amount of sample that can be harvested from a single newborn mouse (**Fig. 27A-C**). These fractions do quantitively contain infectious virus, however; when I subjected the EVs harvested from *in vivo* colon contents to neutralizing antibody treatment, I observed roughly 15% infectivity protection of T1L associated with large *in vivo* EVs and small *in vivo* EVs relative to a free virus control (**Fig. 27D-E**). This relative protection difference was significant when the large EV fraction was compared to free virus but was insignificant when the small EV fraction was compared to free virus, likely due to the variability of the data points (**Fig. 27E**). The range of neutralization protection levels for *in vivo* medium EV-associated T1L was notably broader compared to large EV fractions, with a mean of about 60% protection, but the difference from free virus was not statistically significant (**Fig. 27E**). Thus, though it is extremely variable, it does appear that EV association may provide reovirus in the intestinal tract of a mouse with some amount of protection from antibody neutralization. Given this high amount of variability, however, the biological relevance of this mode of egress is still unclear; further experiments delving into this question will be important in the future.

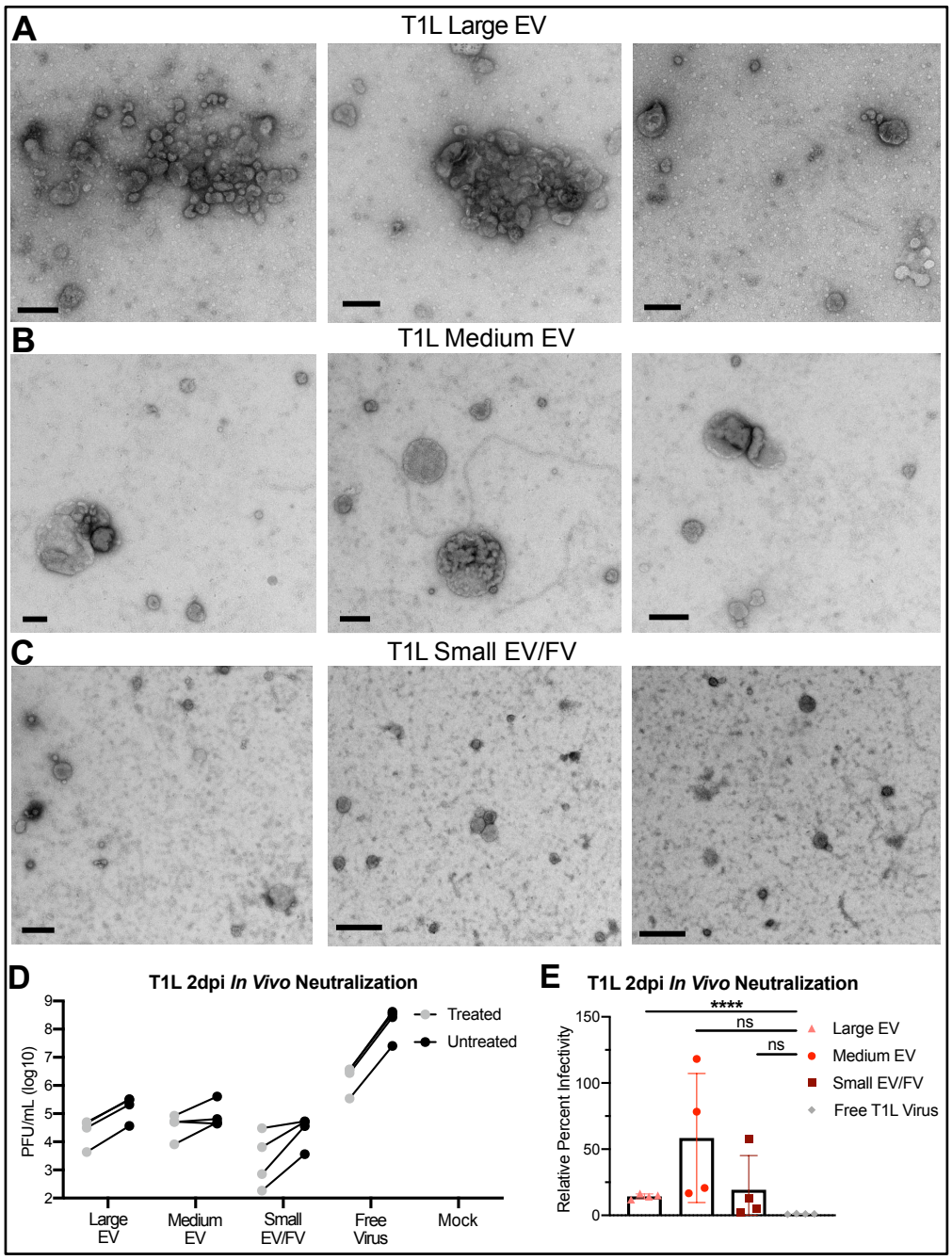
A
T1L Large EV
B
T1L Medium EV
C
T1L Small EV/FV
D
T1L 2dpi *In Vivo* Neutralization
PFU/mL (log10)
9
8
7
6
5
4
3
2
Large EV
Medium EV
Small EV/FV
Free Virus
Mock
Treated
Untreated
E
T1L 2dpi *In Vivo* Neutralization
Relative Percent Infectivity
150
100
50
0
****
ns
ns
Large EV
Medium EV
Small EV/FV
Free T1L Virus

Figure 27. Extracellular reovirus association with large EVs occurs *in vivo*. A litter of 3 day-old black 6 WT mouse pups were inoculated with 1×10^8 T1L PFU/mouse. At 2 d p.i., mice were humanely euthanized, and their colon contents were harvested. (A-C) Large EVs (A), medium EVs (B), and small EVs/free virus (C) were harvested from T1L-infected mouse colon contents via centrifugation. T1L association with each fraction was visualized via negative-stain EM. Scale bar = 200 nm. (D-E) Large EVs, medium EVs, and small EVs/free virus collected from individual mouse colon contents were subjected to mock- treatment or treatment with anti-reovirus σ1 serum. Infectious units were quantified by plaque assay. Plaque titer (D) and relative infectivity level, quantified by dividing the treated infectious units by mock-treated infectious units and multiplying by 100 (E), for each sample are shown. Error bars indicate SD, n = 4 where each data point indicates the colon contents harvested from a single mouse. ****, $P < 0.0001$ by two sample unpaired T test.

Large and medium EV-associated reovirus can mediate multiparticle infection

I was next interested in determining whether EV-mediated egress may alter how reovirus is transported between cells. To determine whether EVs can transport an infectious unit consisting of multiple reovirus particles, I used high-resolution melt (HRM) analysis to detect genotypes of individual viral particles [97]. I co-infected L cells with wild-type (WT) and genetically barcoded (BC) T3D reoviruses, strains which have been previously engineered and validated in our laboratory, and collected cell culture supernatants at 24 h p.i., and enriched for large EV, medium EV, and small EV/free virus fractions (**Fig. 28A**) [97]. I adsorbed fresh L cell monolayers with serially diluted intact EV fractions or with free reovirus particles and then isolated individual plaques. I define a single plaque as a single infectious unit. In the case of a free virus particle, a single infectious unit is likely to be an independent WT particle or an independent BC particle; if an EV bundles multiple particles together, then a single infectious unit could potentially contain multiple WT, multiple BC, or a mixture of multiple WT and multiple BC particles. I genotyped individual viral plaque infectious units using HRM analysis, which distinguishes

WT and BC RNA based on differences in melt temperature conferred by genetic polymorphisms in the barcode (**Fig. 28B**). A multiparticle population containing both WT and BC viruses is anticipated to yield an intermediate melt curve. A multiparticle population containing only WT or only BC viruses, or a mixture that is skewed heavily towards one population or the other, will yield a melt curve indistinguishable from that generated by infection by a single virus particle (**Fig. 29**). In each of four independent experiments, I examined 24 plaques from each fraction, for a total of 96 plaques representing each of the three fractions. While I detected no genotype mixtures in plaques formed from virus in the small EV/free virus fraction, a significant portion of reovirus plaques in the large EV-enriched fraction (~ 6%) contained multiple genomes (**Fig. 28C**). In the medium EV-enriched fraction, I detected statistically significant and slightly higher levels of reovirus plaques containing multiple genomes (~ 11%). Contrastingly, multiple genomes were never detected in plaques formed by small EVs or free virus. Thus, my data suggest that a significant portion of large EVs and medium EVs, but not small EVs, can ferry reovirus between cells as infectious multiparticle bundles.

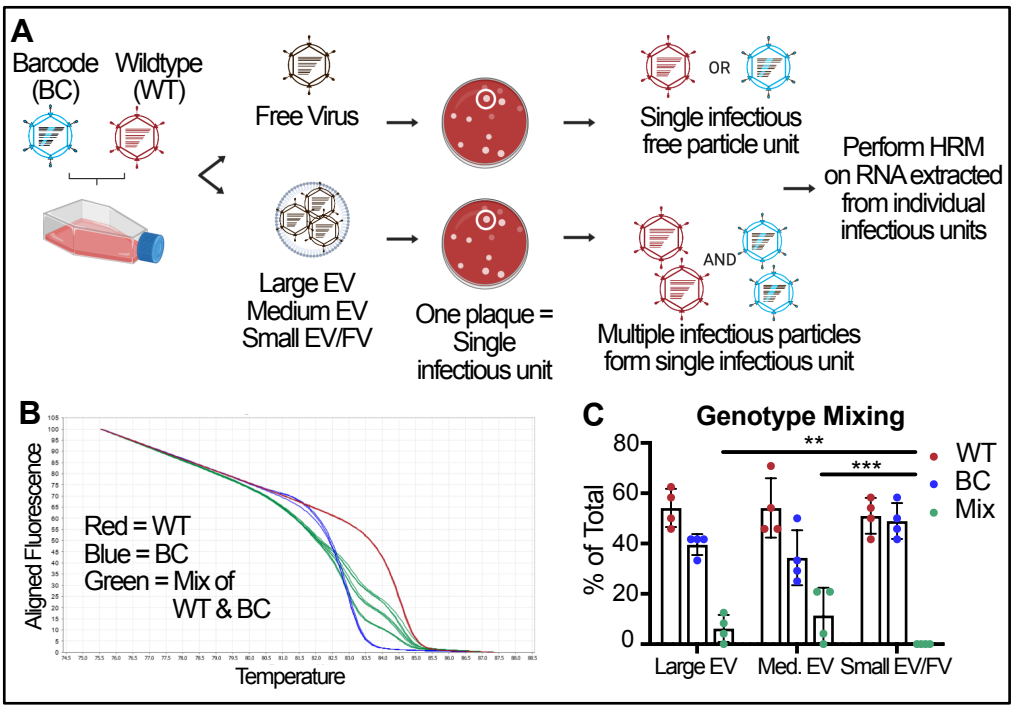

Figure 28. EV-mediated egress permits multiparticle reovirus transport. (A) L cells were coinfected with independent inocula of WT or BC T3D reovirus at an MOI of 10 PFU/cell. At 24 h p.i., large EV, medium EV, and small EV/free virus fractions were harvested from the supernatants using sequential centrifugation and subsequently used to inoculate a plaque assay. Plaques representing individual infectious units, which might be EV-associated bundles or free virus particles, are picked and amplified. Viral RNA was genotyped using HRM. (B) Normalized melt curves for control RNA from WT (red), BC (blue), and 2:1, 1:1, and 1:2 mixtures of WT and BC (green) RNA are shown. (C) Genotype quantitation for the large EV, medium EV, and small EV/free virus fractions as a percentage of total plaques analyzed. Error bars indicate SD. *n* = 24 plaques represented by each data point in four independent experiments. **, $P < 0.01$; ***, $P < 0.001$ by Pearson's chi-squared analysis with pairwise comparisons.

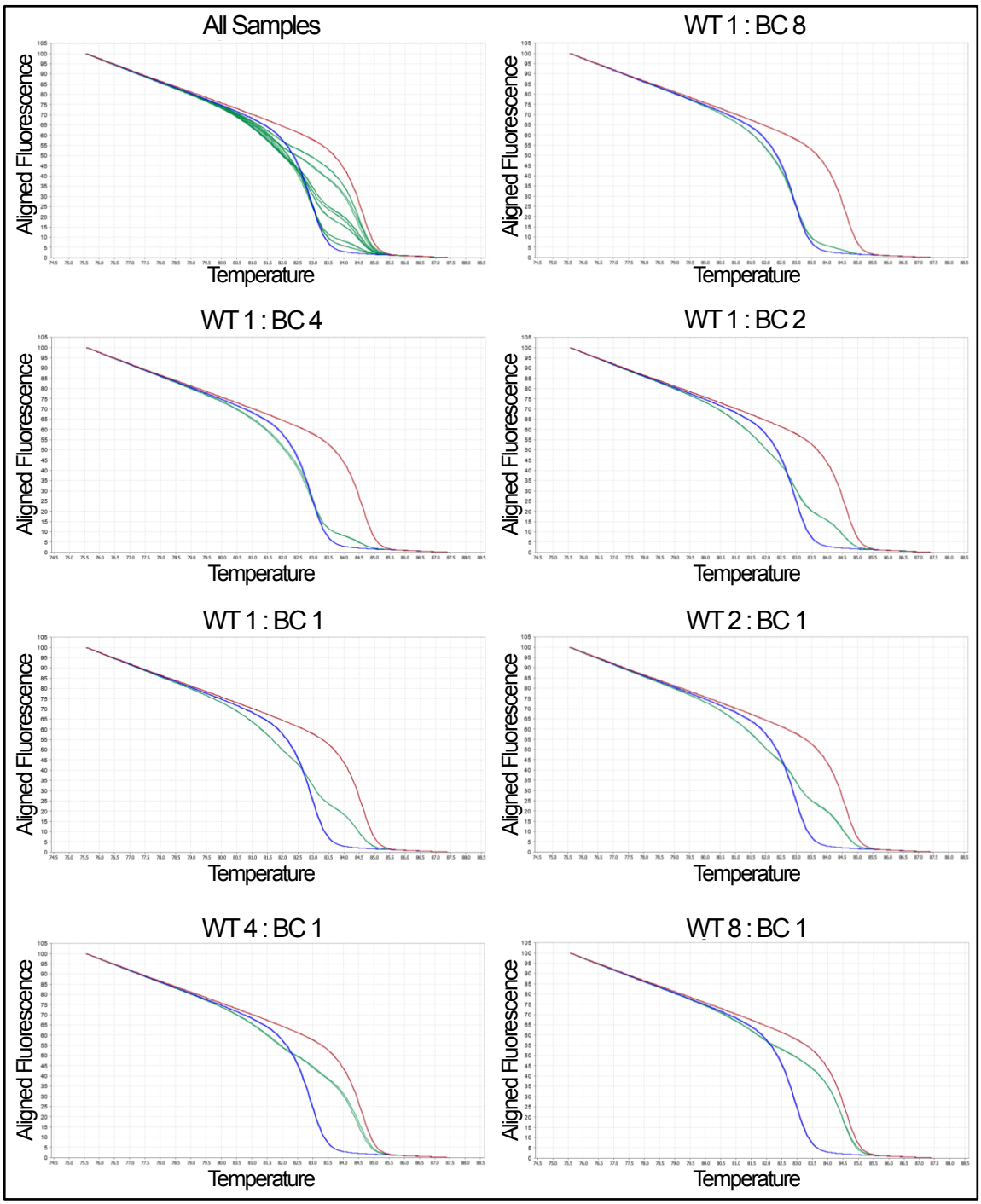

Figure 29. Sensitivity of high-resolution melt analysis. Normalized melt curves for control RNA from WT (red), BC (blue), and mixtures of WT and BC (green) at the indicated ratios are shown.

Reovirus and rotavirus infection enhances EV abundance compared to uninfected cells

I next wanted to more fully understand whether reovirus infection influences EV release on a whole-cell level. To answer this question, I adsorbed L cells with medium alone (mock) or T1L or T3D reovirus, incubated cells for 72 h, and then used sequential differential centrifugation to enrich cell culture supernatants for large EV, medium EV, and small EV/free virus fractions. To compare the relative amounts of protein present in each EV fraction, I used a Coommassie blue-stained SDS-PAGE gel and resolved equal sample volumes (**Fig. 30A**). Compared with uninfected cells, T1L-infected and T3D-infected cells appeared to release material containing significantly increased total protein signal in most EV fractions (**Fig. 30B**). On average, I detected an approximately two-fold increase in released protein in each fraction for infected cells compared to uninfected cells (**Fig. 30C**). To more specifically capture and isolate EVs from the population of cell articles that pellet upon centrifugation, I subjected large EV, medium EV, and small EV/free virus fractions to further separation processing using Annexin V nanobead immunoprecipitation. Annexin V binds phosphatidylserine, which is present on the exterior of most released EVs but is not displayed on the surface of healthy cells. After subjecting equal volumes of immunoprecipitated samples to immunoblotting, I found that, compared to uninfected cells, reovirus infection increased the protein levels associated with released large EV, medium EV, and small EV/free virus fractions (**Fig. 30D**). Although only the difference for the large EV fraction was statistically significant, on average I detected a three-fold to more than four-fold protein signal increase in EV

fractions released from infected cells compared to corresponding EV fractions released from uninfected cells (**Fig. 30E-F**).

I next employed a parallel approach to validate the effects of reovirus infection on EV release. I used a lipophilic dye, DiI, to quantify the EVs released from reovirus-infected cells compared to uninfected cells. Following adsorption with T1L, T3D, or medium alone (mock), I used centrifugation to enrich for large EV, medium EV, and small EV/free virus fractions. I then mixed fractions with DiI to stain membranes and imaged ten randomly selected fields of view by confocal microscopy. To quantify lipid-positive puncta, which likely represent EVs, I used the EVAnalyzer FIJI plugin (**Fig. 30G-H and Fig. 31**) [164]. Although I observed that specific quantities of lipid-stained EV in fields of view varied, overall I detected that lipid-stained EV counts from reovirus-infected cells were significantly higher compared to those released from uninfected cells. The average fold change of released large EVs was notably higher from T3D-infected cells than T1L-infected cells, specifically quantified as a five-fold change versus a two-fold change, (**Fig. 30H**). I theorize that, since T3D induces significantly elevated levels of plasma membrane disruption in L cells, there may be more apoptotic blebs and plasma membrane debris released from T3D-infected L cells, which are most likely to pellet in the large EV fraction. Consistent with findings from the immunoprecipitation assay described above, quantitation of EVs stained with lipophilic dye suggested that reovirus infection typically doubled or tripled the release of most sizes of EVs from L cells (**Fig. 30F, H**). Collectively, these data suggest that reovirus infection enhances the release of EVs of all sizes.

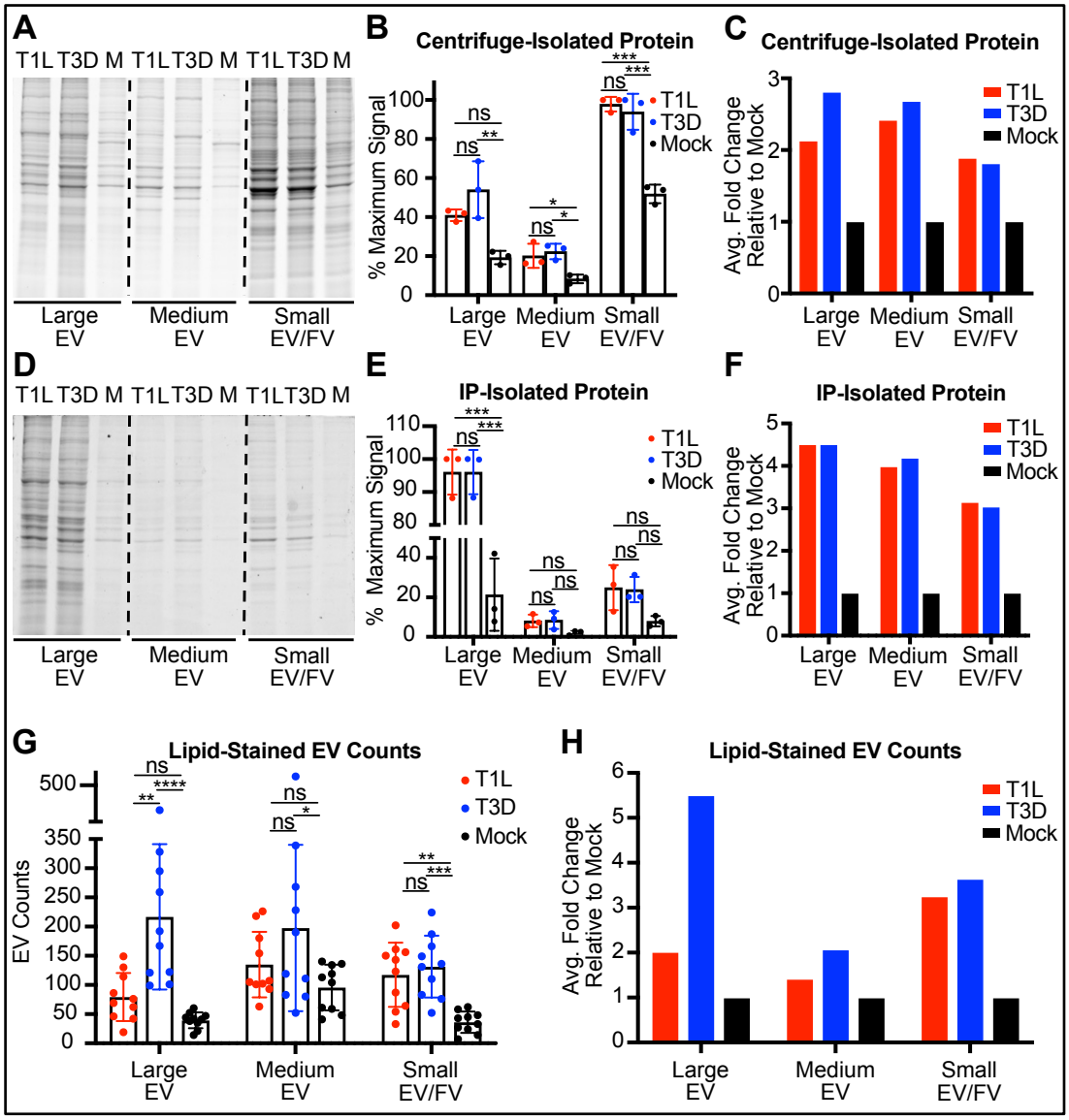
A
T1L T3D M T1L T3D M T1L T3D M
Large EV
Medium EV
Small EV/FV
B
Centrifuge-Isolated Protein
% Maximum Signal
T1L
T3D
Mock
C
Centrifuge-Isolated Protein
Avg. Fold Change Relative to Mock
D
E
IP-Isolated Protein
F
IP-Isolated Protein
G
Lipid-Stained EV Counts
EV Counts
H
Lipid-Stained EV Counts

Figure 30. Reovirus infection enhances EV release compared to uninfected cells. L cells were adsorbed with medium (mock; M) or with three individual clones of T1L or T3D reovirus at an MOI of 1 PFU/cell for 72 h. (A-C) Fractions enriched in large, medium, and small EVs were harvested from supernatants using sequential centrifugation, as previously described, then lysed. Equal lysate volumes were resolved by SDS-PAGE and Coomassie staining (A), three independent experiments were quantified (B), and they were normalized by dividing the average virus-infected value by the average mock-infected value (C). (D-F) Fractions enriched in large, medium, and small EVs were harvested from supernatants using sequential centrifugation, as previously described. Then, EVs were immunoprecipitated using annexin V nanobeads, which bind to phosphatidylserine. Equal volumes of immunoprecipitated material were resolved by SDS-PAGE and Coomassie staining (D), three independent experiments were quantified (E), and normalized by dividing the average virus-infected value by the average mock-infected value (F). (G-H) Fractions enriched in large, medium, and small EVs were harvested from supernatants using sequential centrifugation, as previously described. Each sample was resuspended in an equal volume of salt-balanced buffer, allowed to interact with a fluorescent lipid dye, loaded into the well of a Mattek dish, covered with a sterile glass cover slip, and imaged using confocal microscopy. EVs were counted in 10 random fields of view, each representing an 8 × 8 tile imaging structure (G) and normalized by dividing the average virus-infected value by the average mock-infected value (H). Error bars indicate SD. *, $P < 0.05$; **, $P < 0.01$; ***, $P < 0.001$ by one-way ANOVA with Tukey's multiple comparisons.

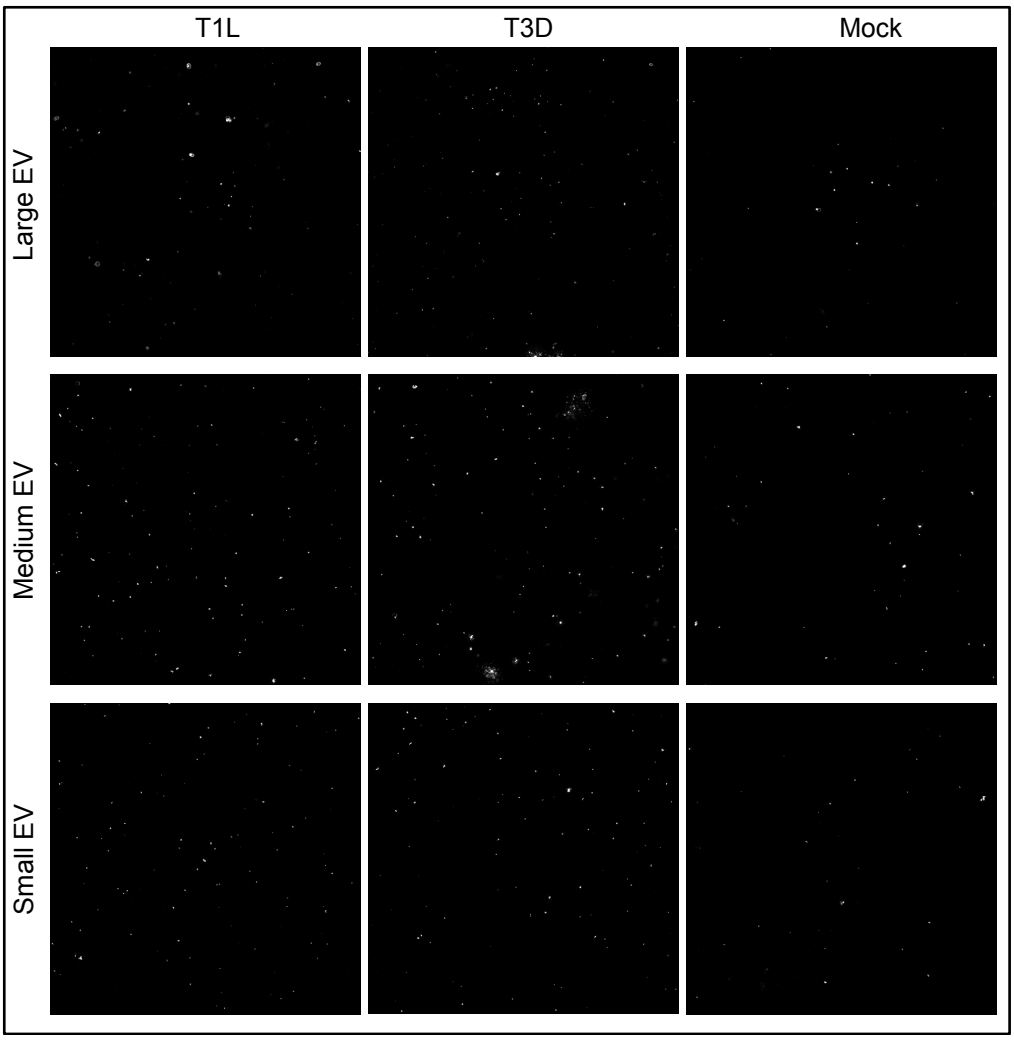

Figure 31. Reovirus infection enhances EV release. Representative confocal images are displayed for a single field of view, which is made up of an 8 × 8 tile imaging structure under 63X oil immersion.

To ensure that the observed reovirus infection-triggered increase in EV abundance was truly a result of EV release and not simply a general change in total protein expression triggered by reovirus infection, I adsorbed L cells with medium alone (mock) or with T1L or T3D and let infection proceed for 72 h. I then harvested the cell monolayer and quantified total protein in cell lysates by Coommassie blue staining (**Fig. 32A**). I detected no significant change nor trend towards a change in total protein expression

between infected cells and uninfected cells, suggesting that reovirus infection itself does not alter cellular protein expression, and that any increase in protein in EV fractions is due to EV release (**Fig. 32B-C**).

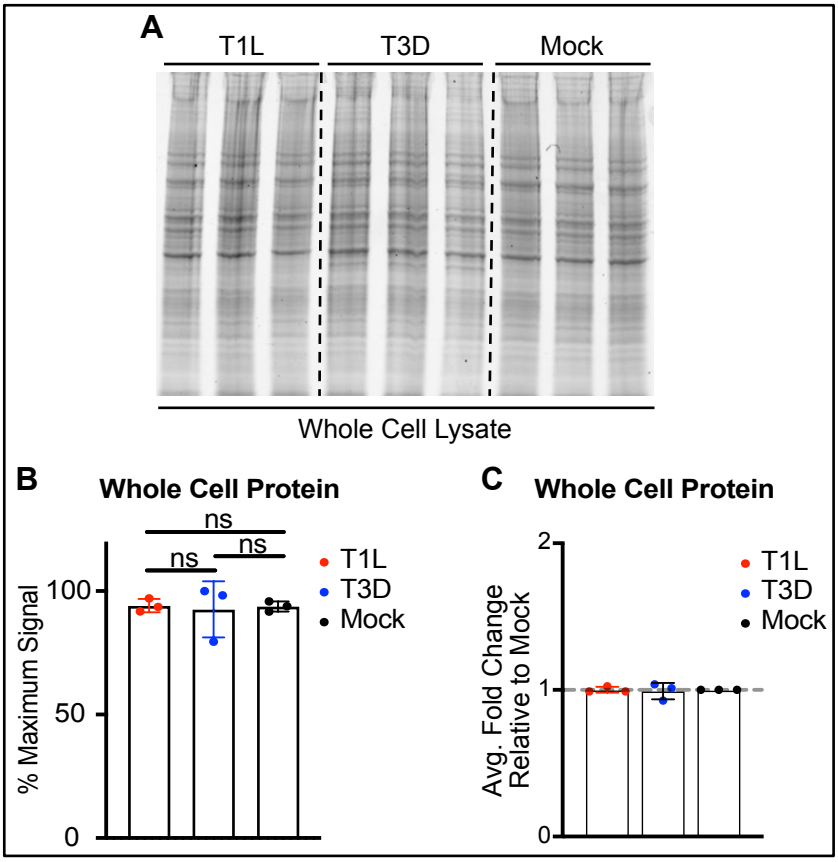

Figure 32. Reovirus infection does not significantly alter whole cell protein expression. L cells were adsorbed with media (mock) or with three individual clones of T1L or T3D reovirus at an MOI of 1 PFU/cell for 72 h. (A-C) Cells were lysed in RIPA buffer, and lysates were resolved by SDS-PAGE and Coomassie staining (A), three independent experiments were quantified (B), and normalized by dividing the average virus-infected value by the average mock-infected value (C). Error bars indicate SD, *n* = 3. Comparisons by one-way ANOVA with Tukey's multiple comparisons.

To determine whether, like reovirus, rotavirus also modulates EV release patterns, I worked with the laboratory of Dr. Andries Zjilstra. We used microflow cytometry to compare the profiles of EV populations released from uninfected MA104 monkey cells or

rotavirus-infected cells over a course of 12 h and 24 h. Our collaborators used a proprietary method using di-8-ANEPPS to stain EV populations, and then utilized microflow cytometry to group similar EV populations based on their size and area [165]. I observe that as soon as 12 h and especially at 24 h, compared to uninfected cells, rotavirus infection significantly upregulates the release of almost all EV populations. Specific, individual EV populations that visually display striking differences are circled for the 24 h timepoint in order to visually compare the increase in abundance between the same uninfected and infected EV populations (**Fig. 33A**). The overall mixture of all EVs present has been quantified as events per minute, and I observe a marked increase of EVs released from infected cells compared to uninfected cells at both the 12 h and 24 h timepoint (**Fig. 33B**). Taken altogether, these data suggest that EV release is upregulated by both reovirus and rotavirus infection.

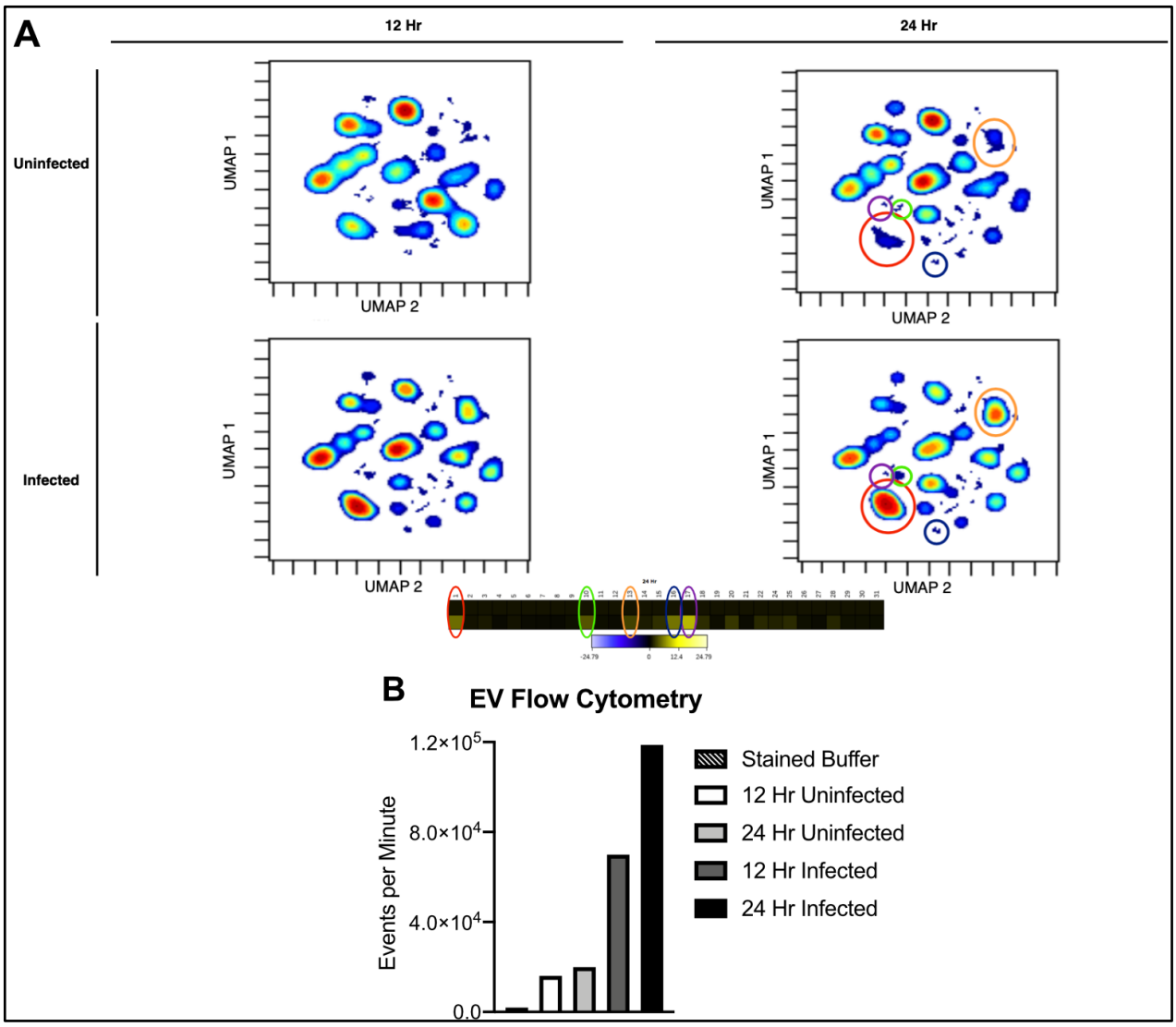
A
12 Hr
24 Hr
Uninfected
Infected
UMAP 1
UMAP 2
B
EV Flow Cytometry
Events per Minute
1.2×10^5
8.0×10^4
4.0×10^4
0.0
Stained Buffer
12 Hr Uninfected
24 Hr Uninfected
12 Hr Infected
24 Hr Infected

Figure 33. Rotavirus infection upregulates the release of EVs compared to uninfected cells. MA104 cells were adsorbed with media alone (uninfected) or with three individual dilution inocula of rSA11 rotavirus at an MOI of 0.1 PFU/cell for 12h or 24h. Whole infected or uninfected supernatant was harvested at each timepoint, cleared of cell debris via centrifugation, and given to our collaborator. EVs were labeled with di-8-ANEPPS and detected via multiparametric imaging flow cytometry. (A) The heterogeneity of resulting EV populations is depicted using Uniform Manifold Approximation Projection. (B) The events per minute for each sample were quantified.

SUMMARY AND RELEVANCE

In this chapter, I sought to understand whether virus egress strategies influence downstream infection of recipient cells. Using two strains of reovirus that differ in membrane disruption efficiency, T1L and T3D, and one strain of rotavirus, I show that virus infection enhances the release of EVs. In some cases, these EVs shield virus particles from antibody-mediated neutralization *in vitro*, though the phenotype is variable in a mouse model. I provide preliminary evidence that outer-capsid proteins, including those that influence apoptosis induction capacity, may be responsible for determining whether virus is protected from neutralization. Furthermore, EV-mediated reovirus transport can ferry collective, multiparticle groups of reovirus between cells. The work described here reveals a potential mechanism by which reovirus may escape immune system defenses and overcome cellular thresholds to infection, enhancing the likelihood of productive infection. These findings enhance our understanding of the influence of egress strategy on virus infection. As further future field-wide studies continue to support EV-mediated egress as a viable route of pathogenic virus transport, there is increasing motivation to re-examine our current viral vaccination strategies, and an improved

understanding of the impacts of EV-associated virus release and spread will continue to advance public health and safety measures [137].

DISCUSSION

EV-facilitated egress may protect reovirus from host immune defenses and from the extracellular environment. T1L and T3D reovirus released from L cells are at least partially shielded from antibody-mediated neutralization and proteolysis and, thus, are likely enclosed within a population of medium EVs (**Fig. 22 - 24**). Our findings echo those observed for JC polyomavirus, enterovirus 71, hepatitis E virus, and HAV, which can also evade antibody-mediated neutralization when they exit cells in EVs [12,69,72-74]. Thus, EV shielding of viruses from extracellular factors including immune defenses and proteases is a recurring strategy by which viruses from distinct families, including reovirus, may more efficiently establish or prolong infection. Given that reovirus is in clinical testing as an oncolytic therapeutic, delivery in an EV could potentially promote reovirus effectiveness as an anti-cancer agent by allowing the virus to evade neutralizing antibodies [101,166-168]. At the present time, however, it is unclear whether neutralization protection occurs with any sort of regularity in a more biologically relevant model. I observed a positive trend towards T1L particle protection mediated most markedly by association with medium EVs harvested from mice, but the level of protection that this association afforded T1L particles was highly varied (**Fig. 27**). Further studies will need to be conducted in the future to ascertain the biological relevance of EV-mediated reovirus egress on infection of downstream cells.

My previous finding indicating that T3D nonstructural σNS protein associates with large and medium EVs in L cells may carry implications for neutralization protection (**Fig. 11**). If T3D particles are buried within remnant replication factory pieces inside of L cell-derived EVs, this additional barrier may help ensure that T3D is protected from antibody-mediated neutralization in L cells; in Caco-2 cells, I do not observe T3D σNS protein association with any EV fractions, and thus I speculate that the extra layer of protection potentially provided by replication factory remnants results in our observed loss in medium EV-mediated T3D protection (**Fig. 11, 21D, 22, 24**). It is possible, then, that the antibody-mediated protection we observe for T3D in L cells is potentially attributed to being buried inside of remnant replication factories that are packaged within medium EVs. However, this mechanism does not explain the protection of T1L in medium EVs derived from L cells or Caco-2 cells (**Fig. 22C and 24B**). Perhaps this "double layer of protection" provided by both an EV shield and a replication factory shield is not required for T1L in order to confer protection in both of these cell types. In some instances, I used negative stain EM and thin section TEM to visualize T1L particles packaged within large membrane-bound organelles that were further packaged inside of L cell-derived medium EVs as internal cargo (**Fig. 13**). Though I am unable to conclude presently how often this phenotype occurs, and whether the virus associated with the smaller membrane-bound structures inside of the medium EV are even infectious, I speculate that this type of packaging may confer the double-layered protection needed for T1L particles to withstand antibody and protease treatment. Reasons for the lack of σNS presence in T3D-infected

Caco-2 cell-derived large and medium EV fractions are currently unclear but could correlate with differences in apoptosis pathways [169-173].

The strain-specific and cell type-dependent neutralization protection of reovirus released in association with medium EVs has potential implications for egress. I observed that while both T1L and T3D reovirus are protected in L cell-derived medium EVs, only T1L was protected in Caco-2-derived medium EVs (**Fig. 24**). One explanation may be that T3D is released in different EV subtypes, both of which are distinct from one another but enriched at the same centrifugation speeds across both cell types. In this scenario, T3D could be packaged internally in the L cell-derived medium EV subtype and bound externally on the Caco-2-derived medium EV subtype. Precedent for a "dual EV egress" strategy exists for encephalomyocarditis virus, which exits cells in two distinct EV subtypes, one of which carries markers derived from the plasma membrane, and one of which carries markers associated with secretory autophagosomes [70]. JC polyoma virus-associating EVs additionally carry markers of both microvesicles and exosomes [69]. Therefore, I can envision a mechanism by which T3D interacts with EV biogenesis pathways to ensure internal packaging and egress within one medium EV subtype in L cells, and then egresses within a different medium EV subtype in Caco-2 cells. This medium EV subtype is either porous and leaves T3D prone to antibody-mediated neutralization, potentially due to T3D's membrane-disruptive capacity, or else T3D is unable to orchestrate internal packaging within this medium EV subtype and is thus instead packaged externally on the medium EV surface. However, given that I am

currently unable to enrich solely for reovirus-containing EVs, further study is needed to discern differences between T1L-associated and T3D-associated medium EVs derived from L cells or Caco-2 cells.

It is currently unclear why neutralization protection of T3D by medium EVs would occur in one cell type but not in another. I found that T3D reovirus and SA11 rotavirus, both of which cause apoptosis and cell membrane disruption **(Fig. 20C and 25B)**, are sensitive to neutralization in medium Caco-2-derived EVs **(Fig. 24D and 25F)**. In contrast, T1L, which does not cause high levels of apoptosis and is primarily nonlytic **(Fig. 20C and 25B)**, was protected from neutralization in both tested cell types **(Fig. 22C and 24B)**. A previous study established that medium EVs derived from Caco-2 cells provided low-level SA11 infectivity protection against antibody-mediated neutralization, and I concurrently observe less than 1% of SA11 neutralization protection by medium EVs derived from Caco-2 cells **(Fig. 25F)** [73]. Though my interpretation of this level of protection significance varies somewhat from the authors' interpretation, overall my findings are quantitatively consistent with the previous study, and I conclude that rSA11 is inefficiently protected by EVs released from Caco-2 cells. I postulate that the capacity to induce apoptosis may influence viral escape in EVs. Preliminary data that I have collected lend strength to this theory; I observed that when T1L virus is conferred increased capacity to induce cell death to a greater extent than WT T1L, there is a corresponding loss in EV-mediated neutralization protection (**Fig. 26B-D**). Reovirus induces apoptosis in L cells, a non-cancerous cell line that differs substantially from Caco-2 cells, which originate from

human colorectal adenocarcinoma [115,163,174]. A link between apoptosis and EV output exists; when caspase inhibitors were applied to Caco-2 cells to inhibit rotavirus SA11 apoptosis induction, the prevalence of EV-associated markers variably increased in large EV-enriched fractions and medium EV-enriched fractions, and decreased in small EV-enriched fractions [89]. Additionally, due to the overexpression of anti-apoptotic molecules in the bcl-2 family and mutations in tumor suppressor genes such as p53, Caco-2 cells lack fully intact apoptosis pathways [169-173]. Sindbis virus-induced apoptosis in HeLa cells results in viral nucleocapsids and viral antigens co-localizing exclusively with EV-like structures budding from the plasma membrane of apoptotic cells [175]. Chikungunya virus-induced apoptosis leads to the formation of EV structures resembling apoptotic bodies, and when individual steps of apoptosis and EV biogenesis are inhibited, virus spread to neighboring cells is impeded [176]. Thus, my data, in conjunction with prior literature, suggest that differences in T3D interactions with apoptosis pathways in L cells and Caco-2 cells might influence interactions with EV biogenesis pathways and reovirus egress strategies. However, because several outer-capsid genes were exchanged between the O.C. hybrid viruses, and not just the apoptosis induction-linked segments S1 and M2, I cannot presently definitively conclude that a change in apoptosis induction capacity is directly responsible for the change in EV-mediated neutralization protection that I have observed.

EVs may contribute to reovirus multiparticle infection. I observed that ~ 18% of tested infectious units released from infected cells contained multiple reovirus genotypes, with more mixed-genotype signal detected in the medium EV fraction, some in the large

EV fraction, and none in the small EV/free virus fraction (**Fig. 28**). To maximize chances of forming mixed virus populations, I used an MOI at which most cells are likely to be co-infected with both WT and BC reoviruses. In previous studies using the same experimental conditions, our laboratory has previously observed both WT and BC RNA co-occupying reovirus factories, sites of assembly prior to egress, and there appeared to be few limitations to WT and BC reovirus reassortment following coinfection at high multiplicity [97]. However, our HRM genotyping strategy is limited in that only infectious units containing relatively even mixtures of WT and BC RNA are likely to be detected. If an EV contains multiple particles of the same parental genome or a substantially higher ratio of one type of genome relative to the other, it is likely to be missed. I observed this phenomenon directly when I mixed different ratios of WT and BC RNA together and visualized the resulting melt curves using HRM analysis. Ratios of more evenly distributed WT and BC RNA, including 1:1 and 1:2, are clearly differentiated from WT-only and BC-only control melt curves (**Fig. 28B and 29**). Ratios on the more uneven end of the spectrum, including 1:4 and 1:8, are skewed closer to the control WT and BC melt curves and are more difficult to differentiate (**Fig. 29**). Thus, my technological approach may underestimate EV-mediated reovirus multiparticle infection.

Multiparticle infection, enabled by EVs, may enhance productive virus infection. A minority of reovirus particles are thought to be infectious [177,178]. When too few particles enter a cell, host barriers may halt virus replication [15,82-85,179]. In contrast with free virus, viral infectivity was enhanced when multiparticle BK polyomavirus, rotavirus, norovirus,

coxsackievirus, poliovirus, and JC polyomavirus associated with EV structures [15,57,69,144,180]. Virus particles may be noninfectious if they contain defective genome or protein elements; RNA viruses including reovirus, which has a segmented genome capable of reassorting to generate genetic diversity, are prone to mutation accumulation because of their lack of a proofreading mechanism [181]. Thus, populations of virus often contain a mosaic of heterogenous quasispecies [182]. When virus particles aggregate in close proximity, viral fitness can be enhanced via complementation [83,183]. For reovirus, the presence of bacteria enhances virulence, with multiparticle infection mediated through adhesion to bacteria proposed as a mechanism [87,161]. Multiparticle aggregation has been shown to increase reovirus complementation during infection, and by rescuing deleterious mutations, the overall fitness of the viral population can be enhanced [86,87,178,184]. *In vivo* studies are needed to determine the biological relevance of EV-associated multiparticle infection.

On a whole-cell level, I observed that T1L and T3D infection enhances the release of all EV sizes (**Fig. 30-31**). Rotavirus infection also produced a similar upregulation of EV release across an entire population of EVs (**Fig. 33**). This appears to be a recurrent theme in the virus-EV field. Large-scale viral modulation of EVs has been demonstrated for multiple viruses: poliovirus remodels intracellular membranes and lipid pools, enterovirus 71 infection induces the formation of autophagosomes, coxsackievirus proteins increase the formation of autophagosomes, Zika virus modulates exosome biogenesis proteins, and Epstein-Barr virus induces the upregulation whole-cell EV protein secretion [15,90,92,93,146,185]. Interestingly, in Chapter II, I indicated that the EVs

released from mock-infected cells were markedly smaller than the EVs released from reovirus-infected cells (**Fig. 12**). I hypothesize that reovirus infection not only increases the abundance of EVs released from cells compared to uninfected cells but may additionally increase the size subpopulations of EVs released from infected cells. It is currently unclear whether reovirus and rotavirus upregulation of EV release is a specific response or a general cell stress response. I have provided evidence that rotavirus infection upregulates EV release, and previous literature suggests that rotavirus protein co-precipitation with EV biogenesis proteins *in vitro* and in human patient samples suggests intracellular association of rotavirus with EV biogenesis pathway molecules compared to uninfected cells, EVs released from rotavirus-infected cells more efficiently inhibited T-cell function and proliferation (**Fig. 33**)[88]. Overall, this suggests that rotavirus is capable of upregulating whole-cell EV release patterns through modulation of specific EV biogenesis proteins, and that these EVs can alter recipient cell function. I theorize that by upregulating EV output, reovirus and rotavirus increase its chances of being released in association with EVs. If released EVs also modulate the host immune system during reovirus infection, as they do for rotavirus, upregulation of EV release may also promote reovirus escape from immune defenses and prolong infection [88,89]. Given that several other viruses, in addition to reovirus, upregulate EV release, I am left to wonder whether EV association is a virus-orchestrated mechanism, or whether this mechanism is a passive one that the host cell triggers in response to general infection which viruses have evolved to take advantage of over time. Further experimentation is needed to reveal the mechanisms and influences of reovirus-mediated upregulation of EV release.

CHAPTER IV: MATERIALS AND METHODS

Cells. Spinner-adapted L cells were grown in Joklik's minimum essential medium (JMEM; U.S. Biological) supplemented to contain 5% fetal bovine serum (FBS; Gibco), 2 mM L-glutamine (Corning), 100 U/ml penicillin (Corning), 100 mg/ml streptomycin (Corning), and 25 ng/ml amphotericin B (Corning). During infection and EV collection, L cells were cultured in serum-free JMEM. Caco-2 cells were maintained in minimum essential medium (MEM; Corning) supplemented to contain 20% FBS, 100 U/ml penicillin, 100 mg/ml streptomycin, 100 U/ml non-essential amino acids (Corning), 100 U/ml HEPES buffer (Corning), 100 U/ml sodium pyruvate (Corning), and 25 ng/ml amphotericin B. During infection and EV collection, Caco-2 cells were cultured in serum-free MEM and kept in a non-polarized, non-differentiated state through maintenance splitting and seeding at sub-confluent levels. MA104 cells were maintained in minimum essential medium (MEM; Corning) supplemented to contain 5% FBS, 100 U/ml penicillin, 100 mg/ml streptomycin, and 25 ng/ml amphotericin B. During infection and EV collection, MA104 cells were cultured in serum-free MEM. Baby hamster kidney cells expressing T7 RNA polymerase controlled by a cytomegalovirus promoter (BHK-T7) were maintained in Dulbecco's minimum essential medium (DMEM; Corning) supplemented to contain 5% FBS, 100 U/ml penicillin, 100 mg/ml streptomycin, and 1 mg/ml Geneticin (Gibco), which was added every other passage. All cells were maintained at 37°C with 5% CO_2.

Viruses. Reovirus strains rsT1L (T1L or WT), rsT3D^I (T3D or WT), rsT3D^I BC (BC), rsT3D^I-rsT1L outer capsid hybrid (T3D-T1L O.C.), and rsT1L-rsT3D^I outer capsid hybrid

(T1L-T3D O.C.) were all engineered using plasmid-based reverse genetics [96]. Strain rsT3D^{I} is a variant of the parental rsT3D prototype strain that contains a T249I mutation that renders viral attachment protein σ1 resistant to proteolytic cleavage [186]. Strain rsT3D^{I} BC is identical to rsT3D^{I} excepting silent genetic "barcode" mutations engineered in each segment [97]. Strain rsT3D^{I}-rsT1L outer capsid hybrid contains a backbone synonymous with parental rsT3D^{I}, with the substitution of rsT1L segments S1, S4, M2, and L2. Strain rsT1L-rsT3D^{I} outer capsid hybrid contains a backbone synonymous with parental rsT1L, with the substitution of rsT3D^{I} segments S1, S4, M2, and L2. Briefly, semi-confluent monolayers of BHK-T7 cells in 6 well plates were transfected with 10 plasmid constructs encoding T1L and T3D reovirus RNAs using TransIT-LT1 transfection reagent (Mirus Bio LLC). After incubation at 37°C for several days, once cytopathic effect was observed, cell lysates were created via two consecutive cycles of freezing and thawing. The resulting lysates were serially diluted and subjected to plaque assay [148]. Three individual plaques per recombinant virus strain were selected and amplified in L cells to make clonal virus stocks. Viral stock titers were quantified via standard plaque assay.

Rotavirus strain rSA11 was also engineered using plasmid-based reverse genetics [186]. Briefly, semi-confluent monolayers of BHK-T7 cells in 6 well plates were transfected with 11 plasmid constructs representing the rSA11 rotavirus genome and plasmids encoding vaccinia virus mRNA capping enzymes and the Nelson Bay virus fusion-associated small transmembrane protein using TransIT-LT1 transfection reagent (Mirus Bio LLC). After incubation at 37°C for several days, once cytopathic effect was observed, cell lysates were created via three consecutive cycles of freezing and thawing. The

resulting lysates were serially diluted and subjected to plaque assay [148]. Three individual plaques per recombinant virus strain were selected and amplified in MA104 cells to make clonal virus stocks. Viral stock titers were quantified via standard plaque assay.

Antibodies. Rabbit polyclonal reovirus antisera [153], rabbit polyclonal antisera directed against the T1L or T3D σ1 head domain [187], mouse monoclonal antibody 2H7 directed against T3D σNS and guinea pig polyclonal antiserum directed against T1L σNS [108,153] were gifts from Dr. Terence Dermody. Rabbit polyclonal rotavirus antiserum was made by Bioqual, Inc. In brief, rSA11 (~ 2.1×10^7 infectious units/ml) was administered intramuscularly on days 0 and 14 with TiterMax Gold adjuvant. Test bleeds were taken days 0, 14, and 28, with final serum harvest day 49. Commercially available TSG101 rabbit polyclonal antibody was shared with me as a gift from the Dr. Heather Pua laboratory (Abcam - ab30871);commercially available ALIX rabbit monoclonal antibody was shared with me as a gift from the Dr. Heather Pua laboratory (Abcam - ab186429); commercially available LC3A/B rabbit polyclonal antibody was shared with me as a gift from the Dr. Alissa Weaver laboratory (Cell Signaling Technologies – 4108S, Lot 2). CD81 mouse monoclonal antibody (Santa Cruz Biotechnology; sc-166029) and AnnexinA1 rabbit polyclonal antibody (ThermoFisher; 71-3400) are commercially available.

Virus Replication Assays. L cells (2×10^5 cells/ml) or Caco-2 cells (4.2×10^5 cells/ml) in complete medium were seeded in 12-well plates and incubated until reaching ~ 90% confluency. Cells were adsorbed in triplicate with media alone (mock) or with three clones

of T1L or T3D at an MOI of 1 PFU/cell (L cells) or 5 PFU/cell (Caco-2 cells). Supernatants were aspirated and replaced with serum-free media post adsorption. Every 24 h for a total of 96 h, plates were stored at -80°C. Then, they were freeze-thawed twice at -80°C and room temperature. Virus titers in the resulting lysates were determined by FFA and calculated based on numbers of infected cells quantified in four countable fields of view per well in duplicate wells, with countable fields containing ~ 50-500 reovirus-positive cells [188]. Cell nuclei were stained with DAPI and reovirus protein stained using a polyclonal anti-reovirus serum, which recognizes both T1L and T3D protein.

Trypan Blue Membrane Disruption Assay. L cells (2×10^5 cells/ml) or Caco-2 cells (4.2×10^5 cells/ml) in complete media were seeded in 12-well plates and incubated until reaching ~ 90% confluency. Cells were adsorbed in triplicate with media alone (mock), with three clones of T1L WT, T3D WT, T1L-T3D O.C. hybrid, or T3D-T1L O.C. hybrid at an MOI of 1 PFU/cell (L cells) or 5 PFU/cell (Caco-2 cells). Caco-2 cells were infected with rSA11 at an MOI of 0.01 PFU/cell. Supernatants were aspirated and replaced with serum-free media post adsorption. Every 24 h for a total of 96 h, cells were gently trypsinized at 37°C and collected via centrifugation at 100 × *g*. Cells were resuspended in equivalent volumes of PBS without Ca^{2+} or Mg^{2+} and 0.4% trypan blue solution (Corning), incubated for 3 min at room temperature, and then 10µl of each sample were promptly applied to a hemacytometer. Live cells per ml and dead cells per ml were counted manually using a compound light microscope for each sample in duplicate using two separate areas of the hemacytometer. In one case (**Fig. 18B**), cells were counted

using a Countess II cell counter using the “Trypan Blue” setting. The resulting quantities are graphed as a percent of stained (trypan-positive) cells. Trypan-positive cells are considered to have a disrupted plasma membrane.

Lactase Dehydrogenase Membrane Damage Assay. L cells (2×10^4 cells/ml) or Caco-2 cells (1.9×10^5 cells/ml) in complete media were seeded in 96-well black-walled plates (Greiner) and incubated until reaching ~ 90% confluency. Cells were adsorbed in triplicate with media alone (mock), with three clones of T1L or T3D at an MOI of 1 PFU/cell (L cells) or 5 PFU/cell (Caco-2 cells). Triplicate wells of uninfected cells were seeded for additional kit-specific controls, including spontaneous LDH release and maximum LDH release. Supernatants were aspirated and replaced with serum-free media post adsorption. Every 24 h for a total of 96 h, cell supernatants were harvested, and plasma membrane damage was quantified in comparison with media-only negative controls and kit-provided positive controls based on the manufacturer protocol (ThermoFisher Scientific, CyQUANT™ LDH Cytotoxicity Assay). Absorbance at 490 and 680 was measured directly upon assay completion using the Biotek Synergy Neo 2 with accompanying Gen 5.309 software.

Extracellular Vesicle Enrichment. To enrich large EV, medium EV, and small EV/free virus populations using sequential centrifugation, serum-free cell supernatants were first harvested from cells. Cell debris was pelleted and discarded following centrifugation at 300 × *g* for 10 min. The resulting supernatant was centrifuged at 2,000 × *g* for 25 min to pellet large EVs, then at 10,000 × *g* for 30 min to pellet medium EVs, and then at 100,000

× *g* for 2 h to pellet a mixed population of small EVs and free virus particles. Pelleted EV fractions were re-suspended in virion storage buffer (5 M NaCl, 1 M $MgCl_2$, 1 M Tris pH 7.4) and stored briefly at 4°C or immediately employed in an assay.

Iodixanol Gradient Separation of Medium EVs, and Small EVs/Free Virus. L cells (1.5 × 10^7 cells/flask) in complete media were seeded in T150 flasks and incubated until ~ 90% confluency. Cell debris, large EVs, and medium EVs were cleared from serum-free T1L-infected or T3D-infected supernatants by sequential differential centrifugation, as described above. The resulting supernatant was concentrated on a 2 ml 60% iodixanol cushion in 0.25 M sucrose and 10 mM Tris, pH 7.5 at 100,000 × *g* for 4 h [189]. Following ultracentrifugation, 3 ml of iodixanol cushion plus concentrated supernatant were collected from the bottom of the ultracentrifuge tube and mixed. The resulting small EV/free virus concentration was loaded into a separate ultracentrifuge tube. Atop this layer, 20%, 10%, and 5% iodixanol layers (diluted from 60% stock with 0.25 M Sucrose; 10 mM Tris pH 7.5) were added sequentially. The gradient was centrifuged at 100,000 × *g* for 18 h. Then, 12 × 1-ml fractions were drawn starting at the top of the gradient. Resulting 1ml fractions were washed with PBS, concentrated at 100,000 × *g* for 2 h, gently pipetted to re-distribute the iodixanol, then concentrated again at 100,000 × *g* for 1 h to allow for separation of small EV populations and free virus populations to density-dependently separate from one another. Following this final centrifugation step, a total of 12 × 1ml fractions were drawn, with fraction 1 at the top of the tube and fraction 12 at the very bottom of the tube. Resulting 1-ml fractions were washed with 1 × PBS and re-

concentrated at 100,000 × g for 2 h, gently pipetted again to re-distribute the iodixanol without disturbing the pellet, then concentrated again at 100,000 × g for 1 h. Pelleted EV fractions were resuspended in virion storage buffer. Equal volumes of each fraction were loaded onto an SDS-PAGE immunoblot, transferred to nitrocellulose, and blocked using Pierce Protein-Free PBS Blocking buffer (ThermoScientific). Many thanks to Dr. Alissa Weaver for allowing us to adapt and employ her protocol.

Medium EVs were harvested from infected cells as described above. Medium EVs were concentrated on a 2 ml 60% iodixanol cushion in 0.25 M sucrose and 10 mM Tris, pH 7.5 at 10,000 × *g* for 30 min [189]. Following ultracentrifugation, 3 ml of iodixanol cushion plus concentrated supernatant were collected from the bottom of the ultracentrifuge tube and mixed. The resulting medium EV concentrate was loaded into a separate ultracentrifuge tube atop a 60% iodixanol layer. Atop this layer, a 35%, 30%, 28%, 24%, 22%, and 20% iodixanol layer (diluted from 60% stock with 0.25 M Sucrose; 10 mM Tris pH 7.5) was added sequentially [152]. The gradient was centrifuged at 100,000 × *g* for 18 h. Then, 24 × 0.5 ml fractions were drawn starting at the top of the gradient. Resulting fractions were washed and resuspended as described above.

Virus-EV Immunoblotting Assays. To determine reovirus protein association with large EVs, medium EVs, and small EVs, L cells (1.5×10^6 cells/flask) or Caco-2 cells (2.5×10^6 cells/flask) in complete media were seeded in T25 cell culture flasks and incubated until ~ 90% confluency. Cells were adsorbed in triplicate with media alone (mock), with three clones of T1L or T3D at an MOI of 1 PFU/cell (L cells) or 5 PFU/cell (Caco-2 cells), then

inocula were aspirated and replaced with serum-free media. Caco-2 cells were infected with rSA11 at an MOI of 0.01 PFU/cell. Inocula were replaced with serum-free media post-adsorption. Cell culture supernatants were collected every 24 h for 96 h. At each timepoint, EV fractions were enriched via sequential differential centrifugation, as described above. Mock-infected cell supernatants were collected at 96 h post infection. Each EV sample was resuspended in 25µl of virion storage buffer and mixed with an equal volume of 2× Bio-Rad Sample buffer containing β-mercaptoethanol. Samples were boiled at 95°C for 5 min and pipetted vigorously to ensure a homogenous suspension. A small volume (10µl) of each sample was loaded onto a 10% hand-cast SDS-polyacrylamide gel, transferred to nitrocellulose, and blocked using Pierce Protein-Free PBS Blocking buffer (ThermoScientific). Reovirus proteins were detected using polyclonal reovirus antiserum (1:1000) and LI-COR IRDye 680LT Goat anti-Rabbit (1:15,000). Small EV marker CD81 was detected using monoclonal anti-CD81 antibody (1:400) and LI-COR IRDye 800LT Goat anti-Mouse (1:15,000). T1L nonstructural protein σNS was detected using guinea pig polyclonal anti-σNS antisera (1:1,000) and LI-COR IRDye 680LT Goat anti-guinea pig (1:15,000) [108]. T3D nonstructural protein σNS was detected using mouse monoclonal anti-σNS antibody 2H7 (1:1,000) and LI-COR IRDye 800LT Goat anti-Mouse (1:15,000) [153]. AnnexinA1 proteins were detected on a separate immunoblot using polyclonal AnnexinA1 antibody (1:250) and LI-COR IRDye 680LT Goat anti-Rabbit (1:15,000). Signal was detected using a Bio-Rad ChemiDoc MP Imaging System. Reovirus λ3, σNS, AnnexinA1, and CD81 protein bands were quantified with adjustment for background using the BioRad ImageLab analysis software. To compare signals from

multiple experiments, the 96 h timepoint value for the small EV/free virus sample was set to 100%, and all other samples were adjusted based on this value.

EV Marker Western blotting. L cells (1.5×10^7 cells/flask) in complete media were seeded in T150 flasks and incubated until ~ 90% confluency. Each flask was adsorbed with media alone (mock) or adsorbed with 1 PFU/cell of T1L or T3D in serum-free media. After 96 h of infection in serum-free media, cell supernatants were harvested. Large EV, medium EV, and small EV/free virus fractions were harvested as described above. To generate mock-infected cell lysates, L cell monolayers were washed with ice-cold PBS. Then, 500 μl of RIPA buffer was added on ice, the flask surface was scraped, and the lysate was collected. All samples were resuspended in virion storage buffer and mixed with an equal volume of 2× Bio-Rad Sample buffer containing β-mercaptoethanol. Samples were boiled at 95°C for 5 min and pipetted vigorously to ensure a homogenous suspension. An equivalent volume (30μl) of each sample was loaded onto a 10% hand-cast SDS-PAGE gel and run at 180V for 50 min. All gels were taken through a standard Western blot protocol, as denoted above, and stained for presence of reovirus protein using a polyclonal anti-reovirus serum (1:1000), or the presence of EV protein using AnnexinA1 (1:250), CD81 (1:400), TSG101 (1:1000), ALIX (1:1000), and LC3A/B (1:250). Secondary antibodies were utilized depending on species specificity, including and LI-COR IRDye 680LT Goat anti-Rabbit (1:15,000) and LI-COR IRDye 800CW Goat anti-Mouse (1:15,000). Blots were imaged using the Bio-Rad ChemiDoc MP Imaging System.

Reovirus-Mock EV Association Assays. L cells (1.5×10^7 cells/flask) in complete medium were seeded in T150 flasks and incubated until ~ 90% confluency. Cells were either adsorbed with T1L or T3D at an MOI of 1 PFU/cell, or with medium only (mock); for every T1L-infected or T3D-infected flask, three mock-infected flasks were seeded and adsorbed. Inocula were aspirated and replaced with serum-free media. After 72 h, reovirus-infected cell culture supernatants were collected and enriched in equal volumes for large EV and medium EV fractions by sequential differential centrifugation to generate the "virus-infected EV' fraction. In parallel, mock-infected cell culture supernatants were collected and enriched in equal volumes for large EV and medium EV fractions by sequential differential centrifugation. These mock-infected EV fractions were incubated at 4°C for 2 h with an equal volume of 1×10^9 PFU/ml free reovirus particles harvested via iodixanol gradient centrifugation to generate the "FV input", or with virion storage buffer. Samples were then re-pelleted at respective centrifugation speeds to obtain the "FV + mock EV" and the "FV + buffer" samples. Equal sample volumes were resolved using SDS-PAGE with Coommassie blue staining, or with immunoblotting using polyclonal reovirus antiserum (1:1000) and LI-COR IRDye 680LT Goat anti-Rabbit (1:15,000). Signal was detected using a Bio-Rad ChemiDoc MP Imaging System. The reovirus λ3 protein band was quantified with adjustment for background using the BioRad ImageLab analysis software.

Detergent, Mechanical, and Storage Virus-EV Disruption Assay. L cells or MA104 cells (1.5×10^7 cells/flask) in complete media were seeded in T150 flasks and incubated

until ~ 90% confluency. L cells were mock-adsorbed with medium or adsorbed with 1PFU/cell of T3D in serum-free medium. MA104 cells were mock-adsorbed with medium or adsorbed with 0.01PFU/cell of rSA11 in serum-free medium. After a period of 72 h, cell supernatant was harvested from each flask and divided into equivalent aliquots. Supernatants were centrifuged as described above to harvest large and medium EVs for detergent-specific samples, or medium EVs only for mechanical/storage-specific samples.

For the detergent-specific samples, the large EV and medium EV fractions were resuspended in a small volume of detergent-free PBS, and equivalent volumes were aliquoted into separate Eppendorf tubes. Large EV and medium EV samples were resuspended in a PBS solution containing 0 – 20% SDS or DOC detergent, and 0 – 40% TritonX-100 or Tween20 detergent. All samples were then vortexed briefly and allowed to incubate at room temperature for 30 min. Samples were then re-centrifuged at 2,000 × g for 25 min and at 10,000 × g for 30 min, respectively, to harvest any large and medium EVs remaining post-detergent treatment.

For mechanical/storage-specific samples, medium EVs were resuspended in a small volume of virion storage buffer, and equivalent volumes were aliquoted into separate Eppendorf tubes. Each sample was either left untreated (“4°C”, “immediate” samples) or subjected to several different treatment conditions (“freeze-thaw” cycles, “freeze-thaw” cycles with 20 min of sonication, sonication for 2 min, sonication for 20 min, treatment with 20% DOC, storage for 1 h at 4°C, storage for 24 h at 4°C, storage for 1 week at 4°C, and storage for 1 week at -80°C). For reovirus freeze-thaw-specific conditions, two cycles of freeze-thaw were used. For rotavirus freeze-thaw-specific

conditions, three cycles of freeze-thaw were used. For sonication-specific conditions, a Qsonica cuphorn sonicator was used. The cuphorn was filled with deionized water and ice to keep the samples cold throughout treatment. The cuphorn was used under 75% amplitude with pulses of 15 s ON, 10 s OFF for a total time of either 2 min or 20 min. Samples were then re-centrifuged at 10,000 × *g* for 30 min to harvest medium EVs remaining after mechanical disruption or storage.

All samples were resuspended in a small volume (25µl) of Tris-based virion storage buffer and mixed with an equal volume of 2X Bio-Rad Sample buffer containing β-mercaptoethanol. Samples were taken through a standard Western blot protocol and stained for presence of reovirus protein using a polyclonal anti-reovirus serum (1:1000), polyclonal anti-rotavirus serum (1:1000), or the presence of EV protein using AnnexinA1 (1:250), in addition to LI-COR IRDye 680LT Goat anti-Rabbit (1:15,000). Blots were imaged using the Bio-Rad ChemiDoc MP Imaging System. One specific protein band was chosen and quantified with adjustment for background noise using the BioRad ImageLab analysis software.

Negative-Stain Transmission Electron Microscopy. For *in vitro* samples, cells (1.5×10^7 cells/flask) or Caco-2 cells (2.0×10^7 cells/flask) in complete media were seeded in T150 flasks and incubated until ~ 90% confluency. Cells were adsorbed with T1L or T3D at an MOI of 1 PFU/cell, or with medium alone (mock-infected), and then inocula were aspirated and replaced with serum-free medium. Caco-2 cells were infected with rSA11 at an MOI of 0.01 PFU/cell. After 72 h for reovirus, or 48 h for rotavirus, cell culture

supernatants were collected and enriched for large EV and medium EV fractions (reovirus) or for medium EVs only (rotavirus) by sequential differential centrifugation. L cell-derived fractions enriched for small EVs and free virus were further separated using density-dependent gradient separation, as described. Caco-2-derived small EVs and free rotavirus were harvested as a mixed population via centrifugation at 100,000 × g for 2 h at 4°C.

For *in vivo* samples, a litter of 3 day-old C57BL/6 WT mice pups were adsorbed with 1×10^8 T1L PFU/mouse. At 2 d post infection, mice were humanely euthanized, and their colon contents were harvested. Large EV, medium EV, and small EV/FV fractions were harvested from colon contents resuspended in 500μl of virion storage buffer via sequential differential centrifugation.

All samples were submitted to the Vanderbilt University Cell Imaging Shared Resource Core under the care of Dr. Evan Krystofiak. Purified samples were adhered to freshly glow discharged carbon coated 300 mesh Cu grids for 30s followed by negative staining using 2% uranyl acetate. Transmission electron microscopy was conducted using a Tecnai T12 operating at 100 keV with an AMT nanosprint5 CMOS camera.

Thin-Section Electron Microscopy. For whole cell samples, L cells (3.8×10^6 cells/dish) in complete medium were seeded in 200 mm dishes and incubated until confluent. For medium EV samples, L cells (1.5×10^7 cells/flask) in complete medium were seeded in T150 flasks and incubated until ~ 90% confluency. Cells were adsorbed with T1L or with T3D at an MOI of 1 PFU/cell. For whole cell samples, after 24 h, cells were washed thrice

with pre-warmed PBS without Ca^{2+} or Mg^{2+} and fixed with 2.5% glutaraldehyde for 1 h at room temperature. For medium EV samples, medium EVs were harvested from T1L-infected L cells via sequential differential centrifugation after 72 h of infection. EVs were washed once with pre-warmed PBS without Ca^{2+} or Mg^{2+} and fixed with 2.5% glutaraldehyde for 1 h at room temperature. After fixation the samples were gently lifted and embedded in 2% low-melt agar. The samples were cryoprotected in graded steps up to 30% glycerol and plunge frozen in liquid ethane. After freezing, the samples were freeze-substituted at -80°C in 1.5% uranyl acetate in methanol for 48 h, then gradually raised to -30°C. Samples were infiltrated with HM-20 Lowicryl under a nitrogen atmosphere and polymerized with UV light for 48 h. Following polymerization, the samples were sectioned at a nominal thickness of 70 nm on a Leica UC7 ultramicrotome and imaged as described above. All samples were submitted to the Vanderbilt University Cell Imaging Shared Resource Core under the care of Dr. Evan Krystofiak.

Confocal Microscopy. L cells (1.25×10^5 cell/ml) were seeded in complete medium in a 24-well plate atop sterile 1 mm glass coverslips and incubated until ~ 90% confluency. Cells were adsorbed with T1L or T3D at an MOI of 1 PFU/cell, or with medium alone (mock-infected), and then inocula were aspirated and replaced with serum-free medium. At 48 h p.i., medium from cells was removed by gentle pipette aspiration and washed once with PBS containing Ca^{2+} and Mg^{2+}. CellBrite Fix Membrane Dye (Biotium, 30090-T) was freshly diluted to 1× concentration using PBS containing Ca^{2+} and Mg^{2+}. To each coverslip, 400µl of CellBrite dye was added and incubated at 37°C for 15 min. Coverslips

were washed thrice with PBS lacking Ca^{2+} and Mg^{2+}, then fixed by adding 400µl of 4% paraformaldehyde for 20 min at room temperature. Coverslips were washed twice with PBS lacking Ca^{2+} and Mg^{2+}, then stained by adding 400µl of reovirus polyclonal antibody serum (1:1000) in 0.5% Triton-X-100 (in PBS -/-) for 1 h 37°C in the dark with occasional gentle rocking by hand. Coverslips were washed twice with PBS lacking Ca^{2+} and Mg^{2+}, then stained by adding 400µl of AlexaFluor goat anti-rabbit Alexa-546 (1:1000) and 1 × DAPI (1:1000) in 0.5% Triton-X-100 (in PBS) for 1.5h at 37°C in the dark with occasional gentle rocking by hand. Coverslips were washed twice with PBS lacking Ca^{2+} and Mg^{2+} and mounted on sterile glass slides containing ProLong™ Gold Antifade Mountant (ThermoFisher P36930). Imaging was conducted using the Zeiss LSM 880 microscope under a 63X oil lens using airyscan Z-stacking.

Quantitation of Extracellular Vesicles Released from Infected and Uninfected Cells.

L cells (1.5×10^7 cells/flask) in complete medium were seeded in T150 flasks and incubated until ~ 90% confluency. Cells were adsorbed with medium alone (mock) or with three clones of T1L or T3D at an MOI of 1 PFU/cell, then inocula were aspirated and replaced with serum-free medium. After 72 h, cell culture supernatants were collected and enriched for large EV, medium EV, and small EV/free virus fractions by sequential differential centrifugation. A subset of samples were resuspended in equal volumes (50µl) of virion storage buffer, resolved by SDS-10% PAGE, and stained with PageBlue Protein Staining Solution (Thermo). Gels were imaged using a Bio-Rad ChemiDoc MP Imaging System, and proteins in entire lanes were quantified using Bio-Rad ImageLab analysis

software. To compare signals from multiple experiments, protein signal was normalized as a percentage of maximum by dividing each adjusted volume value by the highest measured value within the blot.

A subset of samples, which were subjected to annexin V immunoprecipitation (Miltenyi Biotec Annexin V Microbead Immunoprecipitation kit), was resuspended in 200μl of Annexin V Binding Buffer and incubated with Annexin V Microbeads for 2 h at 4°C with rotation. To each resuspended EV sample, 100μl of Annexin V Microbeads were gently added and incubated for 2 h at 4°C on a spinning platform. Samples were then flowed through a Miltenyi Biotec MS Column set onto a Miltenyi Biotec MiniMACS Separator twice over, columns were washed four times with 500μl of 1 × Annexin V Binding Buffer, and eluted via quick plunging. Eluates were resolved by SDS-10% PAGE and PageBlue protein staining , and quantified as described above.

A subset of samples, which were analyzed using confocal microscopy, were resuspended in equal volumes (40μl) of virion storage buffer and stored on ice. Samples were imaged one at a time—each sample was individually mixed with an equal volume of 1 μg/ml of 1,1'-Dioctadecyl-3,3,3',3'-Tetramethylindocarbocyanine Perchlorate resuspended in absolute ethanol (DiI; Invitrogen). The entire 80μl of sample was then loaded into the well of a Mattek 35mm dish (P35G-1.5-14-C), and a sterile 1.4 mm glass coverslip was floated over the top. Each dish was incubated for 5 min at room temperature and then imaged on a Zeiss LSM 880 microscope under a 63× oil lens**.** A total of 10 fields of view per sample, each comprising an 8 × 8 stitched tile, were imaged. DiI-positive puncta in each field were counted using the EVAnalyzer Fiji Software plugin [164], with

threshold settings applied uniformly across separate EV fractions to T1L-infected, T3D-infected, and mock-infected samples.

EV Neutralization Protection Assays. For *in vitro* samples, cells (1.5×10^7 cells/flask) or Caco-2 cells (2.0×10^7 cells/flask) cells in complete media were seeded in T150 flasks and incubated until ~ 90% confluency. Cells were adsorbed with media alone (mock), with three clones of T1L WT, T3D WT, or T1L-T3D O.C. hybrid at an MOI of 1 PFU/cell (L cells) or 5 PFU/cell (Caco-2 cells), then inocula were aspirated and replaced with serum-free media. Caco-2 cells were infected with rSA11 at an MOI of 0.01 PFU/cell. After 72 h for reovirus, or 48 h for rotavirus, cell culture supernatants were enriched for large EVs, medium EVs, and small EVs/free virus by sequential differential centrifugation. Free reovirus separated via iodixanol gradient assay was utilized as a reovirus neutralization control. For rotavirus, a passage 2 stock was utilized as a rotavirus neutralization control.

For *in vivo* samples, a litter of 3 day-old C57BL/6 WT mice pups were adsorbed with 1×10^8 T1L PFU/mouse. At 2 days post infection, mice were humanely euthanized, and their colon contents were harvested. Large EV, medium EV, and small EV/FV fractions were harvested from colon contents resuspended in 500µl of virion storage buffer via sequential differential centrifugation.

Samples were resuspended in virion storage buffer (120µl for *in vitro* samples, 600µl for *in vivo* samples) and divided into two equivalent aliquots. One half of the sample was mock-treated with serum-free medium, and the other half of the sample was treated with T1L or T3D σ1 head-specific antiserum (1:100), or with anti-rotavirus serum (BQ1,

1:100) for 2 h at 4°C. At the 1 h incubation timepoint, samples were mixed via gentle pipetting. Then, virus titer in each sample was quantified by plaque assay using the dilution yielding a range of 40-70 plaques to calculate the titer. The percent infectivity level retained post-neutralization was determined by dividing the treated sample titer by the titer of its untreated counterpart.

EV Protease Protection Assays. L cells (1.5×10^7 cells/flask) in complete medium were seeded in T150 flasks and incubated until ~ 90% confluency. Cells were adsorbed with medium alone (mock) or with three clones of T1L or T3D at an MOI of 1 PFU/cell, then inocula were aspirated and replaced with serum-free medium. After 72 h, cell culture supernatants were enriched for large EVs, medium EVs, and small EVs/free virus by sequential differential centrifugation. Samples were resuspended 200µl of virion storage buffer and divided. One half of the sample (98µl total volume) was mock treated with serum-free medium, and the other half of the sample was treated with 20 µg/ml of 2 mg/ml chymotrypsin stock (Sigma Aldrich) for 1 h at 37°C. After incubation, chymotrypsin activity was neutralized using 2% total volume of 100mM PMSF. Samples were resuspended in equal volumes, resolved by SDS-10% PAGE and immunoblotting. The conversion of EV-associated reovirus from virion to ISVP, evidenced by the loss of σ3 and µ1C proteins, was detected using polyclonal anti-reovirus serum (1:1000). Signal was detected using a Bio-Rad ChemiDoc MP Imaging System. Reovirus σ3 and µ1C protein bands were quantified with adjustment for background using the BioRad ImageLab analysis software.

The percent of σ3 and μ1C protein retained post-protease treatment was determined by dividing the treated sample protein signal by the protein signal of its untreated counterpart.

High-Resolution Melt Analysis of Genotype Mixing. L cells (4×10^5 cells/ml) in complete medium were seeded in 6-well plates and incubated until ~ 90% confluency. Cells were adsorbed with medium alone (mock) or co-infected with three independent dilutions of WT and BC reovirus at an MOI of 10 PFU/cell, then inocula were aspirated and replaced with serum-free medium. After 24 h, cell culture supernatants were collected and enriched for large EV, and medium EV, and small EV/free virus fractions by sequential differential centrifugation. Infectious units were then isolated by plaque assay. A total of 24 well-separated plaques per fraction per replicate were picked and amplified in L cell monolayers in 24-well plates for 2 days. RNA was extracted using TRIzol (Invitrogen), reverse transcribed using random hexamers, and genotyped using HRM, as previously described, using primers specific for the L2 segment [97]. Each sample genotype was called by Applied Biosystems High Resolution Melt Software v3.2 and visually verified by comparison with control reactions containing WT RNA, BC RNA, and mixtures (1:8, 1:4, 1:2, 1:1, 2:1, 4:1, 8:1) of WT and BC RNA.

Rotavirus EV Fingerprinting. MA104 cells (4×10^6 cells/well) in complete medium were seeded in 6-well plates and incubated until ~ 90% confluency. MA104 cells were adsorbed with serum-free medium alone (uninfected) or with three individual dilution inocula of rSA11 rotavirus at an MOI of 0.1 PFU/cell for a period of 12 h or 24 h. Infected

or uninfected supernatants were harvested at each timepoint, cleared of cell debris via centrifugation, and given to our collaborator. EVs were labeled using a proprietary method detailed in the referenced pre-print with di-8-ANEPPS and detected via multiparametric imaging flow cytometry [165]. The events per minute and the heterogeneity of resulting EV populations is depicted using Uniform Manifold Approximation Projection.

Statistical analyses. GraphPad Prism version 10 was used for all statistical analyses. The statistical analyses used are indicated in each figure legend and are denoted separately for each data set. Statistical tests were chosen in consultation with a biostatistician.

Biorender acknowledgement. The following figures were created with Biorender: Figures 1-8, Fig. 10A, 14A, 16A, 22A, 26A, 28A, 34.

CHAPTER V: CONCLUSIONS, DISCUSSION, AND FUTURE DIRECTIONS

SUMMARY OF FINDINGS

Prior to my thesis work, the involvement of EVs in reovirus egress was an entirely undiscovered phenomenon, and the effect of host cell-assisted egress on reovirus infection was a mystery. In Chapter II, I provide evidence that in two separate cell types, infectious units of two reovirus strains with opposing membrane disruption capacities egress both as free virus particles and associated with large and medium EVs, and not with small EVs (**Fig. 34**). This association is not simply artefactual reovirus binding to cell membranes, and instead appears to be a specific and direct association with EV structures that measure, on average, 600-1000 nm in diameter. These EVs are resilient against mechanical disruption and detergent treatment, and can withstand a variety of storage conditions. Reovirus particles appear visually to be packaged inside of EVs that bud from the plasma membrane in a phenotype that is reminiscent of the hallmark biogenesis pattern of microvesicles. In Chapter III, I provide evidence that medium EVs can protect reovirus and rotavirus particles from antibody neutralization and protease degradation in a cell type- and virus strain-dependent manner, and that this protection phenotype may be influenced by the virus's capacity to induce cell death (**Fig. 34**). Such neutralization protection potentially occurs *in vivo* as well, as I observe an overall general trend towards reovirus particle protection by medium EVs harvested from infected mice. Additionally, EVs permit reovirus to be transmitted between cells in multiparticle infection units. Finally, reovirus and rotavirus both enhance the release and abundance of EVs of all sizes during the course of infection.

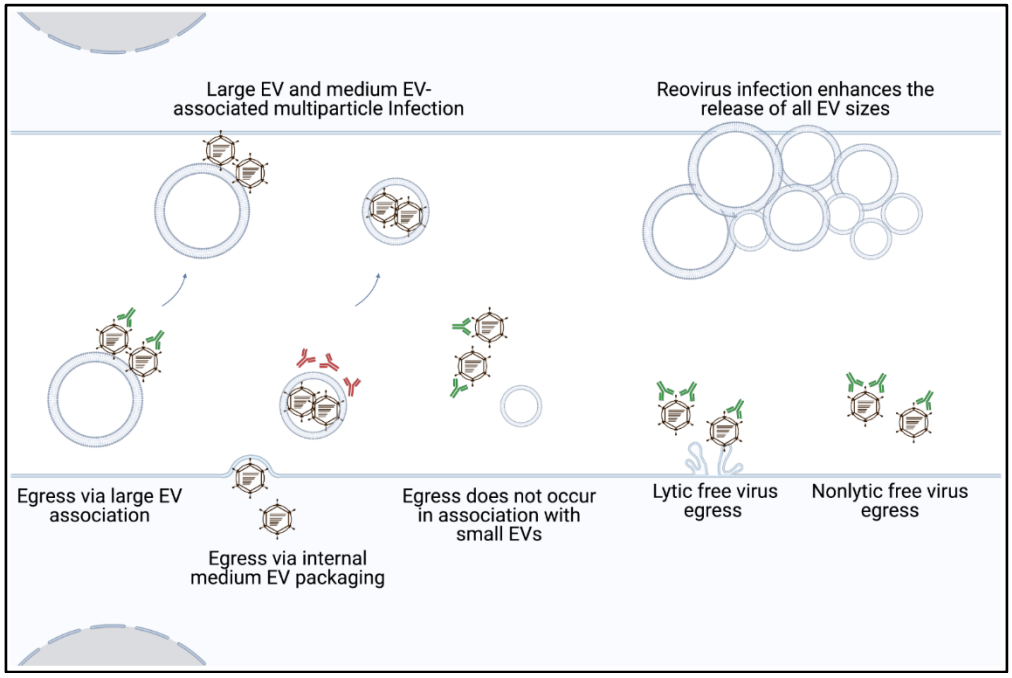

Figure 34. Model of reovirus release and infection in association with EVs. My work indicates that in addition to exiting as free particles, reovirus strains that efficiently or inefficiently disrupt membranes can egress from mouse fibroblast and human colon epithelial cells in association with EVs. Reovirus particles are strain-specifically, cell type-dependently enclosed within and protected from antibody-mediated neutralization by medium EVs. Both large and medium EVs can transport multiple reovirus particles to recipient cells. Furthermore, compared to uninfected cells, reovirus infection enhances cellular release of EVs of all sizes.

DISCUSSION OF EV-FACILITATED AND FREE VIRUS EGRESS AND PROPOSAL OF FUTURE DIRECTIONS

Discussion: A model of EV-mediated and free reovirus egress and enhancement of EV release

Based on the data I have presented here, I foresee a model in which reovirus uses four distinct pathways to egress from infected cells: i) bound on the outside of large EVs, ii) packaged internally as medium EV cargo, iii) as free virus released by membrane lysis,

and iv) as free virus released using a mechanism involving “sorting organelles” and “membranous carriers”, or, alternatively, via an undefined method of egress [10,125].

Reovirus may employ multiple pathways during its egress from an infected cell, and the pathways reovirus uses may vary based on the host cell type and the virus strain in question. Precedent for a “dual EV egress” strategy exists for encephalomyocarditis virus, which exits cells in two distinct EV subtypes [70]. One of the EV subtypes carries markers that originate from the plasma membrane, which is reminiscent of microvesicles, and one of the EV subtypes carries markers that originate from lysosomal and autophagy pathways, which is reminiscent of secretory autophagosomes. Thus, it is possible that infectious units of T1L and T3D associate with both large EVs and with medium EVs, but perhaps association with each EV subpopulation is different.

How does reovirus associate with medium EVs, and what type of EVs are present in the medium EV population? I provide evidence that T1L and T3D are protected from neutralization when associated with medium EV structures (**Fig. 22**). Thus, I think it very likely that reovirus is loaded as cargo on the interior of these EVs. There are a few indicators that the medium EV fraction might be comprised of microvesicles. They are of the correct general size, averaging roughly 600nm in diameter, which falls in line with the average size range detected for microvesicles (**Fig. 12**). Furthermore, two methods of imaging have revealed the same phenomenon—reovirus particles egress in these medium-sized EVs following a pattern in which the plasma membrane curves outward,

encapsulates reovirus particles, and appears to pinch fully off from the rest of the cell (**Fig. 19**). This biogenesis phenotype is strongly reminiscent of the hallmark biogenesis pattern of microvesicles. If the markers that are thought to associate with microvesicles were also consistently and exclusively present in the medium EV fraction from reovirus-infected cells, I would be more confident in defining the reovirus-containing medium EV fraction as microvesicles. However, the microvesicle marker we used, in addition to several others that were not shown, have not specifically segregated with this EV fraction (**Fig. 18)**. EV markers are highly dependent on the cell of origin, and therefore a more thorough and dedicated look at markers specific to L cell-derived EVs is needed; EV markers are widely acknowledged to be heterogenous, often overlapping between EV subpopulations and changing based on the cell's physiology [26]. Additionally, I cannot rule out the potential involvement of secretory autophagosomes in the medium EV fraction—based on their size, secretory autophagosomes would potentially collect in the medium EV fraction. However, when I visualize reovirus egress by confocal microscopy and by TEM, I observe distinct plasma membrane protrusion and budding, which is reminiscent of microvesicles; if these EVs were secretory autophagosomes, I would expect to observe double-membrane vesicles inside of cells that would fuse with the plasma membrane [190]. Thus, it is difficult to define the EV subtype that reovirus associates with in the medium EV fraction, though signs such as size and visual biogenesis pattern point towards microvesicles.

Likewise, how does reovirus associate with large EVs, and can I more definitively identify the type of EVs that are present in the large EV population? T1L and T3D both associate with large EVs derived from both L cells and Caco-2 cells (**Fig. 10B-F, Fig. 21A-C**). I do not think that large EV association is the result of reovirus being loaded as interior EV cargo. Given the evidence that T1L and T3D are both neutralized when associated with large EVs, I think that it is unlikely that reovirus is enclosed by this EV fraction (**Fig. 22 and 124**). Rather, I hypothesize that this association occurs when a portion of the free reovirus particles that are released from infected cells adhere to the exterior of cell debris and large EVs. This hypothesis is supported by prior studies that found that large quantities of infectious reovirus remain associated with cell debris following cell death induction [147]. It is also possible, based on their general size range and the centrifugation speed at which they pellet, that secretory autophagosomes populate the large EV fraction. I do observe autophagosome markers present most strongly in the large EV fraction; though I do not have direct evidence, perhaps secretory autophagosomes populate the large EV fraction and bind reovirus externally, whilst microvesicles populate the medium EV fraction and bind reovirus internally (**Fig. 18**). Reovirus does interact with and extensively remodel many checkpoints along the secretory autophagosome pathway, including inducing autophagic machinery and modulating the pH, size, and abundance of lysosomes; this evidence, if considered alongside the role of lysosomally-derived vesicles in the only other example of reovirus nonlytic egress that we have to-date, leads me to think that it is very possible for reovirus egress to be involved with secretory autophagosomes in some way [124,125].

It is clear that reovirus infection upregulates the abundance of EVs released from cells (**Fig. 30-31**). The EVs harvested from mock-infected large and medium EV fractions averaged around 100-200nm in diameter, and the EVs harvested from reovirus-infected large and medium EV fractions were substantially larger (**Fig. 12**). One caveat, however, is that roughly thrice the number of cells is required to match the abundance of EVs as those released from infected cells; it would be a good idea, in the future, to repeat the negative stain EM imaging of EVs harvested from thrice the number of mock-infected cells (**Fig. 30**). Under pathological conditions, virus infection has been documented to alter the size, composition, and cargo of EVs [191,192]. Therefore, I speculate that not only does reovirus infection upregulate EV abundance, but it specifically upregulates the size of EVs to potentially encourage its own loading into and association with large and medium EVs. These EVs are resilient against mechanical and detergent disruption and can even be stored under a variety of conditions without degrading reovirus-EV association (**Fig. 17**). Thus, if reovirus infection promotes encapsulation inside of medium EVs, this could represent a mechanism of egress in which reovirus ensures it is well-protected from the environmental elements existing outside of a host to a greater extent than perhaps free reovirus would be protected. The question remains, however—if reovirus infection does specifically orchestrate its own loading into said EVs, what cell processes does it modulate in order to accomplish this? Reovirus extensively remodels cellular processes and proteins. Reovirus infection has been shown to upregulate proteins involved in cell structure organization on a whole-cell scale [128]. Reovirus additionally interacts with specific autophagy proteins in order to induce autophagy and

thereby facilitate an enhanced, more productive state of replication and infection [124]. Interestingly, reovirus replication depends on interaction with endoplasmic reticulum-derived vesicles and remodeled membranes, and its egress in one cell type was found to induce relocation and upregulation of lysosomal proteins [106,107,125]. Thus the framework for reovirus-induced cellular modulation of EV release is set, including cell structure and pathway reorganization and membrane remodeling. Perhaps some of the reovirus determinants that participate in these cellular remodeling strategies are the same ones that participate in EV abundance upregulation and cargo loading. I would hypothesize that those reovirus determinants that are structurally located on the exterior of the mature reovirus particle would be the most likely interacting partners for these EV biogenesis molecules, and may play the biggest role in the above scenario. However, at the present time, direct reovirus interaction with specific canonical EV biogenesis pathways is unknown.

Although EV-mediated egress is one strategy that reovirus uses to exit cells, it is not the only route of egress. I observe that a portion of T1L and T3D exit cells as standalone free virus particles that do not associate with any EV fraction (**Fig. 14)**. How, then, is the free reovirus exiting from cells? Bluetongue virus has been previously documented to egress using multiple different egress strategies [54,143]. In addition to inducing cell lysis, bluetongue virus also uses an ESCRT-dependent EV biogenesis pathway to bud nonlytically from the plasma membrane in multiparticle EVs that carry lysosome- and exosome-derived markers. Thus, I hypothesize that T1L and T3D both

follow a similar “dual egress strategy” by which virus escapes the cell in association with medium EVs, while free particles are simultaneously released using an independent egress pathway and potentially bind to the outside of large EVs. I hypothesize that free T3D virus may escape the cell when T3D induces lysis (**Fig. 9B-C and 20C-D**). T1L infection and egress, on the other hand, occurs in the near-complete absence of membrane disruption. This observation falls in line with the nonlytic nature of the large EV- and medium EV-associated T1L egress that I observe but does not explain how the free T1L virus particles that I detect are able to exit cells.

I hypothesize that there is an additional host-assisted mechanism that T1L triggers in order to facilitate nonlytic free virus exit. One prior study reported that T1L free virus egresses nonlytically in HBMEC cells [125]. The authors found that “membranous structures” carrying markers of lysosomal origin bud from reovirus replication factories carrying mature reovirus particles. From these membranous carriers, smaller membrane-bound “sorting organelles” fuse with the plasma membrane to release free virus particles without incurring plasma membrane disruption. I can envision a similar mechanism of T1L free virus release, wherein membrane-bound host cell-derived structures ferry bundles of T1L particles from replication factories to the plasma membrane where the membrane-bound structures then fuse with the plasma membrane to nonlytically release free T1L particles. It is possible that free T3D virus additionally takes advantage of this host cell-assisted nonlytic system as well when free T3D virus escapes during cell lysis. Using thin section TEM to visualize cross-sections of reovirus-infected EVs, I have captured instances

wherein it appears that reovirus virus particles are associated with a host cell membrane-bound structure that are further loaded inside of medium-sized EVs as internal cargo (**Fig. 13**). Perhaps these membrane-bound structures are lysosomally derived, an origin which would agree with previous findings [125]. However, it is unclear whether these virus particles are infectious, as some of the particles do not look whole. Whether this disruption is a feature of the virus being degraded by the smaller membrane-bound structure, or whether this is a technical artefact arising from an imperfect cross-section, is currently unclear. Further investigation will be required to support these preliminary observations. Furthermore, free reovirus may egress using a pathway that is not explained by any of the points presented above. Most of the work I presented in this dissertation has been conducted in L cells, a cell line that has been well-studied. Thus far, no evidence of sorting organelles or membranous carriers has been found. Then again, until the publication of my paper, no evidence of EV-associated reovirus egress had been reported in this cell type either; perhaps this will encourage other researchers to begin delving into the topic of reovirus egress with renewed enthusiasm and interest.

For both EV-facilitated and free virus release, it is required for each virus particle to shuttle from their replication factory of origin towards the plasma membrane. Utilizing the cytoskeletal cell network for such a trafficking event may be the most plausible option to accomplish this goal, and, assuming that medium EVs are indeed microvesicles, may explain how reovirus is loaded into medium EVs at the plasma membrane as internal cargo. The two main cytoskeletal networks present in most cells are microtubules and

actin. Reovirus interacts with microtubules during entry into a cell, and it has been shown that correct sorting of reovirus into specific endosomal compartments relies on reovirus co-localization with microtubule structures [193]. This interaction, however, occurs at the beginning of the replication cycle which is far upstream from the point of reovirus egress. If we focus further downstream in the replication cycle, closer to the timing of reovirus egress, it has been documented that the shape of reovirus replication factories is dependent on microtubule interactions [112]. T1L, which interacts with microtubules, forms morphologically filamentous replication factories. T3D, which does not interact with microtubules at this stage in the replication cycle, forms morphologically globular replication factories. Thus, T1L can possibly take advantage of the microtubule network in order to traffick closer to the plasma membrane, or perhaps as infection progresses, those replication factories which are spindled out closest to the plasma membrane are the ones that egress. A single P208S polymorphism in the μ2 reovirus protein has been documented to exchange the strain-specific filamentous and globular replication factory observed for T1L and T3D [106]. As a future direction, it might be interesting to create a hybrid virus in which the replication factory morphology is exchanged between T1L and T3D to test whether replication factory morphology influences the egress pathway.

Because T3D does not associate with microtubules, there must be another mechanism by which T3D virus trafficks from replication factories towards the plasma membrane. Thus, the role of actin must be considered. A previous study found that rotavirus, which is in the same order as reovirus, is capable of egressing from cells via a

nonlytic actin-dependent mechanism through interaction with lipid rafts [194]. When actin motility was blocked, rotavirus egress was inhibited accordingly [195]. Reovirus may additionally interact with actin—when mature reovirus particles are loaded into membranous carriers in HBMEC cells, filaments resembling actin were observed to tether each reovirus particle to the vesicular carrier as the carrier participated in shuttling reovirus to the plasma membrane for egress [125]. Actin additionally participates in cargo loading of exosomes and in restructuring the plasma membrane during microvesicle biogenesis, and may additionally play a role in microvesicle cargo loading [26]. Though I do not have any direct evidence to support this hypothesis, an actin-dependent mechanism of phytoreovirus-EV trafficking and egress has been elucidated [136]. Therefore, I propose that actin filaments may play a role in shuttling reovirus particles from replication factories to the plasma membrane where reovirus escapes either in association with EVs or as free particles.

Overall, it appears that although T1L and T3D have opposing membrane disruption phenotypes, they both employ a "dual egress strategy" by egressing nonlytically in association with large and medium EVs, and by either lytically or nonlytically releasing free virus particles as well. Though this model seems conceivable, many additional questions remain, and future experimentation is needed to reveal additional insights into the detailed mechanisms of reovirus egress.

<u>Future direction: Evaluation of the EV biogenesis pathways with which reovirus interacts during egress</u>

Above, I discussed the difficulty in assessing the origin of reovirus-associating large and medium EVs given the information we currently have. Though size and biogenesis patterns point toward the reovirus-containing EVs being of microvesicle origin, I do not know enough at the present time to conclude this with certainty. Thus, a careful study addressing the biogenesis pathways reovirus interacts with upon egress will be important in future studies. To determine which EV pathways are required for reovirus egress, cells should be adsorbed with reovirus and then washed to remove unbound virus. Cells will then be left untreated or treated with separate EV inhibitors. 200μM calpeptin will inhibit microvesicle formation, 20μM GW4869 will inhibit exosome formation, 20μM chloroquine will inhibit secretory autophagosomes, and 10μM caspase inhibitors will inhibit apoptotic bleb formation [54,89,196]. As an important set of controls, cell viability using Trypan blue exclusion must be verified, and EV biogenesis and release depletion must also be verified, ideally using immunoblotting for EV-specific markers. Validation of these inhibitors via the use of cell viability and plasma membrane integrity assays will be an important step, as EV inhibitors are known to damage cells. Additionally, these inhibitors may cause off-target inhibitory effects amongst other EV pathways as well, since many of the same biogenesis proteins and molecules are shared between biogenesis pathways, and even at their strongest concentration, it is difficult to completely abolish EV biogenesis. After a period of inhibitor treatment, EV fractions should be isolated, and samples then immunoblotted for markers of exosomes, microvesicles, apoptotic blebs, secretory autophagosomes, and anti-virus serum. If reovirus egress is dependent upon a specific EV pathway or subpopulation, then EV-inhibited cells should show a markedly decreased

amount of virus signal associated with the medium EV fraction compared to untreated cells. These studies would help to determine the EV pathways that are required for EV-facilitated reovirus egress.

To validate and compliment the above findings, I propose the use of EM and confocal imaging to visualize reovirus egress. Using thin section TEM to look at the cross-section of infected cells, it may be possible to glean further information about the cellular and vesicular structures that reovirus associates with during egress, and to capture further instances of reovirus egress patterns (**Fig. 19A-B**). Using thin section TEM to visualize cross-sections of EVs may additionally be informative in interpreting how reovirus is packaged into or around large and medium EVs. To interrogate the colocalization of reovirus more specifically with specific EV pathways, once inhibitor studies have elucidated the most likely EV pathway(s) with which reovirus interacts, antibody-based staining of key molecules associated with that pathway(s) can be applied, in addition to reovirus staining. If super-resolution confocal microscopy is applied, it may be possible to quantify the level of reovirus co-localization with the targeted pathway. Furthermore, once a likely EV biogenesis pathway is identified, tools such as EV marker-stained intestinal organoid modeling can be used to better visualize EV egress in a more biologically relevant system, and EV marker-tagged EV populations that reovirus enhances upon infection could be identified using a technique similar to EV Fingerprinting [165]. These studies would further define the EV pathway and EV subpopulation with which reovirus interacts during its escape from a cell.

Discussion: EV-mediated neutralization and protease protection—implications for reovirus infection and the role of apoptosis.

In Chapter III, I revealed that medium EVs confer immune protection and protease degradation resistance on reovirus. Because T1L and T3D are specifically shielded from these extracellular stressors, it is likely that they are enclosed within medium EVs released from L cells, and that they are strain-specifically enclosed in medium EVs derived from Caco-2 cells (**Fig. 22-24**). This phenomenon is not exclusive to reovirus—EVs of various subtypes have been discovered to enable viruses including JC polyomavirus, enterovirus 71, hepatitis E virus, and HAV in evading antibody-mediated neutralization [12,69,72-74]. Therefore, multiple viruses across evolutionarily distinct families are shielded from immune defenses by EVs that are capable of internally packaging and protecting them. This represents a recurring strategy by which multiple viruses, reovirus included, can stealthily evade immune detection and neutralization to potentially prolong virus infection. Not only can EVs create a physical shield around these virus particles, but EVs enable nonlytic virus egress. By leaving cell plasma membranes intact, the cell immune responses such as necrosis, damage associated molecule release, and pathogen-associated molecule release which are usually upregulated during lytic egress are instead dampened [197]. Additionally, the phosphatidylserine that is generally exposed universally on the EV surface dampens the immune response by triggering anti-inflammatory immunosuppressive cytokine signals [75]. Phosphatidylserine also stimulates phagocytic uptake which facilitates EV binding to recipient cells. Thus, the shielding characteristics of medium EVs may help protect reovirus from immune system defenses

when reovirus is in the extracellular environment, the immunosuppressive characteristics of EVs may help reovirus evade immune detection, and the “eat me” characteristics of EVs may help reovirus ensure more efficient cellular uptake.

Although EV protection may be advantageous in some situations, in others, it may be a hinderance. I observe a trend towards medium EV-facilitated reovirus protection when protease treatment is applied (**Fig. 23**). T3D is highly sensitive to proteolytic cleavage in the intestine, to the detriment of T3D’s capacity to infect and spread *in vivo*; thus, such protease degradation protection elicited by medium EV encapsulation is likely to represent a potential mechanism whereby T3D is able to more successfully withstand the extracellular gut environment to engender more successful spread throughout a host. However, most reovirus strains do not feature this protease cleavage site, and thus, for more reovirus strains including T1L, conversion to ISVP is advantageous to ensuring a productive infection. Thus, protease degradation protection is potentially not advantageous for its infection cycle *in vivo.* Protection within a medium EV might present reovirus with a disadvantage, in which ISVP conversion is blockaded inside medium EVs and thus, *in vivo* infection and spread may not be as efficient. If reovirus is bound externally on large EVs, however, intestinal proteases would still be able to interact with reovirus, leading to ISVP conversion; therefore, perhaps large EV association is more advantageous to the reovirus replication cycle than protection within a medium EV, which may protect virus from immune attack but may hinder its ability to replicate.

I hypothesize that the capacity to induce apoptosis plays a role in the apparent cell type- and reovirus strain-dependent difference in EV-facilitated neutralization protection that I observe in L cells and Caco-2 cells (**Fig. 22 and 24**). In general, viral infection may be linked to apoptosis induction and EV biogenesis; dengue virus titer was enhanced upon overexpression of ALIX, a protein which is involved in apoptosis regulation and in ESCRT EV biogenesis pathways, and viral production was impeded when Alix was knocked down [198-202]. Additionally, EVs derived from virus-infected cells can play a modulatory role resulting in apoptosis and function dysregulation in recipient cells. Caco-2-derived EVs harvested from rotavirus-infected cells induced cell death in recipient CD4+ T cells [88]. EVs carrying HIV, Epstein-Barr virus, Rift Valley fever virus, Ebola virus, and Japanese encephalitis virus proteins induced neuronal cell death, T-lymphocyte cell death, T-cell and monocytic cell apoptosis, T cell apoptosis, and neuronal cell death, respectively [91,203-206]. Furthermore, apoptosis induction in infected cells may regulate viral escape in EVs. In HeLa cells, Sindbis alphavirus-induced apoptosis results in viral nucleocapsids and antigens co-localizing exclusively with EV-like structures that appear to bud from the plasma membrane of apoptotic cells [175]. Also in HeLa cells, chikungunya virus-induced apoptosis led to the formation of EV structures resembling apoptotic bodies [176]. When individual steps of the apoptosis and EV biogenesis were inhibited, chikungunya virus spread to neighboring cells was markedly impeded [176]. Therefore, documented precedent exists by which virus-induced apoptosis modulates whole-cell EV release patterns, impacts productive viral infection, modulates EV signaling to upregulate cell death in recipient cells, and affects EV-mediated viral escape. Thus, I imagine a

model in which T3D successfully induces apoptosis in L cells, which are not cancer-originating and are thus apoptosis-competent, and thus orchestrates its own internal packaging inside fully intact, neutralization-protective EVs [115,163]. Caco-2 cells, on the other hand, originate from a human colorectal adenocarcinoma and do not have fully intact apoptosis pathways [169,171-174,207,208]. Because Caco-2 cells are at least partially apoptosis-incompetent, T3D may not interact successfully with EV biogenesis pathways to orchestrate internal packaging, and is instead released lytically as free virus particles which may stick to the surface of medium EVs, but which offer no protection against antibody-mediated neutralization [147]. Thus, reovirus apoptosis induction may contribute to strain-specific variation in EV-mediated neutralization protection in Caco-2 cells. My preliminary findings, in which I exchange apoptosis induction capacity between T1L and T3D, lend support to this theory that apoptosis induction capacity potentially influences the capacity for EVs to bestow protection on reovirus particles (**Fig. 26**).

Overall, it is apparent that there exists a scenario in which EV-facilitated release significantly facilitates protection of reovirus particles while they transit between cells, potentially even prolonging reovirus infection by downregulating immune detection and response and upregulating the frequency with which reovirus enters permissive cells. The capacity to induce apoptosis may play a role in how reovirus is protected from degradation depending on the virus strain and host cell interaction pattern. However, the biological relevance of these theories remain untested, and future experimentation is required to determine how important these observations are *in vivo.*

Future direction: Identification of the reovirus determinants influencing EV-facilitated neutralization protection

In Chapter II, I observed that EV-facilitated neutralization protection of reovirus occurred in a cell type- and virus stain-dependent manner (**Fig. 22 and 24**). I additionally provided preliminary evidence suggesting a potential role for the reovirus outer capsid in determining whether EVs shield reovirus particles (**Fig. 26**). I hypothesize that two of the reovirus outer capsid determinants, S1 and M2, will play the largest role in influencing the protection phenotype due to their involvement in reovirus apoptosis induction capacity, for reasons I have discussed in detail in this chapter. Though I have provided the preliminary data to support the promising nature of this line of inquiry, much work remains in order to elucidate this gap in knowledge.

To begin this study, validation of the two hybrid viruses that I have engineered, T1L-T3D O.C. and T3D-T1L O.C., will be important. Electropherotyping of multiple hybrid virus clones for both hybrid viruses will be important to ensure that correct segment incorporation has successfully taken place. I do not foresee issues with successful segment incorporation. A growth curve timecourse of both of these viruses in Caco-2 cells will need to be compared to their WT parents in order to determine whether outer capsid exchange impacts viral replication in host cells. Based on the replication efficiency displayed by their WT counterparts, I expect that segment exchange may improve replication efficiency somewhat for the T1L-T3D O.C. virus, and somewhat lessen the replication efficiency for the T3D-T1L O.C. virus (**Fig. 20A-B**). I have already validated the impact of outer capsid exchange on reovirus plasma membrane disruption (**Fig. 26B**).

These initial experiments would define any baseline similarities and differences between the hybrid viruses and their WT parents.

Next, the association of each hybrid virus with EV fractions must be defined. Each of the steps detailed here will need to be compared to WT virus as a baseline control. I propose harvesting large, medium, and small EV fractions from hybrid-infected Caco-2 cells and comparing their structural and nonstructural protein association and infectious unit association with each EV fraction. I expect that nonstructural protein from both T1L-T3D O.C. and T3D-T1L O.C. will not associate with any EV fraction based on my evidence that nonstructural protein from neither parental virus associates with any EV fractions (**Fig. 21D**). I suspect that structural protein association of the T1L-T3D O.C. virus with each EV fractions may reach more equivalent proportions, and the T3D-T1L O.C. virus protein association with the medium EV fraction may lessen (**Fig. 21A-B**). Then, I propose visualization of this virus-EV association using negative stain EM imaging of large EV, medium EV, and density-separated small EV and free virus fractions. I have never pursued imaging of Caco-2-derived EVs for WT virus, and thus do not have any baseline on which to form a strong expectation; however, based on infectious unit association of both WT T1L and T3D with large, medium, and small EV/free virus fractions that do not change phenotype markedly between the WT strains, I expect to visualize hybrid virus particles associated with large EVs and medium EVs (**Fig. 21C**). Additionally, because both WT virus strains are neutralized when associated with the small EV fraction, and this does not appear to change between strains, I postulate that the small EV/FV fraction

contains a population of free hybrid virus particles that can be separated from the small EV population (**Fig. 24**). These experiments will define whether the reovirus outer capsid contributes to reovirus interaction with different EV subtypes during egress.

Finally, I would subject both O.C. hybrid viruses to a plaque reduction neutralization assay in comparison with WT virus as a baseline control. Based on my preliminary data, in which outer capsid exchange induced an “intermediate” membrane disruption and protection phenotype, I would expect the same “intermediate” EV-mediated protection phenotype for the O.C. hybrid viruses (**Fig. 26B-D**). Specifically, I observe that the T1L-T3D O.C. virus protection facilitated by medium EV association is not fully abolished by the T3D outer capsid, and instead retains about 20% protection (**Fig. 26D**). Compared to T1L WT virus, this represents a roughly 60% decrease in medium EV-mediated protection. I expect that the T3D-T1L O.C. virus would also display an “intermediate” protection phenotype. Roughly 5% of WT T3D virus infectivity is protected via medium EV association; I expect that the T3D-T1L O.C. hybrid would be rescued to a substantial degree, but that rescue would not be wholly and completely restored (**Fig. 22E**). If any of these segment exchange protection phenotypes prove to be promising, I propose creating several new viruses featuring a parental backbone with single segment exchanged between the two virus strains. These single segment exchanges would include all of the outer capsid determinants (S1, S4, M2, L2), and would allow us to identify which segment specifically is the most responsible for inducing EV-mediated neutralization protection. I would additionally include a double-segment exchanged virus featuring both an S1 and M2 combination, because both of these

segment determinants are thought to contribute most heavily to the capacity of reovirus to induce apoptosis, and these two segments may need to be present as interacting partners on the same virus particle in order to induce the highest amount of apoptosis possible. These experiments would illuminate the impact of the reovirus outer capsid on EV-mediated antibody neutralization protection, and may potentially pinpoint apoptosis induction capacity as a contributing factor.

Discussion: EV-mediated egress implications for multiparticle reovirus infection

It has previously been established that, in general, standalone particles of free virus are not efficient at establishing productive infection in host cells [15,209]. Although it may seem more intuitive that free virus particles would "cover more ground" and spread throughout cells with greater efficiency than their aggregated counterparts, this may in fact be a less productive route of infection. In contrast with free virus units, viral infectivity was enhanced when multiparticle BK polyomavirus, rotavirus, norovirus, poliovirus, and coxsackievirus associated with EV structures [15,57,68,69,144,180]. For reovirus specifically, the presence of bacteria enhances virulence, and it has been thought that multiparticle infection mediated through virus adhesion to bacterial cells is a potential mechanism of this observed phenotype [87,161]. A potential explanation for multiparticle infection generating enhanced productive infection is that host cell barriers may present an obstacle to virus replication when too few numbers of virus particles enter individual host cells [15,179]. EVs can aggregate numerous virus particles into a simultaneous collective group, thus increasing the viral load of a host cell and potentially removing host cell

barriers to initial viral replication by minimizing the amount of time needed to advance viral protein accumulation to the point that host cell defenses can be overcome and productive replication can take hold [83]. Aggregation of multiple reovirus particles into a single, collective infectious unit that simultaneously infects a host cell may allow reovirus to overcome host cell barriers to infection quickly and efficiently. Thus, by aggregating multiparticle populations of reovirus into single infectious units, egress in large and medium EVs potentially represents a biologically advantageous strategy that allows reovirus to infect cells with greater efficiency and thus replicate with higher productivity than their free reovirus counterparts. Multiparticle aggregation has been shown to increase reovirus complementation during infection, and by rescuing deleterious mutations, the overall fitness of the viral population can be enhanced [15,86,87,178,184]. Virion aggregation of vesicular stomatitis virus was found to accelerate early infection fitness in multiple cell types [83]. Genetic complementation amongst a pool of aggregated virions may initially protect against deleterious mutations [210]. Thus, large EV- and medium EV-mediated multiparticle infection potentially augments the conditions that favor reovirus genetic complementation, which may grant reovirus a greater chance of complementing and rescuing otherwise defective genome segments to confer an enhanced infectious advantage.

Using HRM, I detected lower amounts of EV-associated reovirus multiparticle units than I had previously anticipated based on prior EM imaging in which many large and medium EVs appeared to associate with clusters of virus particles (**Fig. 12**). I hypothesize

that it is possible that EVs do indeed contain higher amounts of multiparticle reovirus units, but that there exists preferential packaging of the same parental genome type into one EV. Evidence exists that viral cargo may be selectively packaged in EVs. Coxsackievirus-containing EVs appear to selectively package “sibling” viruses of the same parental origin which feature fewer genomic mutations [144]. Furthermore, cellular EV machinery appears to interact with and select for mature HAV capsid domains during exosome packaging, and activated rotavirus which features a cleaved VP4 nucleocapsid is selectively packaged in EVs [57,211]. A similar selective packaging mechanism has been observed for reovirus. Host cell-derived membranous structures termed “sorting organelles” and “membranous carriers” selectively package large multiparticle groups of mature, fully assembled reovirus particles at sites of reovirus replication before trafficking to the plasma membrane for release of free virus particle [125]. Why this packaging mechanism is selective is, at the present time, a mystery, because it is unclear how complete, mature particles are distinguished from "empty" reovirus particles. Overall, however, an EV machinery-dependent mechanism may exist by which multiple sibling reovirus particles of the same genomic origin are selected for packaging into the same EV. Although I have shown that our WT and BC viruses have the same replication efficiency in cells, it is possible that one virus’s genomic fingerprint is selected for (as with coxsackievirus), or possibly that something exists in the capsid topology (as with HAV or rotavirus) that is selected for EV association or EV loading over the other virus. However, given that the proteins are identical between the WT and BC reovirus particles, this may not be the most likely explanation. Perhaps there is greater likelihood that reovirus replication factories

are more heavily weighted towards one genotype or the other, and so the same becomes true for outgoing viruses in specific regions of the cell. A previous lab member's work suggests that replication factories contain a mix of WT and BC segments, but the imaging method used to carry out these experiments was not sensitive and likely did not detect many of the genomes present within each factory [97]. This selective packaging strategy may represent the primary mechanism by which the majority of EV-associated reovirus units are loaded, and a minority of EVs may exist in which selection has failed or been altered, allowing a mixed population to be packaged within EVs, which is the population that I capture using HRM. Thus, I potentially only currently detect the "tip of the iceberg" of multiparticle reovirus-EV release; further studies into the molecular mechanism orchestrating reovirus-EV packaging will illuminate our collective understanding further.

Future direction: Assessment of the effect of Caco-2-derived EV-facilitated egress on reovirus infection and EV abundance

Questions regarding EV-facilitated multiparticle transport of reovirus between Caco-2 cells, as well as whether reovirus infection enhances the release of EVs in Caco-2 cells, still remain unanswered. I am interested in a fuller characterization of the downstream impacts of Caco-2-derived EV egress on reovirus infection of Caco-2 cells, particularly as they relate to multiparticle infection. I would utilize the same methods I have detailed here in L cells and apply that same methodology to Caco-2 cells—this would include using HRM to investigate the level of multiparticle transport facilitated by Caco-2-derived large, medium, and small EVs, and using parallel immunoprecipitation capture and confocal imaging analysis of large, medium, and small EV fractions

harvested from uninfected and reovirus-infected cells. I expect that both reovirus strains, like rotavirus in Caco-2 cells and also similar to what I observe of reovirus infection in L cells, would enhance the abundance of released EVs. Additionally, I expect that T3D multiparticle infection may actually be enhanced in Caco-2 cells. During the course of my work with Caco-2-derived EVs, I have noticed that harvested EVs are very markedly "stickier" than L cell-derived EVs, and thus, I hypothesize that this "stickiness" might promote more EVs to cluster together into larger units. T3D infectious units associate with all EV fractions (**Fig. 21C**). Although T3D is not protected in either large or medium EVs, I suspect that it is still bound on the exterior of these EV fractions. This association phenotype may be enough to ensure efficient multiparticle transport; given my observation that EVs derived from Caco-2 cells stick to one another with much higher affinity than L cell-derived EVs, I anticipate that Caco-2-derived EVs may clump and cluster together to create larger and more frequent multiparticle T3D units. To investigate T1L multiparticle infection, I would propose the engineering of a barcoded T1L particle virus. Using these WT and BC T1L viruses, I would test the T1L multiparticle transport efficiency of L cell-derived and Caco-2-derived large and medium EVs. I would expect that large- and medium-EV association would also promote T1L multiparticle infection; however, I wonder whether T1L multiparticle infection might be less than T3D, given the slower replication rate I have observed for T1L in Caco-2 cells compared to T3D.

Discussion: EV-mediated egress implications for reovirus entry

By combining my multiparticle transport data with my neutralization protection data, I obtain interesting insight into how reovirus interacts with and is packaged in different sizes of EV fractions. In L cells, multiparticle transmission of T3D is mediated by large EVs and for medium EVs, and I see this finding recapitulated visually when I observe reovirus association with large EVs and medium EVs via negative-stain EM. However, only in medium L cell-derived EVs is T3D protected; I see no such T3D protection conferred by large L cell EVs. Thus, I hypothesize that multiple T3D particles are adhered externally on large EVs, and additionally packaged internally in medium EVs.

This observation leads me to ponder the difference that packaging phenotype might play on overall reovirus entry and interaction with cell receptors. Canonically, reovirus uptake is facilitated via binding to sialic acid and JAM-A expressed at the plasma membrane, whereas EV uptake into cells can be mediated via a variety of phagocytic and fusion pathways [10,26]. Some viruses such as murine norovirus and poliovirus cannot infect cells when associated with EVs, and thus appear to retain their reliance on canonical cell receptors [15,57]. I question whether the reovirus particles that are packaged externally on the outside of large EVs may actually be more infectious than those packaged internally inside medium EVs, because the reovirus particles packaged externally still benefit from the advantages of multiparticle transport that I have discussed above but retain access to sialic acid and JAM-A cell surface receptors. If a reovirus particle is loaded as interior cargo inside of a medium EV, there are a variety of pathways, including direct plasma membrane fusion, by which an EV may interact with a cell, and not all of them will be the

correct pathway required by reovirus for productive infection. In a previous study, the entry mechanisms of non-enveloped HAV compared to quasi-enveloped HAV were investigated [212]. Both types of HAV were capable of infecting human liver cells, and both particle types entered host cells using an endocytic-like mechanism; however, uncoating and disassembly of non-enveloped HAV occurred early in the infectious cycle, whereas the quasi-enveloped HAV underwent further trafficking to lysosomes before subsequent degradation. Overall, these data suggest that envelopment can distinctly affect late-stage replication. Thus, by retaining canonical cell surface receptor interaction, reovirus may be more likely to enter cells and be sorted to the early and late endocytic pathways which are crucial for productive reovirus replication [213]. However, endocytosis is a very common, and in some cases preferred, mechanism of cell uptake for EVs [214-216]. Thus, perhaps the likelihood of endocytic uptake is a high enough probability that the reovirus population as a whole is not markedly adversely impacted.

The influence of EV-enclosed reovirus on reovirus's ability to proceed from the point of entry through the rest of the replication cycle must additionally be considered. Multiparticle transport on the exterior of a large EV may ensure that reovirus is able to become transcriptionally active. When reovirus enters into the endosome, acidification triggers uncoating and transcription activation. If reovirus is packaged inside an EV that is inside of an endosome, as I suspect it is inside of medium EVs, it must first escape the EV in order for uncoating and activation to occur. If reovirus is bound on the outside of large EVs, then it would not need to cross an additional membrane in order to access the

endosomal compartment. Reovirus protein μ1 has been documented to play an important role in interacting with endosomal membranes to ensure virus is released into the cytoplasm in order to continue the replication cycle [213,217]. Thus, I hypothesize that if indeed this model of reovirus entry is true, then the μ1 protein may play an important role in interacting with the EV encapsulating reovirus particles to penetrate through the EV and into the endosomal compartment. As a future direction, it would be interesting to utilize several μ1 mutants, which have previously been engineered to contain various mutations in the ϕ region and have been documented to alter the rate of endosomal membrane penetration [218]. By comparing free μ1 WT and mutant viruses with EV-associated WT and μ1 mutant viruses, it may be possible to ascertain whether μ1 plays a role in penetrating the EV to promote release into the endosome and thus ensure that the replication cycle can proceed. This would also potentially shed light on the potential roadblock that EVs may or may not cause reovirus, by forcing reovirus to penetrate across two membranes—one EV, and one endosomal—in order to access the cell cytoplasm.

By altering how virus particles interact with and rely on host cell receptors to gain entry, EVs may potentially alter viral tropism. EVs can deliver viruses and viral genomes to non-susceptible cells, as previous studies indicate that EV-transported JC polyomavirus and BK polyomavirus do not require canonical receptors, suggesting an alternative entry pathway [56,80]. Thus, EV-associated reovirus may not be reliant on canonical cell surface receptors in order to gain cell entry, which may give the reovirus that is associated with medium EVs a distinct advantage over the reovirus that is

associated with large EVs. Packaging within medium EVs not only affords reovirus the benefits of multiparticle transport and immune evasion/ suppression, but also may be more advantageous because the more promiscuous nature of EV binding to cells may act as a potential pathway for reovirus to infect non-canonical cell types and thus establish a broader cell tropism than what reovirus has traditionally been attributed. This would depend on reovirus entry through the endosomal pathway, which EVs are capable of an in fact accomplish frequently as a common method of uptake, but which may not always occur depending on the individual EV's uptake pathway. Thus, reovirus association with large EVs and with medium EVs may confer separate advantages. Future studies illuminating the impact of reovirus-EV packaging on receptor reliance will provide insight into this hypothesis, and may allow us additional insight into the extent to which EV association enhances productive reovirus infection of recipient cells.

Future direction: Assessment of EV-facilitated egress on reovirus entry and tropism

Above, I discussed the implications of EV-facilitated egress and transport on the capacity of reovirus to enter cells and replicate efficiently. Going forward, it will be important to understand this gap in knowledge in order to gain a fuller understanding of how EV-mediated reovirus exit impacts reovirus infection and spread. To determine whether EV association impacts reovirus interaction with canonical cell receptors, including sialic acid and JAM-A molecules, I propose pre-treating L cells with inhibitory antibodies to block reovirus interaction with these receptors. Neuraminidase treatment will block sialic acid, and monoclonal antibody AF1077 will block JAM-A [114,219]. By treating

cells with individual reagents, both reagents in tandem, or mock-treating cells, it will be possible to further delineate exactly what receptors, if any, are required for reovirus entry. Blockaded and non-blockaded cells will then be treated with either free reovirus or with large EV-associated and medium EV-associated reovirus, washed to remove unbound virus, and then infectious units of virus will be quantified. Based on prior studies investigating BK polyomavirus-EV entry, which binds to sialic acid similar to reovirus and utilizes receptor-independent entry pathways when contained in EVs, in addition to the noted propensity for EVs to enter cells via the endocytic pathway, I anticipate that EV association will permit reovirus to bind to cells whose canonical receptors are blocked [56]. These studies will allow us to gain insight into the influence of EV association on reovirus cell receptor reliance.

If reovirus binding to cells no longer requires canonical receptors, it would be valuable to know whether EV-associated reovirus is still being sorted into the endosomal pathway. By treating cells with ammonium chloride, endosomal acidification is halted, and thus reovirus replication is impaired [220]. If large EV- or medium EV-associated reovirus allows particles to enter cells in the endocytic pathway, then reovirus replication will be halted to similar levels as a free virus control. If either of these EV fractions cause reovirus to enter cells using an alternative entry pathway, then reovirus endosomal-dependent uptake will not be abolished to the levels observed for free virus. If EV-associated reovirus enters using a pathway that is not the endocytic pathway, it is highly unlikely that this virus would represent infectious virus; further studies testing the validity of this statement will

be illuminating in further our understanding the impact of EV association on reovirus replication.

I expressed an idea above that perhaps large EVs permit more efficient reovirus binding and could escape the endosomal compartment more easily compared to medium EVs, due to their differences in binding reovirus on the exterior or interior, respectively. To test this hypothesis, I would propose harvesting large EVs and medium EVs from L cells and apply equal infectious units of each fraction and of free virus to L cell monolayers. Every 2 h over a total course of 8 h, I would quantify reovirus protein in cells infected with each fraction. If medium EVs, which likely enclose reovirus, interfere with reovirus's ability to bind and enter cells, or if they impact reovirus's ability to escape the endosomal compartment, then protein accumulation in the cells will be lower compared to free virus. If large EVs do indeed bind reovirus externally, then I would expect reovirus particles to receive no replication interference, and thus protein accumulation in cells will be roughly equivalent compared to free virus. These studies would help to determine whether EV association alters the capacity of reovirus to escape the endosomal compartment.

It would additionally be interesting to determine whether EV containment permits reovirus to infect cells that are not susceptible to free virus infection. Chinese hamster ovary (CHO) cells are not susceptible to reovirus binding [221,222]. I would use EVs harvested from L cells as the "producer" EV, because these EVs have received the most characterization, and use the CHO cells as the recipient cell line. While the species origins of mouse L cells and hamster CHO cells are not identical to one another, they are at least

both rodents, and thus this closer species similarity should help ensure that the EVs harvested from L cells are capable of interacting with the CHO cells [223]. I would harvest EVs from T1L-infected and T3D-infected L cells, and administer these EVs to a monolayer of CHO cells. In parallel, I would administer similar number of non-permissive cells with free virus, to ensure that the CHO cells are truly not susceptible. After binding and infection, I would stain the CHO cells for reovirus protein to determine if the EVs released from L cells permitted reovirus to infect this cell line. These studies may help increase knowledge of the impact of EV-facilitated egress on virus tropism.

CONCLUDING REMARKS AND PUBLIC HEALTH RELEVANCE

Altogether, my work suggests that in addition to egressing as free independent particles, in a virus strain- and cell type-dependent manner, reovirus egresses from two distinct cell types enclosed in medium-sized, immune- and protease-protective EVs that can promote multiparticle infection. Virus-associated routes of egress confer distinct advantages to improve productive virus infection [8]. EVs can enable high multiplicity multiparticle packaging and transport of large groups of virus particles between cells that assist the virus in overcoming cell barriers to infection, potentially provide an enclosed space to increase the likelihood of genetic complementation to rescue otherwise noninfectious particles, shield virus cargo from immune detection and neutralization, deliver an immunosuppressive and anti-inflammatory signal, facilitate virus uptake through a variety of often non-canonical pathways, and permit nonlytic egress which is less likely to sound the immune system alarms [12,14,15,56,75,160]. Thus, EV-associated reovirus egress

represents a route of infection that is primed for increasing and prolonging productive reovirus infection. Although I do not yet know if this egress strategy is replicated in a human model, it is likely that EV-associated egress does represent a biologically meaningful exit pathway, because the literature points to this mechanism of transmission being utilized by evolutionary diverse viruses. Several highly pathogenic viruses, including rotavirus, norovirus, poliovirus, coxsackievirus, HAV, and Zika virus among others, utilize EVs as infectious vehicles of egress [12,15,24,57,90]. A greater understanding of the implications and impacts of EV-associated virus release and spread are thus necessary to continue improving public health and safety [81]. The findings I illustrate in this dissertation may broadly enhance our understanding of viral egress strategies and may potentially apply to other more pathogenic viruses. EVs can also be harnessed in a therapeutic aspect, as evidenced by the rise of EV studies in the tumor microenvironment and the recent FDA approval of utilizing HAV as a drug to destroy skin cancer cells [224]. Continued studies building on these findings may help future clinical studies that focus on targeting and delivering therapeutic EV-contained oncolytic reovirus to tumor sites.

REFERENCES

1. Dulbecco, R., and Vogt, M. (1953). Some problems of animal virology as studied by the plaque technique. Cold Spring Harb Symp Quant Biol *18*, 273-279. 10.1101/sqb.1953.018.01.039.
2. Más, V., and Melero, J.A. (2013). Entry of enveloped viruses into host cells: membrane fusion. Subcell Biochem *68*, 467-487. 10.1007/978-94-007-6552-8_16.
3. Rossmann, M.G. (2013). Structure of viruses: a short history. Q Rev Biophys *46*, 133-180. 10.1017/s0033583513000012.
4. Hurley, J.H. (2015). ESCRTs are everywhere. Embo j *34*, 2398-2407. 10.15252/embj.201592484.
5. Lindenbach, B.D. (2013). Virion assembly and release. Curr Top Microbiol Immunol *369*, 199-218. 10.1007/978-3-642-27340-7_8.
6. Welsch, S., Müller, B., and Kräusslich, H.G. (2007). More than one door - Budding of enveloped viruses through cellular membranes. FEBS Lett *581*, 2089-2097. 10.1016/j.febslet.2007.03.060.
7. Bird, S.W., Maynard, N.D., Covert, M.W., and Kirkegaard, K. (2014). Nonlytic viral spread enhanced by autophagy components. Proc Natl Acad Sci U S A *111*, 13081-13086. 10.1073/pnas.1401437111.
8. Altan-Bonnet, N. (2016). Extracellular vesicles are the Trojan horses of viral infection. Curr Opin Microbiol *32*, 77-81. 10.1016/j.mib.2016.05.004.
9. Altan-Bonnet, N., Perales, C., and Domingo, E. (2019). Extracellular vesicles: Vehicles of en bloc viral transmission. Virus Res *265*, 143-149. 10.1016/j.virusres.2019.03.023.
10. Roth, A.N., Aravamudhan, P., Fernández de Castro, I., Tenorio, R., Risco, C., and Dermody, T.S. (2021). Ins and Outs of Reovirus: Vesicular Trafficking in Viral Entry and Egress. Trends Microbiol *29*, 363-375. 10.1016/j.tim.2020.09.004.
11. Pletan, M.L., and Tsai, B. (2022). Non-enveloped virus membrane penetration: New advances leading to new insights. PLoS Pathog *18*, e1010948. 10.1371/journal.ppat.1010948.
12. Feng, Z., Hensley, L., McKnight, K.L., Hu, F., Madden, V., Ping, L., Jeong, S.H., Walker, C., Lanford, R.E., and Lemon, S.M. (2013). A pathogenic picornavirus acquires an envelope by hijacking cellular membranes. Nature *496*, 367-371. 10.1038/nature12029.
13. Nagashima, S., Jirintai, S., Takahashi, M., Kobayashi, T., Tanggis, Nishizawa, T., Kouki, T., Yashiro, T., and Okamoto, H. (2014). Hepatitis E virus egress depends on the exosomal pathway, with secretory exosomes derived from multivesicular bodies. J Gen Virol *95*, 2166-2175. 10.1099/vir.0.066910-0.
14. Robinson, S.M., Tsueng, G., Sin, J., Mangale, V., Rahawi, S., McIntyre, L.L., Williams, W., Kha, N., Cruz, C., Hancock, B.M., et al. (2014). Coxsackievirus B exits the host cell in shed microvesicles displaying autophagosomal markers. PLoS Pathog *10*, e1004045. 10.1371/journal.ppat.1004045.
15. Chen, Y.H., Du, W., Hagemeijer, M.C., Takvorian, P.M., Pau, C., Cali, A., Brantner, C.A., Stempinski, E.S., Connelly, P.S., Ma, H.C., et al. (2015).

Phosphatidylserine vesicles enable efficient en bloc transmission of enteroviruses. Cell *160*, 619-630. 10.1016/j.cell.2015.01.032.
16. Théry, C., Witwer, K.W., Aikawa, E., Alcaraz, M.J., Anderson, J.D., Andriantsitohaina, R., Antoniou, A., Arab, T., Archer, F., Atkin-Smith, G.K., et al. (2018). Minimal information for studies of extracellular vesicles 2018 (MISEV2018): a position statement of the International Society for Extracellular Vesicles and update of the MISEV2014 guidelines. J Extracell Vesicles *7*, 1535750. 10.1080/20013078.2018.1535750.
17. Rybak, K., and Robatzek, S. (2019). Functions of Extracellular Vesicles in Immunity and Virulence. Plant Physiol *179*, 1236-1247. 10.1104/pp.18.01557.
18. Colombo, M., Raposo, G., and Théry, C. (2014). Biogenesis, secretion, and intercellular interactions of exosomes and other extracellular vesicles. Annu Rev Cell Dev Biol *30*, 255-289. 10.1146/annurev-cellbio-101512-122326.
19. Keller, S., Ridinger, J., Rupp, A.K., Janssen, J.W., and Altevogt, P. (2011). Body fluid derived exosomes as a novel template for clinical diagnostics. J Transl Med *9*, 86. 10.1186/1479-5876-9-86.
20. Théry, C., Amigorena, S., Raposo, G., and Clayton, A. (2006). Isolation and characterization of exosomes from cell culture supernatants and biological fluids. Curr Protoc Cell Biol *Chapter 3*, Unit 3.22. 10.1002/0471143030.cb0322s30.
21. Lässer, C., Alikhani, V.S., Ekström, K., Eldh, M., Paredes, P.T., Bossios, A., Sjöstrand, M., Gabrielsson, S., Lötvall, J., and Valadi, H. (2011). Human saliva, plasma and breast milk exosomes contain RNA: uptake by macrophages. J Transl Med *9*, 9. 10.1186/1479-5876-9-9.
22. Schorey, J.S., Cheng, Y., Singh, P.P., and Smith, V.L. (2015). Exosomes and other extracellular vesicles in host-pathogen interactions. EMBO Rep *16*, 24-43. 10.15252/embr.201439363.
23. Deatherage, B.L., and Cookson, B.T. (2012). Membrane vesicle release in bacteria, eukaryotes, and archaea: a conserved yet underappreciated aspect of microbial life. Infect Immun *80*, 1948-1957. 10.1128/iai.06014-11.
24. Robinson, D.G., Ding, Y., and Jiang, L. (2016). Unconventional protein secretion in plants: a critical assessment. Protoplasma *253*, 31-43. 10.1007/s00709-015-0887-1.
25. Willms, E., Johansson, H.J., Mäger, I., Lee, Y., Blomberg, K.E., Sadik, M., Alaarg, A., Smith, C.I., Lehtiö, J., El Andaloussi, S., Wood, M.J., and Vader, P. (2016). Cells release subpopulations of exosomes with distinct molecular and biological properties. Sci Rep *6*, 22519. 10.1038/srep22519.
26. van Niel, G., D'Angelo, G., and Raposo, G. (2018). Shedding light on the cell biology of extracellular vesicles. Nat Rev Mol Cell Biol *19*, 213-228. 10.1038/nrm.2017.125.
27. Mohan, A., Agarwal, S., Clauss, M., Britt, N.S., and Dhillon, N.K. (2020). Extracellular vesicles: novel communicators in lung diseases. Respir Res *21*, 175. 10.1186/s12931-020-01423-y.

28. Kalra, H., Drummen, G.P., and Mathivanan, S. (2016). Focus on Extracellular Vesicles: Introducing the Next Small Big Thing. Int J Mol Sci *17*, 170. 10.3390/ijms17020170.
29. Klumperman, J., and Raposo, G. (2014). The complex ultrastructure of the endolysosomal system. Cold Spring Harb Perspect Biol *6*, a016857. 10.1101/cshperspect.a016857.
30. Stein, J.M., and Luzio, J.P. (1991). Ectocytosis caused by sublytic autologous complement attack on human neutrophils. The sorting of endogenous plasma-membrane proteins and lipids into shed vesicles. Biochem J *274 (Pt 2)*, 381-386. 10.1042/bj2740381.
31. Pollet, H., Conrard, L., Cloos, A.S., and Tyteca, D. (2018). Plasma Membrane Lipid Domains as Platforms for Vesicle Biogenesis and Shedding? Biomolecules *8*. 10.3390/biom8030094.
32. Mathivanan, S., Ji, H., and Simpson, R.J. (2010). Exosomes: extracellular organelles important in intercellular communication. J Proteomics *73*, 1907-1920. 10.1016/j.jprot.2010.06.006.
33. Lötvall, J., Hill, A.F., Hochberg, F., Buzás, E.I., Di Vizio, D., Gardiner, C., Gho, Y.S., Kurochkin, I.V., Mathivanan, S., Quesenberry, P., et al. (2014). Minimal experimental requirements for definition of extracellular vesicles and their functions: a position statement from the International Society for Extracellular Vesicles. J Extracell Vesicles *3*, 26913. 10.3402/jev.v3.26913.
34. Jeppesen, D.K., Fenix, A.M., Franklin, J.L., Higginbotham, J.N., Zhang, Q., Zimmerman, L.J., Liebler, D.C., Ping, J., Liu, Q., Evans, R., et al. (2019). Reassessment of Exosome Composition. Cell *177*, 428-445.e418. 10.1016/j.cell.2019.02.029.
35. Minciacchi, V.R., You, S., Spinelli, C., Morley, S., Zandian, M., Aspuria, P.J., Cavallini, L., Ciardiello, C., Reis Sobreiro, M., Morello, M., et al. (2015). Large oncosomes contain distinct protein cargo and represent a separate functional class of tumor-derived extracellular vesicles. Oncotarget *6*, 11327-11341. 10.18632/oncotarget.3598.
36. Gasser, O., Hess, C., Miot, S., Deon, C., Sanchez, J.C., and Schifferli, J.A. (2003). Characterisation and properties of ectosomes released by human polymorphonuclear neutrophils. Exp Cell Res *285*, 243-257. 10.1016/s0014-4827(03)00055-7.
37. Li, C.J., Liu, Y., Chen, Y., Yu, D., Williams, K.J., and Liu, M.L. (2013). Novel proteolytic microvesicles released from human macrophages after exposure to tobacco smoke. Am J Pathol *182*, 1552-1562. 10.1016/j.ajpath.2013.01.035.
38. Martínez de Lizarrondo, S., Roncal, C., Calvayrac, O., Rodríguez, C., Varo, N., Purroy, A., Lorente, L., Rodríguez, J.A., Doeuvre, L., Hervás-Stubbs, S., et al. (2012). Synergistic effect of thrombin and CD40 ligand on endothelial matrix metalloproteinase-10 expression and microparticle generation in vitro and in vivo. Arterioscler Thromb Vasc Biol *32*, 1477-1487. 10.1161/atvbaha.112.248773.

39. Del Conde, I., Shrimpton, C.N., Thiagarajan, P., and López, J.A. (2005). Tissue-factor-bearing microvesicles arise from lipid rafts and fuse with activated platelets to initiate coagulation. Blood *106*, 1604-1611. 10.1182/blood-2004-03-1095.
40. Mezouar, S., Darbousset, R., Dignat-George, F., Panicot-Dubois, L., and Dubois, C. (2015). Inhibition of platelet activation prevents the P-selectin and integrin-dependent accumulation of cancer cell microparticles and reduces tumor growth and metastasis in vivo. Int J Cancer *136*, 462-475. 10.1002/ijc.28997.
41. Booth, A.M., Fang, Y., Fallon, J.K., Yang, J.M., Hildreth, J.E., and Gould, S.J. (2006). Exosomes and HIV Gag bud from endosome-like domains of the T cell plasma membrane. J Cell Biol *172*, 923-935. 10.1083/jcb.200508014.
42. Caruso, S., and Poon, I.K.H. (2018). Apoptotic Cell-Derived Extracellular Vesicles: More Than Just Debris. Front Immunol *9*, 1486. 10.3389/fimmu.2018.01486.
43. Turiák, L., Misják, P., Szabó, T.G., Aradi, B., Pálóczi, K., Ozohanics, O., Drahos, L., Kittel, A., Falus, A., Buzás, E.I., and Vékey, K. (2011). Proteomic characterization of thymocyte-derived microvesicles and apoptotic bodies in BALB/c mice. J Proteomics *74*, 2025-2033. 10.1016/j.jprot.2011.05.023.
44. Lleo, A., Zhang, W., McDonald, W.H., Seeley, E.H., Leung, P.S., Coppel, R.L., Ansari, A.A., Adams, D.H., Afford, S., Invernizzi, P., and Gershwin, M.E. (2014). Shotgun proteomics: identification of unique protein profiles of apoptotic bodies from biliary epithelial cells. Hepatology *60*, 1314-1323. 10.1002/hep.27230.
45. Taylor, R.C., Cullen, S.P., and Martin, S.J. (2008). Apoptosis: controlled demolition at the cellular level. Nat Rev Mol Cell Biol *9*, 231-241. 10.1038/nrm2312.
46. Feng, Y., Yao, Z., and Klionsky, D.J. (2015). How to control self-digestion: transcriptional, post-transcriptional, and post-translational regulation of autophagy. Trends Cell Biol *25*, 354-363. 10.1016/j.tcb.2015.02.002.
47. Cuervo, A.M. (2010). The plasma membrane brings autophagosomes to life. Nat Cell Biol *12*, 735-737. 10.1038/ncb0810-735.
48. Mutsafi, Y., and Altan-Bonnet, N. (2018). Enterovirus Transmission by Secretory Autophagy. Viruses *10*. 10.3390/v10030139.
49. Jiang, S., Dupont, N., Castillo, E.F., and Deretic, V. (2013). Secretory versus degradative autophagy: unconventional secretion of inflammatory mediators. J Innate Immun *5*, 471-479. 10.1159/000346707.
50. Ejlerskov, P., Rasmussen, I., Nielsen, T.T., Bergström, A.L., Tohyama, Y., Jensen, P.H., and Vilhardt, F. (2013). Tubulin polymerization-promoting protein (TPPP/p25α) promotes unconventional secretion of α-synuclein through exophagy by impairing autophagosome-lysosome fusion. J Biol Chem *288*, 17313-17335. 10.1074/jbc.M112.401174.
51. Nilsson, P., Loganathan, K., Sekiguchi, M., Matsuba, Y., Hui, K., Tsubuki, S., Tanaka, M., Iwata, N., Saito, T., and Saido, T.C. (2013). Aβ secretion and plaque formation depend on autophagy. Cell Rep *5*, 61-69. 10.1016/j.celrep.2013.08.042.

52. Peng, H., Liu, B., Yves, T.D., He, Y., Wang, S., Tang, H., Ren, H., Zhao, P., Qi, Z., and Qin, Z. (2018). Zika Virus Induces Autophagy in Human Umbilical Vein Endothelial Cells. Viruses *10*. 10.3390/v10050259.
53. Cao, B., Parnell, L.A., Diamond, M.S., and Mysorekar, I.U. (2017). Inhibition of autophagy limits vertical transmission of Zika virus in pregnant mice. J Exp Med *214*, 2303-2313. 10.1084/jem.20170957.
54. Labadie, T., Sullivan, E., and Roy, P. (2020). Multiple Routes of Bluetongue Virus Egress. Microorganisms *8*. 10.3390/microorganisms8070965.
55. Buckingham, E.M., Jarosinski, K.W., Jackson, W., Carpenter, J.E., and Grose, C. (2016). Exocytosis of Varicella-Zoster Virus Virions Involves a Convergence of Endosomal and Autophagy Pathways. J Virol *90*, 8673-8685. 10.1128/jvi.00915-16.
56. Handala, L., Blanchard, E., Raynal, P.I., Roingeard, P., Morel, V., Descamps, V., Castelain, S., Francois, C., Duverlie, G., Brochot, E., and Helle, F. (2020). BK Polyomavirus Hijacks Extracellular Vesicles for En Bloc Transmission. J Virol *94*. 10.1128/jvi.01834-19.
57. Santiana, M., Ghosh, S., Ho, B.A., Rajasekaran, V., Du, W.L., Mutsafi, Y., De Jésus-Diaz, D.A., Sosnovtsev, S.V., Levenson, E.A., Parra, G.I., et al. (2018). Vesicle-Cloaked Virus Clusters Are Optimal Units for Inter-organismal Viral Transmission. Cell Host Microbe *24*, 208-220.e208. 10.1016/j.chom.2018.07.006.
58. Ramakrishnaiah, V., Thumann, C., Fofana, I., Habersetzer, F., Pan, Q., de Ruiter, P.E., Willemsen, R., Demmers, J.A., Stalin Raj, V., Jenster, G., et al. (2013). Exosome-mediated transmission of hepatitis C virus between human hepatoma Huh7.5 cells. Proc Natl Acad Sci U S A *110*, 13109-13113. 10.1073/pnas.1221899110.
59. Bukong, T.N., Momen-Heravi, F., Kodys, K., Bala, S., and Szabo, G. (2014). Exosomes from hepatitis C infected patients transmit HCV infection and contain replication competent viral RNA in complex with Ago2-miR122-HSP90. PLoS Pathog *10*, e1004424. 10.1371/journal.ppat.1004424.
60. Longatti, A., Boyd, B., and Chisari, F.V. (2015). Virion-independent transfer of replication-competent hepatitis C virus RNA between permissive cells. J Virol *89*, 2956-2961. 10.1128/jvi.02721-14.
61. Gu, J., Wu, J., Fang, D., Qiu, Y., Zou, X., Jia, X., Yin, Y., Shen, L., and Mao, L. (2020). Exosomes cloak the virion to transmit Enterovirus 71 non-lytically. Virulence *11*, 32-38. 10.1080/21505594.2019.1705022.
62. Martelli, F., Macera, L., Spezia, P.G., Medici, C., Pistello, M., Guasti, D., Romagnoli, P., Maggi, F., and Giannecchini, S. (2018). Torquetenovirus detection in exosomes enriched vesicles circulating in human plasma samples. Virol J *15*, 145. 10.1186/s12985-018-1055-y.
63. Vora, A., Zhou, W., Londono-Renteria, B., Woodson, M., Sherman, M.B., Colpitts, T.M., Neelakanta, G., and Sultana, H. (2018). Arthropod EVs mediate dengue virus transmission through interaction with a tetraspanin domain

containing glycoprotein Tsp29Fb. Proc Natl Acad Sci U S A *115*, E6604-e6613. 10.1073/pnas.1720125115.
64. Zhou, W., Woodson, M., Neupane, B., Bai, F., Sherman, M.B., Choi, K.H., Neelakanta, G., and Sultana, H. (2018). Exosomes serve as novel modes of tick-borne flavivirus transmission from arthropod to human cells and facilitates dissemination of viral RNA and proteins to the vertebrate neuronal cells. PLoS Pathog *14*, e1006764. 10.1371/journal.ppat.1006764.
65. Silvas, J.A., Popov, V.L., Paulucci-Holthauzen, A., and Aguilar, P.V. (2016). Extracellular Vesicles Mediate Receptor-Independent Transmission of Novel Tick-Borne Bunyavirus. J Virol *90*, 873-886. 10.1128/jvi.02490-15.
66. Wang, T., Fang, L., Zhao, F., Wang, D., and Xiao, S. (2018). Exosomes Mediate Intercellular Transmission of Porcine Reproductive and Respiratory Syndrome Virus. J Virol *92*. 10.1128/jvi.01734-17.
67. Chivero, E.T., Bhattarai, N., Rydze, R.T., Winters, M.A., Holodniy, M., and Stapleton, J.T. (2014). Human pegivirus RNA is found in multiple blood mononuclear cells in vivo and serum-derived viral RNA-containing particles are infectious in vitro. J Gen Virol *95*, 1307-1319. 10.1099/vir.0.063016-0.
68. Arantes, T.S., Rodrigues, R.A., Dos Santos Silva, L.K., Oliveira, G.P., de Souza, H.L., Khalil, J.Y., de Oliveira, D.B., Torres, A.A., da Silva, L.L., Colson, P., et al. (2016). The Large Marseillevirus Explores Different Entry Pathways by Forming Giant Infectious Vesicles. J Virol *90*, 5246-5255. 10.1128/jvi.00177-16.
69. Morris-Love, J., Gee, G.V., O'Hara, B.A., Assetta, B., Atkinson, A.L., Dugan, A.S., Haley, S.A., and Atwood, W.J. (2019). JC Polyomavirus Uses Extracellular Vesicles To Infect Target Cells. mBio *10*. 10.1128/mBio.00379-19.
70. van der Grein, S.G., Defourny, K.A.Y., Rabouw, H.H., Galiveti, C.R., Langereis, M.A., Wauben, M.H.M., Arkesteijn, G.J.A., van Kuppeveld, F.J.M., and Nolte-'t Hoen, E.N.M. (2019). Picornavirus infection induces temporal release of multiple extracellular vesicle subsets that differ in molecular composition and infectious potential. PLoS Pathog *15*, e1007594. 10.1371/journal.ppat.1007594.
71. Bern, C., Martines, J., de Zoysa, I., and Glass, R.I. (1992). The magnitude of the global problem of diarrhoeal disease: a ten-year update. Bull World Health Organ *70*, 705-714.
72. Mao, L., Wu, J., Shen, L., Yang, J., Chen, J., and Xu, H. (2016). Enterovirus 71 transmission by exosomes establishes a productive infection in human neuroblastoma cells. Virus Genes *52*, 189-194. 10.1007/s11262-016-1292-3.
73. Iša, P., Pérez-Delgado, A., Quevedo, I.R., López, S., and Arias, C.F. (2020). Rotaviruses Associate with Distinct Types of Extracellular Vesicles. Viruses *12*. 10.3390/v12070763.
74. Takahashi, M., Tanaka, T., Takahashi, H., Hoshino, Y., Nagashima, S., Jirintai, Mizuo, H., Yazaki, Y., Takagi, T., Azuma, M., et al. (2010). Hepatitis E Virus (HEV) strains in serum samples can replicate efficiently in cultured cells despite the coexistence of HEV antibodies: characterization of HEV virions in blood circulation. J Clin Microbiol *48*, 1112-1125. 10.1128/jcm.02002-09.

75. Birge, R.B., Boeltz, S., Kumar, S., Carlson, J., Wanderley, J., Calianese, D., Barcinski, M., Brekken, R.A., Huang, X., Hutchins, J.T., et al. (2016). Phosphatidylserine is a global immunosuppressive signal in efferocytosis, infectious disease, and cancer. Cell Death Differ *23*, 962-978. 10.1038/cdd.2016.11.
76. Théry, C., Ostrowski, M., and Segura, E. (2009). Membrane vesicles as conveyors of immune responses. Nat Rev Immunol *9*, 581-593. 10.1038/nri2567.
77. Nakai, W., Yoshida, T., Diez, D., Miyatake, Y., Nishibu, T., Imawaka, N., Naruse, K., Sadamura, Y., and Hanayama, R. (2016). A novel affinity-based method for the isolation of highly purified extracellular vesicles. Sci Rep *6*, 33935. 10.1038/srep33935.
78. Maginnis, M.S. (2018). Virus-Receptor Interactions: The Key to Cellular Invasion. J Mol Biol *430*, 2590-2611. 10.1016/j.jmb.2018.06.024.
79. Marsh, M., and Helenius, A. (2006). Virus entry: open sesame. Cell *124*, 729-740. 10.1016/j.cell.2006.02.007.
80. O'Hara, B.A., Morris-Love, J., Gee, G.V., Haley, S.A., and Atwood, W.J. (2020). JC Virus infected choroid plexus epithelial cells produce extracellular vesicles that infect glial cells independently of the virus attachment receptor. PLoS Pathog *16*, e1008371. 10.1371/journal.ppat.1008371.
81. Zhang, M., Ghosh, S., Li, M., Altan-Bonnet, N., and Shuai, D. (2022). Vesicle-Cloaked Rotavirus Clusters are Environmentally Persistent and Resistant to Free Chlorine Disinfection. Environ Sci Technol *56*, 8475-8484. 10.1021/acs.est.2c00732.
82. Leeks, A., Segredo-Otero, E.A., Sanjuán, R., and West, S.A. (2018). Beneficial coinfection can promote within-host viral diversity. Virus Evol *4*, vey028. 10.1093/ve/vey028.
83. Andreu-Moreno, I., and Sanjuán, R. (2018). Collective Infection of Cells by Viral Aggregates Promotes Early Viral Proliferation and Reveals a Cellular-Level Allee Effect. Curr Biol *28*, 3212-3219.e3214. 10.1016/j.cub.2018.08.028.
84. Stiefel, P., Schmidt, F.I., Dörig, P., Behr, P., Zambelli, T., Vorholt, J.A., and Mercer, J. (2012). Cooperative vaccinia infection demonstrated at the single-cell level using FluidFM. Nano Lett *12*, 4219-4227. 10.1021/nl3018109.
85. Zaritsky, L.A., Bedsaul, J.R., and Zoon, K.C. (2015). Virus Multiplicity of Infection Affects Type I Interferon Subtype Induction Profiles and Interferon-Stimulated Genes. J Virol *89*, 11534-11548. 10.1128/jvi.01727-15.
86. Erickson, A.K., Jesudhasan, P.R., Mayer, M.J., Narbad, A., Winter, S.E., and Pfeiffer, J.K. (2018). Bacteria Facilitate Enteric Virus Co-infection of Mammalian Cells and Promote Genetic Recombination. Cell Host Microbe *23*, 77-88.e75. 10.1016/j.chom.2017.11.007.
87. Berger, A.K., Yi, H., Kearns, D.B., and Mainou, B.A. (2017). Bacteria and bacterial envelope components enhance mammalian reovirus thermostability. PLoS Pathog *13*, e1006768. 10.1371/journal.ppat.1006768.
88. Barreto, A., Rodríguez, L.S., Rojas, O.L., Wolf, M., Greenberg, H.B., Franco, M.A., and Angel, J. (2010). Membrane vesicles released by intestinal epithelial

cells infected with rotavirus inhibit T-cell function. Viral Immunol *23*, 595-608. 10.1089/vim.2009.0113.
89. Bautista, D., Rodríguez, L.S., Franco, M.A., Angel, J., and Barreto, A. (2015). Caco-2 cells infected with rotavirus release extracellular vesicles that express markers of apoptotic bodies and exosomes. Cell Stress Chaperones *20*, 697-708. 10.1007/s12192-015-0597-9.
90. Zhou, W., Woodson, M., Sherman, M.B., Neelakanta, G., and Sultana, H. (2019). Exosomes mediate Zika virus transmission through SMPD3 neutral Sphingomyelinase in cortical neurons. Emerg Microbes Infect *8*, 307-326. 10.1080/22221751.2019.1578188.
91. Keryer-Bibens, C., Pioche-Durieu, C., Villemant, C., Souquère, S., Nishi, N., Hirashima, M., Middeldorp, J., and Busson, P. (2006). Exosomes released by EBV-infected nasopharyngeal carcinoma cells convey the viral latent membrane protein 1 and the immunomodulatory protein galectin 9. BMC Cancer *6*, 283. 10.1186/1471-2407-6-283.
92. Huang, S.C., Chang, C.L., Wang, P.S., Tsai, Y., and Liu, H.S. (2009). Enterovirus 71-induced autophagy detected in vitro and in vivo promotes viral replication. J Med Virol *81*, 1241-1252. 10.1002/jmv.21502.
93. Mohamud, Y., Shi, J., Qu, J., Poon, T., Xue, Y.C., Deng, H., Zhang, J., and Luo, H. (2018). Enteroviral Infection Inhibits Autophagic Flux via Disruption of the SNARE Complex to Enhance Viral Replication. Cell Rep *22*, 3292-3303. 10.1016/j.celrep.2018.02.090.
94. Cypryk, W., Lorey, M., Puustinen, A., Nyman, T.A., and Matikainen, S. (2017). Proteomic and Bioinformatic Characterization of Extracellular Vesicles Released from Human Macrophages upon Influenza A Virus Infection. J Proteome Res *16*, 217-227. 10.1021/acs.jproteome.6b00596.
95. Zicari, S., Arakelyan, A., Palomino, R., Fitzgerald, W., Vanpouille, C., Lebedeva, A., Schmitt, A., Bomsel, M., Britt, W., and Margolis, L. (2018). Human cytomegalovirus-infected cells release extracellular vesicles that carry viral surface proteins. Virology *524*, 97-105. 10.1016/j.virol.2018.08.008.
96. Kobayashi, T., Ooms, L.S., Ikizler, M., Chappell, J.D., and Dermody, T.S. (2010). An improved reverse genetics system for mammalian orthoreoviruses. Virology *398*, 194-200. 10.1016/j.virol.2009.11.037.
97. Thoner, T.W., Jr., Meloy, M.M., Long, J.M., Diller, J.R., Slaughter, J.C., and Ogden, K.M. (2022). Reovirus Efficiently Reassorts Genome Segments during Coinfection and Superinfection. J Virol *96*, e0091022. 10.1128/jvi.00910-22.
98. Tai, J.H., Williams, J.V., Edwards, K.M., Wright, P.F., Crowe, J.E., Jr., and Dermody, T.S. (2005). Prevalence of reovirus-specific antibodies in young children in Nashville, Tennessee. J Infect Dis *191*, 1221-1224. 10.1086/428911.
99. Selb, B., and Weber, B. (1994). A study of human reovirus IgG and IgA antibodies by ELISA and western blot. J Virol Methods *47*, 15-25. 10.1016/0166-0934(94)90062-0.
100. Bouziat, R., Hinterleitner, R., Brown, J.J., Stencel-Baerenwald, J.E., Ikizler, M., Mayassi, T., Meisel, M., Kim, S.M., Discepolo, V., Pruijssers, A.J., et al. (2017).

Reovirus infection triggers inflammatory responses to dietary antigens and development of celiac disease. Science *356*, 44-50. 10.1126/science.aah5298.
101. Chaurasiya, S., Fong, Y., and Warner, S.G. (2021). Oncolytic Virotherapy for Cancer: Clinical Experience. Biomedicines *9*. 10.3390/biomedicines9040419.
102. Dermody, T., Parker, J., and Sherry, B. (2013). Chapter 44. Orthoreoviruses. Fields Virology. David M. Knipe, Peter M. Howley.(ed.).
103. Sutherland, D.M., Aravamudhan, P., and Dermody, T.S. (2018). An Orchestra of Reovirus Receptors: Still Searching for the Conductor. Adv Virus Res *100*, 223-246. 10.1016/bs.aivir.2017.10.005.
104. Dietrich, M.H., Ogden, K.M., Katen, S.P., Reiss, K., Sutherland, D.M., Carnahan, R.H., Goff, M., Cooper, T., Dermody, T.S., and Stehle, T. (2017). Structural Insights into Reovirus σ1 Interactions with Two Neutralizing Antibodies. J Virol *91*. 10.1128/jvi.01621-16.
105. Tyler, K.L., Mann, M.A., Fields, B.N., and Virgin, H.W.t. (1993). Protective anti-reovirus monoclonal antibodies and their effects on viral pathogenesis. J Virol *67*, 3446-3453. 10.1128/jvi.67.6.3446-3453.1993.
106. Tenorio, R., Fernández de Castro, I., Knowlton, J.J., Zamora, P.F., Lee, C.H., Mainou, B.A., Dermody, T.S., and Risco, C. (2018). Reovirus σNS and μNS Proteins Remodel the Endoplasmic Reticulum to Build Replication Neo-Organelles. mBio *9*. 10.1128/mBio.01253-18.
107. Fernández de Castro, I., Zamora, P.F., Ooms, L., Fernández, J.J., Lai, C.M., Mainou, B.A., Dermody, T.S., and Risco, C. (2014). Reovirus forms neo-organelles for progeny particle assembly within reorganized cell membranes. mBio *5*. 10.1128/mBio.00931-13.
108. Becker, M.M., Peters, T.R., and Dermody, T.S. (2003). Reovirus sigma NS and mu NS proteins form cytoplasmic inclusion structures in the absence of viral infection. J Virol *77*, 5948-5963. 10.1128/jvi.77.10.5948-5963.2003.
109. Lee, C.H., Raghunathan, K., Taylor, G.M., French, A.J., Tenorio, R., Fernández de Castro, I., Risco, C., Parker, J.S.L., and Dermody, T.S. (2021). Reovirus Nonstructural Protein σNS Recruits Viral RNA to Replication Organelles. mBio *12*, e0140821. 10.1128/mBio.01408-21.
110. Bussiere, L.D., Choudhury, P., Bellaire, B., and Miller, C.L. (2017). Characterization of a Replicating Mammalian Orthoreovirus with Tetracysteine-Tagged μNS for Live-Cell Visualization of Viral Factories. J Virol *91*. 10.1128/jvi.01371-17.
111. Ooms, L.S., Kobayashi, T., Dermody, T.S., and Chappell, J.D. (2010). A post-entry step in the mammalian orthoreovirus replication cycle is a determinant of cell tropism. J Biol Chem *285*, 41604-41613. 10.1074/jbc.M110.176255.
112. Parker, J.S., Broering, T.J., Kim, J., Higgins, D.E., and Nibert, M.L. (2002). Reovirus core protein mu2 determines the filamentous morphology of viral inclusion bodies by interacting with and stabilizing microtubules. J Virol *76*, 4483-4496. 10.1128/jvi.76.9.4483-4496.2002.
113. Tenorio, R., Fernández de Castro, I., Knowlton, J.J., Zamora, P.F., Sutherland, D.M., Risco, C., and Dermody, T.S. (2019). Function, Architecture, and

Biogenesis of Reovirus Replication Neoorganelles. Viruses *11*. 10.3390/v11030288.
114. Sutherland, D.M., Aravamudhan, P., Dietrich, M.H., Stehle, T., and Dermody, T.S. (2018). Reovirus Neurotropism and Virulence Are Dictated by Sequences in the Head Domain of the Viral Attachment Protein. J Virol *92*. 10.1128/jvi.00974-18.
115. Tyler, K.L., Squier, M.K., Rodgers, S.E., Schneider, B.E., Oberhaus, S.M., Grdina, T.A., Cohen, J.J., and Dermody, T.S. (1995). Differences in the capacity of reovirus strains to induce apoptosis are determined by the viral attachment protein sigma 1. J Virol *69*, 6972-6979. 10.1128/jvi.69.11.6972-6979.1995.
116. Pruijssers, A.J., Hengel, H., Abel, T.W., and Dermody, T.S. (2013). Apoptosis induction influences reovirus replication and virulence in newborn mice. J Virol *87*, 12980-12989. 10.1128/jvi.01931-13.
117. Berger, A.K., and Danthi, P. (2013). Reovirus activates a caspase-independent cell death pathway. mBio *4*, e00178-00113. 10.1128/mBio.00178-13.
118. Clarke, P., Richardson-Burns, S.M., DeBiasi, R.L., and Tyler, K.L. (2005). Mechanisms of apoptosis during reovirus infection. Curr Top Microbiol Immunol *289*, 1-24. 10.1007/3-540-27320-4_1.
119. DeBiasi, R.L., Robinson, B.A., Sherry, B., Bouchard, R., Brown, R.D., Rizeq, M., Long, C., and Tyler, K.L. (2004). Caspase inhibition protects against reovirus-induced myocardial injury in vitro and in vivo. J Virol *78*, 11040-11050. 10.1128/jvi.78.20.11040-11050.2004.
120. Rodgers, S.E., Barton, E.S., Oberhaus, S.M., Pike, B., Gibson, C.A., Tyler, K.L., and Dermody, T.S. (1997). Reovirus-induced apoptosis of MDCK cells is not linked to viral yield and is blocked by Bcl-2. J Virol *71*, 2540-2546. 10.1128/jvi.71.3.2540-2546.1997.
121. Weiner, H.L., Drayna, D., Averill, D.R., Jr., and Fields, B.N. (1977). Molecular basis of reovirus virulence: role of the S1 gene. Proc Natl Acad Sci U S A *74*, 5744-5748. 10.1073/pnas.74.12.5744.
122. Rubin, D.H., and Fields, B.N. (1980). Molecular basis of reovirus virulence. Role of the M2 gene. J Exp Med *152*, 853-868. 10.1084/jem.152.4.853.
123. Lemieux, R., Lemay, G., and Millward, S. (1987). The viral protein sigma 3 participates in translation of late viral mRNA in reovirus-infected L cells. J Virol *61*, 2472-2479. 10.1128/jvi.61.8.2472-2479.1987.
124. Kemp, V., Dautzenberg, I.J.C., Limpens, R.W., van den Wollenberg, D.J.M., and Hoeben, R.C. (2017). Oncolytic Reovirus Infection Is Facilitated by the Autophagic Machinery. Viruses *9*. 10.3390/v9100266.
125. Fernández de Castro, I., Tenorio, R., Ortega-González, P., Knowlton, J.J., Zamora, P.F., Lee, C.H., Fernández, J.J., Dermody, T.S., and Risco, C. (2020). A modified lysosomal organelle mediates nonlytic egress of reovirus. J Cell Biol *219*. 10.1083/jcb.201910131.
126. Sharpe, A.H., and Fields, B.N. (1981). Reovirus inhibition of cellular DNA synthesis: role of the S1 gene. J Virol *38*, 389-392. 10.1128/jvi.38.1.389-392.1981.

127. Poggioli, G.J., Dermody, T.S., and Tyler, K.L. (2001). Reovirus-induced sigma1s-dependent G(2)/M phase cell cycle arrest is associated with inhibition of p34(cdc2). J Virol *75*, 7429-7434. 10.1128/jvi.75.16.7429-7434.2001.
128. Berard, A.R., Cortens, J.P., Krokhin, O., Wilkins, J.A., Severini, A., and Coombs, K.M. (2012). Quantification of the host response proteome after mammalian reovirus T1L infection. PLoS One *7*, e51939. 10.1371/journal.pone.0051939.
129. Desmet, E.A., Anguish, L.J., and Parker, J.S. (2014). Virus-mediated compartmentalization of the host translational machinery. mBio *5*, e01463-01414. 10.1128/mBio.01463-14.
130. Gardet, A., Breton, M., Fontanges, P., Trugnan, G., and Chwetzoff, S. (2006). Rotavirus spike protein VP4 binds to and remodels actin bundles of the epithelial brush border into actin bodies. J Virol *80*, 3947-3956. 10.1128/jvi.80.8.3947-3956.2006.
131. Berkova, Z., Crawford, S.E., Trugnan, G., Yoshimori, T., Morris, A.P., and Estes, M.K. (2006). Rotavirus NSP4 induces a novel vesicular compartment regulated by calcium and associated with viroplasms. J Virol *80*, 6061-6071. 10.1128/jvi.02167-05.
132. Connolly, J.L., Barton, E.S., and Dermody, T.S. (2001). Reovirus binding to cell surface sialic acid potentiates virus-induced apoptosis. J Virol *75*, 4029-4039. 10.1128/jvi.75.9.4029-4039.2001.
133. Lai, C.M., Mainou, B.A., Kim, K.S., and Dermody, T.S. (2013). Directional release of reovirus from the apical surface of polarized endothelial cells. mBio *4*, e00049-00013. 10.1128/mBio.00049-13.
134. Excoffon, K.J., Guglielmi, K.M., Wetzel, J.D., Gansemer, N.D., Campbell, J.A., Dermody, T.S., and Zabner, J. (2008). Reovirus preferentially infects the basolateral surface and is released from the apical surface of polarized human respiratory epithelial cells. J Infect Dis *197*, 1189-1197. 10.1086/529515.
135. Mohl, B.P., and Roy, P. (2014). Bluetongue virus capsid assembly and maturation. Viruses *6*, 3250-3270. 10.3390/v6083250.
136. Miyazaki, N., Nakagawa, A., and Iwasaki, K. (2013). Life cycle of phytoreoviruses visualized by electron microscopy and tomography. Front Microbiol *4*, 306. 10.3389/fmicb.2013.00306.
137. Kerviel, A., Zhang, M., and Altan-Bonnet, N. (2021). A New Infectious Unit: Extracellular Vesicles Carrying Virus Populations. Annu Rev Cell Dev Biol *37*, 171-197. 10.1146/annurev-cellbio-040621-032416.
138. Desrochers, L.M., Antonyak, M.A., and Cerione, R.A. (2016). Extracellular Vesicles: Satellites of Information Transfer in Cancer and Stem Cell Biology. Dev Cell *37*, 301-309. 10.1016/j.devcel.2016.04.019.
139. Crescitelli, R., Lässer, C., Szabó, T.G., Kittel, A., Eldh, M., Dianzani, I., Buzás, E.I., and Lötvall, J. (2013). Distinct RNA profiles in subpopulations of extracellular vesicles: apoptotic bodies, microvesicles and exosomes. J Extracell Vesicles *2*. 10.3402/jev.v2i0.20677.
140. Pegtel, D.M., and Gould, S.J. (2019). Exosomes. Annu Rev Biochem *88*, 487-514. 10.1146/annurev-biochem-013118-111902.

141. Cocucci, E., Racchetti, G., and Meldolesi, J. (2009). Shedding microvesicles: artefacts no more. Trends Cell Biol *19*, 43-51. 10.1016/j.tcb.2008.11.003.
142. Osteikoetxea, X., Sódar, B., Németh, A., Szabó-Taylor, K., Pálóczi, K., Vukman, K.V., Tamási, V., Balogh, A., Kittel, Á., Pállinger, É., and Buzás, E.I. (2015). Differential detergent sensitivity of extracellular vesicle subpopulations. Org Biomol Chem *13*, 9775-9782. 10.1039/c5ob01451d.
143. Wirblich, C., Bhattacharya, B., and Roy, P. (2006). Nonstructural protein 3 of bluetongue virus assists virus release by recruiting ESCRT-I protein Tsg101. J Virol *80*, 460-473. 10.1128/jvi.80.1.460-473.2006.
144. Bou, J.V., Geller, R., and Sanjuán, R. (2019). Membrane-Associated Enteroviruses Undergo Intercellular Transmission as Pools of Sibling Viral Genomes. Cell Rep *29*, 714-723.e714. 10.1016/j.celrep.2019.09.014.
145. Ponpuak, M., Mandell, M.A., Kimura, T., Chauhan, S., Cleyrat, C., and Deretic, V. (2015). Secretory autophagy. Curr Opin Cell Biol *35*, 106-116. 10.1016/j.ceb.2015.04.016.
146. Hurwitz, S.N., Nkosi, D., Conlon, M.M., York, S.B., Liu, X., Tremblay, D.C., and Meckes, D.G., Jr. (2017). CD63 Regulates Epstein-Barr Virus LMP1 Exosomal Packaging, Enhancement of Vesicle Production, and Noncanonical NF-κB Signaling. J Virol *91*. 10.1128/jvi.02251-16.
147. Spendlove, R.S., Lennette, E.H., Knight, C.O., and Chin, J.N. (1966). Production in FL cells of infectious and potentially infectious reovirus. J Bacteriol *92*, 1036-1040. 10.1128/jb.92.4.1036-1040.1966.
148. Coombs, K.M. (2023). Mammalian Reoviruses: Propagation, Quantification, and Storage. Curr Protoc *3*, e716. 10.1002/cpz1.716.
149. Kowal, E.J.K., Ter-Ovanesyan, D., Regev, A., and Church, G.M. (2017). Extracellular Vesicle Isolation and Analysis by Western Blotting. Methods Mol Biol *1660*, 143-152. 10.1007/978-1-4939-7253-1_12.
150. Chuo, S.T., Chien, J.C., and Lai, C.P. (2018). Imaging extracellular vesicles: current and emerging methods. J Biomed Sci *25*, 91. 10.1186/s12929-018-0494-5.
151. Lobb, R.J., Becker, M., Wen, S.W., Wong, C.S., Wiegmans, A.P., Leimgruber, A., and Möller, A. (2015). Optimized exosome isolation protocol for cell culture supernatant and human plasma. J Extracell Vesicles *4*, 27031. 10.3402/jev.v4.27031.
152. Crescitelli, R., Lässer, C., and Lötvall, J. (2021). Isolation and characterization of extracellular vesicle subpopulations from tissues. Nat Protoc *16*, 1548-1580. 10.1038/s41596-020-00466-1.
153. Becker, M.M., Goral, M.I., Hazelton, P.R., Baer, G.S., Rodgers, S.E., Brown, E.G., Coombs, K.M., and Dermody, T.S. (2001). Reovirus sigmaNS protein is required for nucleation of viral assembly complexes and formation of viral inclusions. J Virol *75*, 1459-1475. 10.1128/jvi.75.3.1459-1475.2001.
154. Colletti, M., Ceglie, D., Di Giannatale, A., and Nazio, F. (2020). Autophagy and Exosomes Relationship in Cancer: Friends or Foes? Front Cell Dev Biol *8*, 614178. 10.3389/fcell.2020.614178.

155. Gillian, A.L., Schmechel, S.C., Livny, J., Schiff, L.A., and Nibert, M.L. (2000). Reovirus protein sigmaNS binds in multiple copies to single-stranded RNA and shares properties with single-stranded DNA binding proteins. J Virol *74*, 5939-5948. 10.1128/jvi.74.13.5939-5948.2000.
156. Zamora, P.F., Hu, L., Knowlton, J.J., Lahr, R.M., Moreno, R.A., Berman, A.J., Prasad, B.V.V., and Dermody, T.S. (2018). Reovirus Nonstructural Protein σNS Acts as an RNA Stability Factor Promoting Viral Genome Replication. J Virol *92*. 10.1128/jvi.00563-18.
157. Hessvik, N.P., and Llorente, A. (2018). Current knowledge on exosome biogenesis and release. Cell Mol Life Sci *75*, 193-208. 10.1007/s00018-017-2595-9.
158. Xie, S., Zhang, Q., and Jiang, L. (2022). Current Knowledge on Exosome Biogenesis, Cargo-Sorting Mechanism and Therapeutic Implications. Membranes (Basel) *12*. 10.3390/membranes12050498.
159. Gorshkov, A., Purvinsh, L., Brodskaia, A., and Vasin, A. (2022). Exosomes as Natural Nanocarriers for RNA-Based Therapy and Prophylaxis. Nanomaterials (Basel) *12*. 10.3390/nano12030524.
160. Mirabelli, C., and Wobus, C.E. (2018). All Aboard! Enteric Viruses Travel Together. Cell Host Microbe *24*, 183-185. 10.1016/j.chom.2018.07.012.
161. Kuss, S.K., Best, G.T., Etheredge, C.A., Pruijssers, A.J., Frierson, J.M., Hooper, L.V., Dermody, T.S., and Pfeiffer, J.K. (2011). Intestinal microbiota promote enteric virus replication and systemic pathogenesis. Science *334*, 249-252. 10.1126/science.1211057.
162. Sung, P.S., Huang, T.F., and Hsieh, S.L. (2019). Extracellular vesicles from CLEC2-activated platelets enhance dengue virus-induced lethality via CLEC5A/TLR2. Nat Commun *10*, 2402. 10.1038/s41467-019-10360-4.
163. Danthi, P., Kobayashi, T., Holm, G.H., Hansberger, M.W., Abel, T.W., and Dermody, T.S. (2008). Reovirus apoptosis and virulence are regulated by host cell membrane penetration efficiency. J Virol *82*, 161-172. 10.1128/jvi.01739-07.
164. Schürz, M., Danmayr, J., Jaritsch, M., Klinglmayr, E., Benirschke, H.M., Matea, C.T., Zimmerebner, P., Rauter, J., Wolf, M., Gomes, F.G., et al. (2022). EVAnalyzer: High content imaging for rigorous characterisation of single extracellular vesicles using standard laboratory equipment and a new open-source ImageJ/Fiji plugin. J Extracell Vesicles *11*, e12282. 10.1002/jev2.12282.
165. Lersner, A.K.v., Fernandes, F.C.L., Ozawa, P.M.M., Lima, S.M., Vagner, T., Sung, B.H., Wehbe, M., Franze, K., Wilson, J.T., Irish, J.M., et al. (2022). EV Fingerprinting: Resolving extracellular vesicle heterogeneity using multi-parametric flow cytometry. bioRxiv, 2022.2011.2010.515864. 10.1101/2022.11.10.515864.
166. Hashiro, G., Loh, P.C., and Yau, J.T. (1977). The preferential cytotoxicity of reovirus for certain transformed cell lines. Arch Virol *54*, 307-315. 10.1007/bf01314776.

167. Duncan, M.R., Stanish, S.M., and Cox, D.C. (1978). Differential sensitivity of normal and transformed human cells to reovirus infection. J Virol *28*, 444-449. 10.1128/jvi.28.2.444-449.1978.
168. Coffey, M.C., Strong, J.E., Forsyth, P.A., and Lee, P.W. (1998). Reovirus therapy of tumors with activated Ras pathway. Science *282*, 1332-1334. 10.1126/science.282.5392.1332.
169. Merchant, A.K., Loney, T.L., and Maybaum, J. (1996). Expression of wild-type p53 stimulates an increase in both Bax and Bcl-xL protein content in HT29 cells. Oncogene *13*, 2631-2637.
170. Li, X., Marani, M., Mannucci, R., Kinsey, B., Andriani, F., Nicoletti, I., Denner, L., and Marcelli, M. (2001). Overexpression of BCL-X(L) underlies the molecular basis for resistance to staurosporine-induced apoptosis in PC-3 cells. Cancer Res *61*, 1699-1706.
171. Ruemmele, F.M., Dionne, S., Qureshi, I., Sarma, D.S., Levy, E., and Seidman, E.G. (1999). Butyrate mediates Caco-2 cell apoptosis via up-regulation of pro-apoptotic BAK and inducing caspase-3 mediated cleavage of poly-(ADP-ribose) polymerase (PARP). Cell Death Differ *6*, 729-735. 10.1038/sj.cdd.4400545.
172. Moss, S.F., Scholes, J.V., and Holt, P.R. (1996). Abnormalities of epithelial apoptosis in multistep colorectal neoplasia demonstrated by terminal deoxyuridine nick end labeling. Dig Dis Sci *41*, 2238-2247. 10.1007/bf02071407.
173. el-Mahdani, N., Vaillant, J.C., Guiguet, M., Prévot, S., Bertrand, V., Bernard, C., Parc, R., Béréziat, G., and Hermelin, B. (1997). Overexpression of p53 mRNA in colorectal cancer and its relationship to p53 gene mutation. Br J Cancer *75*, 528-536. 10.1038/bjc.1997.92.
174. Lea, T. (2015). Caco-2 Cell Line. In The Impact of Food Bioactives on Health: in vitro and ex vivo models, K. Verhoeckx, P. Cotter, I. López-Expósito, C. Kleiveland, T. Lea, A. Mackie, T. Requena, D. Swiatecka, and H. Wichers, eds. (Springer
Copyright 2015, The Author(s).), pp. 103-111. 10.1007/978-3-319-16104-4_10.
175. Rosen, A., Casciola-Rosen, L., and Ahearn, J. (1995). Novel packages of viral and self-antigens are generated during apoptosis. J Exp Med *181*, 1557-1561. 10.1084/jem.181.4.1557.
176. Krejbich-Trotot, P., Denizot, M., Hoarau, J.J., Jaffar-Bandjee, M.C., Das, T., and Gasque, P. (2011). Chikungunya virus mobilizes the apoptotic machinery to invade host cell defenses. Faseb j *25*, 314-325. 10.1096/fj.10-164178.
177. Diller, J.R., Halloran, S.R., Koehler, M., Dos Santos Natividade, R., Alsteens, D., Stehle, T., Dermody, T.S., and Ogden, K.M. (2020). Reovirus σ1 Conformational Flexibility Modulates the Efficiency of Host Cell Attachment. J Virol *94*. 10.1128/jvi.01163-20.
178. Klasse, P.J. (2015). Molecular determinants of the ratio of inert to infectious virus particles. Prog Mol Biol Transl Sci *129*, 285-326. 10.1016/bs.pmbts.2014.10.012.
179. Cuevas, J.M., Durán-Moreno, M., and Sanjuán, R. (2017). Multi-virion infectious units arise from free viral particles in an enveloped virus. Nat Microbiol *2*, 17078. 10.1038/nmicrobiol.2017.78.

180. Zhang, M., Ghosh, S., Kumar, M., Santiana, M., Bleck, C.K.E., Chaimongkol, N., Altan-Bonnet, N., and Shuai, D. (2021). Emerging Pathogenic Unit of Vesicle-Cloaked Murine Norovirus Clusters is Resistant to Environmental Stresses and UV(254) Disinfection. Environ Sci Technol *55*, 6197-6205. 10.1021/acs.est.1c01763.
181. Domingo, E., García-Crespo, C., Lobo-Vega, R., and Perales, C. (2021). Mutation Rates, Mutation Frequencies, and Proofreading-Repair Activities in RNA Virus Genetics. Viruses *13*. 10.3390/v13091882.
182. Domingo, E., Sheldon, J., and Perales, C. (2012). Viral quasispecies evolution. Microbiol Mol Biol Rev *76*, 159-216. 10.1128/mmbr.05023-11.
183. Shirogane, Y., Watanabe, S., and Yanagi, Y. (2019). Cooperation between different variants: A unique potential for virus evolution. Virus Res *264*, 68-73. 10.1016/j.virusres.2019.02.015.
184. Bordería, A.V., Isakov, O., Moratorio, G., Henningsson, R., Agüera-González, S., Organtini, L., Gnädig, N.F., Blanc, H., Alcover, A., Hafenstein, S., et al. (2015). Group Selection and Contribution of Minority Variants during Virus Adaptation Determines Virus Fitness and Phenotype. PLoS Pathog *11*, e1004838. 10.1371/journal.ppat.1004838.
185. Jackson, W.T., Giddings, T.H., Jr., Taylor, M.P., Mulinyawe, S., Rabinovitch, M., Kopito, R.R., and Kirkegaard, K. (2005). Subversion of cellular autophagosomal machinery by RNA viruses. PLoS Biol *3*, e156. 10.1371/journal.pbio.0030156.
186. Kobayashi, T., Antar, A.A., Boehme, K.W., Danthi, P., Eby, E.A., Guglielmi, K.M., Holm, G.H., Johnson, E.M., Maginnis, M.S., Naik, S., et al. (2007). A plasmid-based reverse genetics system for animal double-stranded RNA viruses. Cell Host Microbe *1*, 147-157. 10.1016/j.chom.2007.03.003.
187. Boehme, K.W., Guglielmi, K.M., and Dermody, T.S. (2009). Reovirus nonstructural protein sigma1s is required for establishment of viremia and systemic dissemination. Proc Natl Acad Sci U S A *106*, 19986-19991. 10.1073/pnas.0907412106.
188. Thoner, T.W., Jr., Ye, X., Karijolich, J., and Ogden, K.M. (2021). Reovirus Low-Density Particles Package Cellular RNA. Viruses *13*. 10.3390/v13061096.
189. Jimenez, L., Yu, H., McKenzie, A.J., Franklin, J.L., Patton, J.G., Liu, Q., and Weaver, A.M. (2019). Quantitative Proteomic Analysis of Small and Large Extracellular Vesicles (EVs) Reveals Enrichment of Adhesion Proteins in Small EVs. J Proteome Res *18*, 947-959. 10.1021/acs.jproteome.8b00647.
190. Wang, X., Huynh, H., Gjörloff-Wingren, A., Monosov, E., Stridsberg, M., Fukuda, M., and Mustelin, T. (2002). Enlargement of secretory vesicles by protein tyrosine phosphatase PTP-MEG2 in rat basophilic leukemia mast cells and Jurkat T cells. J Immunol *168*, 4612-4619. 10.4049/jimmunol.168.9.4612.
191. Kutchy, N.A., Peeples, E.S., Sil, S., Liao, K., Chivero, E.T., Hu, G., and Buch, S. (2020). Extracellular Vesicles in Viral Infections of the Nervous System. Viruses *12*. 10.3390/v12070700.

192. Candelario, K.M., and Steindler, D.A. (2014). The role of extracellular vesicles in the progression of neurodegenerative disease and cancer. Trends Mol Med *20*, 368-374. 10.1016/j.molmed.2014.04.003.
193. Mainou, B.A., Zamora, P.F., Ashbrook, A.W., Dorset, D.C., Kim, K.S., and Dermody, T.S. (2013). Reovirus cell entry requires functional microtubules. mBio *4*. 10.1128/mBio.00405-13.
194. Trejo-Cerro, Ó., Eichwald, C., Schraner, E.M., Silva-Ayala, D., López, S., and Arias, C.F. (2018). Actin-Dependent Nonlytic Rotavirus Exit and Infectious Virus Morphogenetic Pathway in Nonpolarized Cells. J Virol *92*. 10.1128/jvi.02076-17.
195. Gardet, A., Breton, M., Trugnan, G., and Chwetzoff, S. (2007). Role for actin in the polarized release of rotavirus. J Virol *81*, 4892-4894. 10.1128/jvi.02698-06.
196. Catalano, M., and O'Driscoll, L. (2020). Inhibiting extracellular vesicles formation and release: a review of EV inhibitors. J Extracell Vesicles *9*, 1703244. 10.1080/20013078.2019.1703244.
197. Schaefer, L. (2014). Complexity of danger: the diverse nature of damage-associated molecular patterns. J Biol Chem *289*, 35237-35245. 10.1074/jbc.R114.619304.
198. Thepparit, C., Khongwichit, S., Ketsuwan, K., Libsittikul, S., Auewarakul, P., and Smith, D.R. (2019). Dengue virus requires apoptosis linked gene-2-interacting protein X (ALIX) for viral propagation. Virus Res *261*, 65-71. 10.1016/j.virusres.2018.12.015.
199. Missotten, M., Nichols, A., Rieger, K., and Sadoul, R. (1999). Alix, a novel mouse protein undergoing calcium-dependent interaction with the apoptosis-linked-gene 2 (ALG-2) protein. Cell Death Differ *6*, 124-129. 10.1038/sj.cdd.4400456.
200. Chatellard-Causse, C., Blot, B., Cristina, N., Torch, S., Missotten, M., and Sadoul, R. (2002). Alix (ALG-2-interacting protein X), a protein involved in apoptosis, binds to endophilins and induces cytoplasmic vacuolization. J Biol Chem *277*, 29108-29115. 10.1074/jbc.M204019200.
201. Bissig, C., and Gruenberg, J. (2014). ALIX and the multivesicular endosome: ALIX in Wonderland. Trends Cell Biol *24*, 19-25. 10.1016/j.tcb.2013.10.009.
202. Khadka, S., Vangeloff, A.D., Zhang, C., Siddavatam, P., Heaton, N.S., Wang, L., Sengupta, R., Sahasrabudhe, S., Randall, G., Gribskov, M., et al. (2011). A physical interaction network of dengue virus and human proteins. Mol Cell Proteomics *10*, M111.012187. 10.1074/mcp.M111.012187.
203. Rahimian, P., and He, J.J. (2016). Exosome-associated release, uptake, and neurotoxicity of HIV-1 Tat protein. J Neurovirol *22*, 774-788. 10.1007/s13365-016-0451-6.
204. Lenassi, M., Cagney, G., Liao, M., Vaupotic, T., Bartholomeeusen, K., Cheng, Y., Krogan, N.J., Plemenitas, A., and Peterlin, B.M. (2010). HIV Nef is secreted in exosomes and triggers apoptosis in bystander CD4+ T cells. Traffic *11*, 110-122. 10.1111/j.1600-0854.2009.01006.x.
205. Pleet, M.L., Mathiesen, A., DeMarino, C., Akpamagbo, Y.A., Barclay, R.A., Schwab, A., Iordanskiy, S., Sampey, G.C., Lepene, B., Nekhai, S., Aman, M.J.,

and Kashanchi, F. (2016). Ebola VP40 in Exosomes Can Cause Immune Cell Dysfunction. Front Microbiol *7*, 1765. 10.3389/fmicb.2016.01765.
206. Mukherjee, S., Akbar, I., Kumari, B., Vrati, S., Basu, A., and Banerjee, A. (2019). Japanese Encephalitis Virus-induced let-7a/b interacted with the NOTCH-TLR7 pathway in microglia and facilitated neuronal death via caspase activation. J Neurochem *149*, 518-534. 10.1111/jnc.14645.
207. Ruemmele, F.M., Schwartz, S., Seidman, E.G., Dionne, S., Levy, E., and Lentze, M.J. (2003). Butyrate induced Caco-2 cell apoptosis is mediated via the mitochondrial pathway. Gut *52*, 94-100. 10.1136/gut.52.1.94.
208. Levine, A.J. (1997). p53, the cellular gatekeeper for growth and division. Cell *88*, 323-331. 10.1016/s0092-8674(00)81871-1.
209. Sanjuán, R. (2018). Collective properties of viral infectivity. Curr Opin Virol *33*, 1-6. 10.1016/j.coviro.2018.06.001.
210. Segredo-Otero, E., and Sanjuán, R. (2019). The effect of genetic complementation on the fitness and diversity of viruses spreading as collective infectious units. Virus Res *267*, 41-48. 10.1016/j.virusres.2019.05.005.
211. González-López, O., Rivera-Serrano, E.E., Hu, F., Hensley, L., McKnight, K.L., Ren, J., Stuart, D.I., Fry, E.E., and Lemon, S.M. (2018). Redundant Late Domain Functions of Tandem VP2 YPX(3)L Motifs in Nonlytic Cellular Egress of Quasi-enveloped Hepatitis A Virus. J Virol *92*. 10.1128/jvi.01308-18.
212. Rivera-Serrano, E.E., González-López, O., Das, A., and Lemon, S.M. (2019). Cellular entry and uncoating of naked and quasi-enveloped human hepatoviruses. Elife *8*. 10.7554/eLife.43983.
213. Mainou, B.A., and Dermody, T.S. (2012). Transport to late endosomes is required for efficient reovirus infection. J Virol *86*, 8346-8358. 10.1128/jvi.00100-12.
214. Montecalvo, A., Larregina, A.T., Shufesky, W.J., Stolz, D.B., Sullivan, M.L., Karlsson, J.M., Baty, C.J., Gibson, G.A., Erdos, G., Wang, Z., et al. (2012). Mechanism of transfer of functional microRNAs between mouse dendritic cells via exosomes. Blood *119*, 756-766. 10.1182/blood-2011-02-338004.
215. Morelli, A.E., Larregina, A.T., Shufesky, W.J., Sullivan, M.L., Stolz, D.B., Papworth, G.D., Zahorchak, A.F., Logar, A.J., Wang, Z., Watkins, S.C., Falo, L.D., Jr., and Thomson, A.W. (2004). Endocytosis, intracellular sorting, and processing of exosomes by dendritic cells. Blood *104*, 3257-3266. 10.1182/blood-2004-03-0824.
216. Escrevente, C., Keller, S., Altevogt, P., and Costa, J. (2011). Interaction and uptake of exosomes by ovarian cancer cells. BMC Cancer *11*, 108. 10.1186/1471-2407-11-108.
217. Kim, J.W., Lyi, S.M., Parrish, C.R., and Parker, J.S. (2011). A proapoptotic peptide derived from reovirus outer capsid protein {micro}1 has membrane-destabilizing activity. J Virol *85*, 1507-1516. 10.1128/jvi.01876-10.
218. Danthi, P., Coffey, C.M., Parker, J.S., Abel, T.W., and Dermody, T.S. (2008). Independent regulation of reovirus membrane penetration and apoptosis by the mu1 phi domain. PLoS Pathog *4*, e1000248. 10.1371/journal.ppat.1000248.

219. Lai, C.M., Boehme, K.W., Pruijssers, A.J., Parekh, V.V., Van Kaer, L., Parkos, C.A., and Dermody, T.S. (2015). Endothelial JAM-A promotes reovirus viremia and bloodstream dissemination. J Infect Dis *211*, 383-393. 10.1093/infdis/jiu476.
220. Canning, W.M., and Fields, B.N. (1983). Ammonium chloride prevents lytic growth of reovirus and helps to establish persistent infection in mouse L cells. Science *219*, 987-988. 10.1126/science.6297010.
221. Konopka-Anstadt, J.L., Mainou, B.A., Sutherland, D.M., Sekine, Y., Strittmatter, S.M., and Dermody, T.S. (2014). The Nogo receptor NgR1 mediates infection by mammalian reovirus. Cell Host Microbe *15*, 681-691. 10.1016/j.chom.2014.05.010.
222. Aravamudhan, P., Guzman-Cardozo, C., Urbanek, K., Welsh, O.L., Konopka-Anstadt, J.L., Sutherland, D.M., and Dermody, T.S. (2022). The Murine Neuronal Receptor NgR1 Is Dispensable for Reovirus Pathogenesis. J Virol *96*, e0005522. 10.1128/jvi.00055-22.
223. Long, W.F., and Burke, D.C. (1971). Interferon production by double-stranded RNA: a comparison of induction by reovirus to that by a synthetic double-stranded polynucleotide. J Gen Virol *12*, 1-11. 10.1099/0022-1317-12-1-1.
224. Zhang, Y., Wu, J., Zhang, H., Wei, J., and Wu, J. (2020). Extracellular Vesicles-Mimetic Encapsulation Improves Oncolytic Viro-Immunotherapy in Tumors With Low Coxsackie and Adenovirus Receptor. Front Bioeng Biotechnol *8*, 574007. 10.3389/fbioe.2020.574007.